

Summer 2021

The Effect of Through Thickness Reinforcement on Debonding Behavior of Skin/Stringer Configuration

Yogaraja Sridhar
Old Dominion University, ysrid001@odu.edu

Follow this and additional works at: https://digitalcommons.odu.edu/mae_etds



Part of the [Aerospace Engineering Commons](#), and the [Mechanical Engineering Commons](#)

Recommended Citation

Sridhar, Yogaraja. "The Effect of Through Thickness Reinforcement on Debonding Behavior of Skin/Stringer Configuration" (2021). Master of Science (MS), Thesis, Mechanical & Aerospace Engineering, Old Dominion University, DOI: 10.25777/x4vy-ms41
https://digitalcommons.odu.edu/mae_etds/338

This Thesis is brought to you for free and open access by the Mechanical & Aerospace Engineering at ODU Digital Commons. It has been accepted for inclusion in Mechanical & Aerospace Engineering Theses & Dissertations by an authorized administrator of ODU Digital Commons. For more information, please contact digitalcommons@odu.edu.

**THE EFFECT OF THROUGH THICKNESS REINFORCEMENT ON DEBONDING
BEHAVIOR OF SKIN/STRINGER CONFIGURATION**

by

Yogaraja Sridhar

B.E. November 2018, Madras Institute of Technology, Anna University, India

A Thesis submitted to the Faculty of
Old Dominion University in Partial Fulfillment of the
Requirements for the Degree of

MASTER OF SCIENCE

MECHANICAL AND AEROSPACE ENGINEERING

OLD DOMINION UNIVERSITY

August 2021

Approved by:

Dr.Oleksandr Kravchenko (Director)

Dr.Krishnand Kaipa (Member)

Dr. Mileta Tomovic (Member)

ABSTRACT

THE EFFECT OF THROUGH THICKNESS REINFORCEMENT ON BONDED SKIN AND STRINGER SPECIMENS USING ADHESIVE LAYER

Yogaraja Sridhar
Old Dominion University, 2021
Director: Dr. Oleksandr Kravchenko

Investigation of this study is to determine the crack propagation and disbonding in the bonded region of the skin and stringer specimen. An adhesive layer has been used to bond the skin and stringer by using a heat press operation. After the bonding, a drilling method has been adopted to install the through thickness reinforcement in the specimen. The key role of the through thickness reinforcement is to increase the stiffness and strength of the panels and to prevent the crack propagation or disbonding of the panels. The reinforcement was installed in pure (Pristine) samples and in defect samples where an initial defect was placed in between the skin and stringer panels before the bonding process to compare the efficiency of the through thickness reinforcement in both the cases. The effect of spacing of the through thickness reinforcement along the longitudinal direction of the specimens were studied. Two different spacing of the reinforcement was installed in both pure and defect samples. A three point bending test and Tensile tests were carried out to inspect the crack propagation and failure of the specimens. The strength and stiffness of the specimens for both the spacings are compared using the respective Load-Displacement plots. Also, an Ultrasonic scanner was used to analyze the location and size of the crack in the specimen after the tests were completed. In addition, Digital Image Correlation (DIC) was equipped to understand the displacement measurements during the experiment

ACKNOWLEDGEMENTS

I would like to express my gratitude to my thesis advisor Dr. Oleksandr G. Kravchenko for his continuous guidance, funding and having faith in me throughout my master's journey. I would like to specially thank my advisor for supporting and motivating me during the pandemic which helped me to overcome my challenges.

Secondly, I specially thank Siavash Sattar for guiding me on using the Digital Image Correlation system and all other lab mates in our Composite Modeling and Manufacturing lab, Old Dominion University without which the research would have not been completed.

I would like to thank my family for their support and belief in me. Without them I could not have pursued my dream of completing my master's degree. I would also like to thank my friends who have been encouraging me in difficult situations and throughout my journey.

NOMENCLATURE

3PB Three Point Bending

DIC Digital Image Correlation.

MTS MTS Systems Corporation

TTR Through Thickness Reinforcement

VCCT Virtual Crack Closure Techniqu

TABLE OF CONTENTS

Chapter	Page
LIST OF FIGURES	vii
CHAPTER 1	1
1.1 Motivation.....	1
1.2 Thesis Goals.....	3
CHAPTER 2	4
2.1 Effect of Mechanical Fastening on Skin-Stringer Specimen.....	5
2.2 FEM Modeling of Skin-Stringer Structures.....	7
2.3 Effect of Adhesive Layer in Bonded Joints	9
2.4 Effect of Tufting on Skin/Stringer Panels.....	13
2.4.1 Effect of Z-pining Method on Skin/Stringer Panels	16
2.4.2 Effect of Welding on Bonded Plates.....	18
2.5 Effect Of Through Thickness Reinforcement in Laminated Composite Structures ...	19
CHAPTER 3	23
3.1 Fabrication of Skin-Stringer Specimen.....	24
3.2 Curing Process of the Prepreg Fabric	26
3.3 Bonding Process of Skin-Stringer Panels	28
3.4 Installation of Through Thickness Reinforcement (TTR)	29
3.5 Fabrication of Skin-Stringer Specimens for Tensile Test.....	33

3.6 Ultrasonic Scanning using Omniscan	34
3.9 Simulation of Skin/Stringer Sample Using Finite Element Analysis	40
CHAPTER 4	48
4.1 Comparison of Pristine Skin-Stringer Sample and Sample with Initial Disbond	48
4.2 Effect of 1/2" TTR Spacing on Skin-Stringer Debonding Behavior	54
4.3 Effect of 1/4" TTR Spacing on Skin-Stringer Debonding Behavior	60
4.4 Effect of 1/2" and 1/4" TTR Spacing on Failed Skin-Stringer Panels	70
4.5 Effect of TTR in Tensile test	72
4.6 Ultrasonic Scanning of Skin-Stringer Specimens	76
4.7 Simulation Results of Skin/Stringer Specimen	83
CHAPTER 5	86
REFERENCES	88

LIST OF FIGURES

Figure	Page
1 A fuselage with mechanically fastened skin and stringers.	2
2 A fuselage with adhesively bonded and cured skin and stringers	2
3 Finite element mesh of skin -stringer [1].	5
4 STAGS model of skin-stringer specimen from NASA study [5].	6
5 FEM modeling of skin-stringer specimen [3].	8
6 Initial crack modeled in the defect specimen [3].	8
7 Load-Displacement plot for linear and Non-linear analysis [3].	9
8 Adhesive AV138 specimen [8].	11
9 Adhesive silkforce 7888 specimen [8].	12
10 Load-Displacement plot for brittle and ductile adhesives [8].	13
11 a) Un-tufted specimen and b) tufted reinforcement in the specimen [10].	14
12 Kuka robot performing the tufting reinforcement [9].	15
13 Load-Displacement curve of skin-stringer specimen [9].	16
14 Simplification of skin-stringer specimen [12].	17
15 Grid configuration of Z-pins [12].	17
16 Stress-Strain curves for a) pristine sample and b) Z-pins inserted samples [12].	18
17 Load-Displacement plot for resistance welding specimens [14].	19

Figure	Page
18 Defect specimens with TTR [2]	20
19 Specimen with TTR positioned in the undamaged area [2].	21
20 Specimen with TTR positioned in delamination area [2].	21
21 Aspect ratio of rods used for TTR in specimens [15].	22
22 Tensile and Flexural tests setup for skin-stringer specimen.	23
23 Unidirectional carbon fiber prepreg fabric.	24
24 Vacuum bagging of the skin-stringer laminate	25
25 Wabash Heat Press.....	26
26 Skin laminate after curing.	27
27 Stringer laminate	27
28 Protomax Waterjet	29
29 Completely cured skin-stringer plate	29
30 a) Top view and b) Side view of the TTR configuration with ¼ inch spacing,c)dremel equipment and d) sawyer robot drilling machine.	30
31 Epoxy Resin and Hardener.	32
32 TTR installed skin-stringer sample	33
33 Tabs bonding to the skin-stringer specimen.	34
34 Interface of the Omniscan.	35

Figure	Page
35 Part & Weld screen of Omniscan.....	36
36 Setup screen of the Omniscan Sx.....	37
37 Confirmation screen for checking the probe elements.	38
38 a)Calibration for scanning the specimens b) Example of setting Gate A thickness of pristine sample c) Image of the transducer scanning the sample with water as scanning gel.	40
39 Modeled Skin Surface.....	41
40 Partitioned Layers of Skin Specimen.....	41
41 Modeled Stringer Specimen.....	42
42 Partitioned Layers of Stringer Specimen	42
43 Properties of the Cohesive Elements	44
44 ABAQUS modelling of cohesive element.....	44
45 Orientation of the plies in Skin/Stringer Specimen.	45
46 Interactions Settings Used for Skin/Stringer Sample.....	46
47 Boundary conditions of the Skin/Stringer Sample.....	47
48 DIC images of displacement for the pristine skin/stringer sample.	50
49 a) Load vs Displacement plot for pristine vs defect skin-stringer samples b) Crack propagation behavior of pristine and defect samples.....	51
50 DIC images of displacement for initial debonded skin/stringer samples.	52

Figure	Page
51 Load vs Displacement plot for pristine vs pristine repaired TTR.....	54
52 DIC images of displacement for ½ inch spaced TTR in pristine skin/stringer sample.	55
53 Load vs Displacement for defect vs TTR repaired defect.	56
54 DIC image of displacement for ½ inch spaced TTR in initial disbond sample.	57
55 Behavior of crack propagation for defect vs defect with 1/2” TTR samples.....	59
56 Load vs Displacement curves for ½ inch spaced TTR vs ¼ inch spaced TTR.	61
57 DIC image of displacement for ¼ inch spaced TTR in pristine skin/stringer sample.	62
58 Behavior of crack propagation for pristine vs pristine with 1/4” spaced TTR.	63
59 Load vs Displacement plots for ½ inch and ¼ inch spaced TTR defect skin/stringer.....	64
60 a) DIC images of displacement for ¼ inch spaced TTR in defect skin/stringer sample b) Behavior of crack propagation in defect with 1/2" vs defect with 1/4" spaced TTR samples.....	66
61 Effectiveness of TTR spacing on pristine and initially disbanded skin/stringer samples.	67
62 Comparison of crack initiation load in all sample groups.	69
63 Load vs Displacement for completely failed and repaired specimens.....	71
64 Effectiveness of TTR on repaired skin/stringer specimens.	72
65 Failed Pristine with TTR Skin/Stringer.	73
66 Tensile test results of skin-stringer specimens.....	74

Figure	Page
67 Crack in the defect skin/stringer sample.	74
68 DIC image of displacement of pristine skin/stringer with ¼ inch spaced TTR.	75
69 DIC image of displacement of the defect skin/stringer sample with ¼ inch spaced TTR.	76
70 Ultrasonic scanning image of pristine skin/stringer sample.	77
71 Ultrasonic scanning image of defect skin/stringer samples.	78
72 Ultrasonic scanning image of defect sample with ½ inch spaced TTR.	79
73 Ultrasonic scanning image of pristine with ½ inch spaced TTR.	80
74 Ultrasonic scanning of defect skin/stringer sample with ¼ inch TTR.	81
75 Ultrasonic scanning for pristine samples with ¼ inch spaced TTR.	82
76 Stress concentration of skin/stringer specimen.	83
77 Failure of cohesive layer at the load of 495 N.	84
78 Failure of cohesive layer at the load of 620 N.	84
79 Load vs Displacement of ABAQUS for pristine skin/stringer sample.	85

CHAPTER 1

INTRODUCTION

1.1 Motivation

The use of Carbon epoxy composite structure is increasing in the aerospace industry rather than conventional metals used before. The manufacturing of a commercial aircraft is a lengthy process where each part of the aircraft is built separately and then assembled. For example, the fuselage of the aircraft and wing are manufactured separately and then joined together. The wings are attached with help of spurs and the skin of the fuselage are being fastened to the stringers. The Skin and stringer are present at the outer layer of the fuselage and run along the longitudinal direction of the wing (Figures 1 and 2). When the aircraft is being operated the skin and stringers play a vital role in uniformly distributing the Aerodynamic Loads throughout the structure thus preventing failure at a particular point. Research proves that the use of mechanical fastening [20] in bonding the skin and stringer generate high stress concentration at the location of the holes which causes the material to fail and might lead to catastrophic failure because the method of bolt clamping influences the ultimate strength of the material. Composites are used more in manufacturing because of its lighter weight and high strength and stiffness, the curing and bonding process of the composites have also become promising rather than the use of fasteners but the critical problem that is faced by the composites in the aerospace sectors are the disbonding or the delamination problem of the skin and stringer [2]. The delamination in composites can compromise the safety and performance of the structure and reduce the mechanical toughness properties which also leads to catastrophic failure, so several different techniques are being adopted to avoid the failure through delamination of the composites.

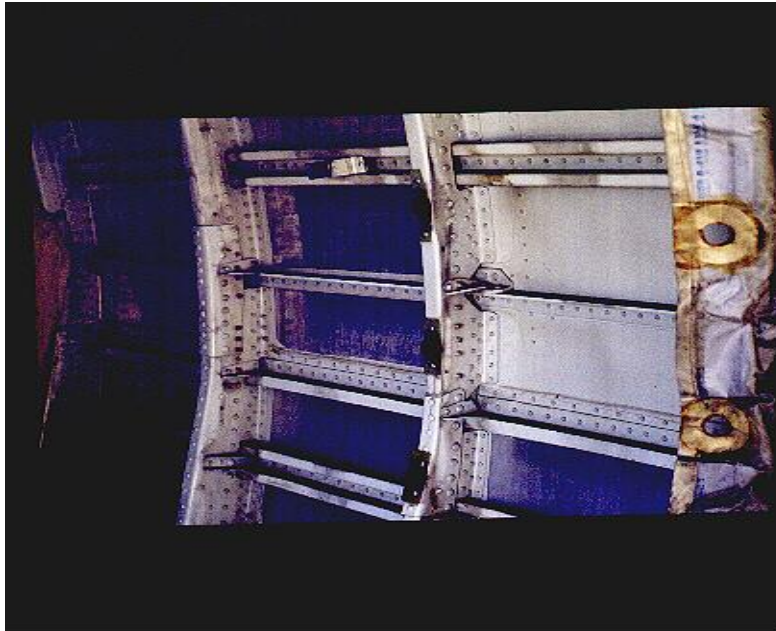


Figure 1 A fuselage with mechanically fastened skin and stringers.



Figure 2 A fuselage with adhesively bonded and cured skin and stringers

1.2 Thesis Goals

The Goal of the research is to improve the efficiency of the adhesively bonded skin and stringer configuration with the Through Thickness Reinforcement (TTR) methods. The TTR are installed with two different spacings in both the pristine skin/stringer samples and samples with initial Teflon defect placed during the bonding process to imitate an initial crack at the corner, where the stress concentration is expected. The 3-point bending (3PB) and the tensile tests are carried out to investigate the efficiency of the samples with TTR. Additionally, completely failed samples were also repaired with the respective TTR spacing to understand the crack propagation and recovered strength of the rebounded skin/stringer elements. Finally, the comparison between the two different spacing is performed for a better understanding of the crack propagation and the stiffness of the structure.

CHAPTER 2

LITERATURE REVIEW

Most research indicates that the use of adhesive layer between the skin and stringer are more efficient than the method of mechanical fastening, welding, and bolting [23]. The use of adhesive layer for the bonding process of the skin and stringer has been increasing in aerospace applications. During operating conditions, the bonded specimens are introduced to bending and twisting where the disbanding and/or delamination of the skin and stringer occurs, and they start to fail on the edges of the stringer. The delamination crack propagates until failure occurs, which can develop in quasi-static or fatigue loading conditions. Several studies have been performed on this problem in both numerical and experimental methods. Simulations using Finite Element Method (FEM) are used to predict the failure of the skin and stringer [1,20] and samples are fabricated and tested for comparing with experimental studies. To avoid the delamination, different methods of reinforcement was suggested such as tufting and Z-pinning [2,15]. The through thickness reinforcement was constructed on the sample to increase the strength of the bonded specimen and arrest the crack propagation to avoid failure. The scope of this study was adopted from the research of through thickness reinforcement (TTR) where the sample is fabricated using a particular orientation of carbon fiber prepreg and then different spacings were installed to understand the efficiency of the TTR on the specimen under three-point bending and tensile tests. Certain studies assume that the fuselage is designed to have cracks while operating, which may cause the skin to buckle [4] so samples with initial defect were also investigated under similar loading conditions.

2.1 Effect of Mechanical Fastening on Skin-Stringer Specimen

A study by I.H Marshall et al. [1] investigated the bonding problem by creating a 3-dimensional Finite element model of a plate with open hole. This model (Figure 3) was simulated to understand the stress concentrations near the hole when the plate is subjected to loading. The main objective of the study is to analyze the effect of bolting and stacking sequence of the skin-stringer. The simulation of the model was displacement controlled and symmetric boundary conditions were defined at the edge nodes of the model.

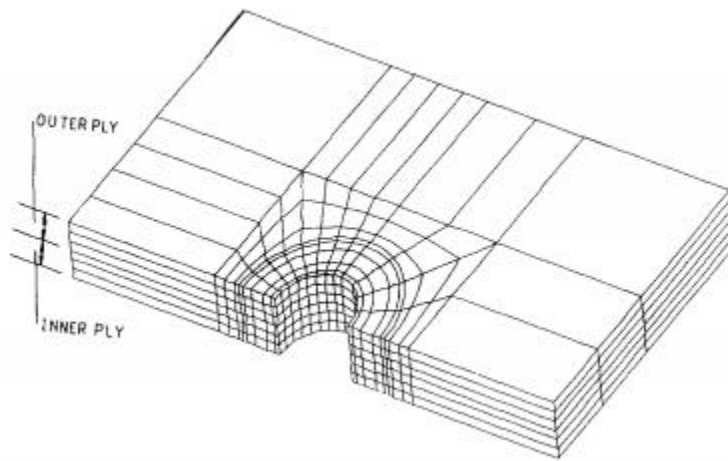


Figure 3 Finite element mesh of skin -stringer [1].

The investigation of the study proved that when the load is applied the interlaminar, stresses were found maximum near the holes on the top surface. Also, it was understood the behavior of the stresses near the hole in the open hole model is seen to be similar for the skin/stringer samples. The failure of the specimen starts at the region around the holes when the load is higher, and the delamination of the skin and stringer starts when the clamping does not improve the joint strength. It is also proved from the study that when the crack in bolted specimens starts, the crack

propagation grows non-linearly as the loads keeps increasing, and the major disadvantage is that the peak load cannot be determined because of the non-linear crack propagation.

A NASA research by Richard et al. [5] had used Structural Analysis of General Shells (STAGS) which is a special platform to model the fastened elements to perform the simulations (Figure 4). The major advantage of STAGS is to include the effect of material non-linearities during the analysis. Simulations for specimens with an initial defect can be modeled using STAGS and it calculates the crack propagation using the strain energy release rate. The results of this study were presented for pristine and defect skin/stringer panels, respectively. For pristine skin/stringer panel it was shown that the presence of nonlinear crack growth as the displacement gradient during the analysis was found to be higher and because of this complexity it was difficult to determine the critical location at peak load [1,5].

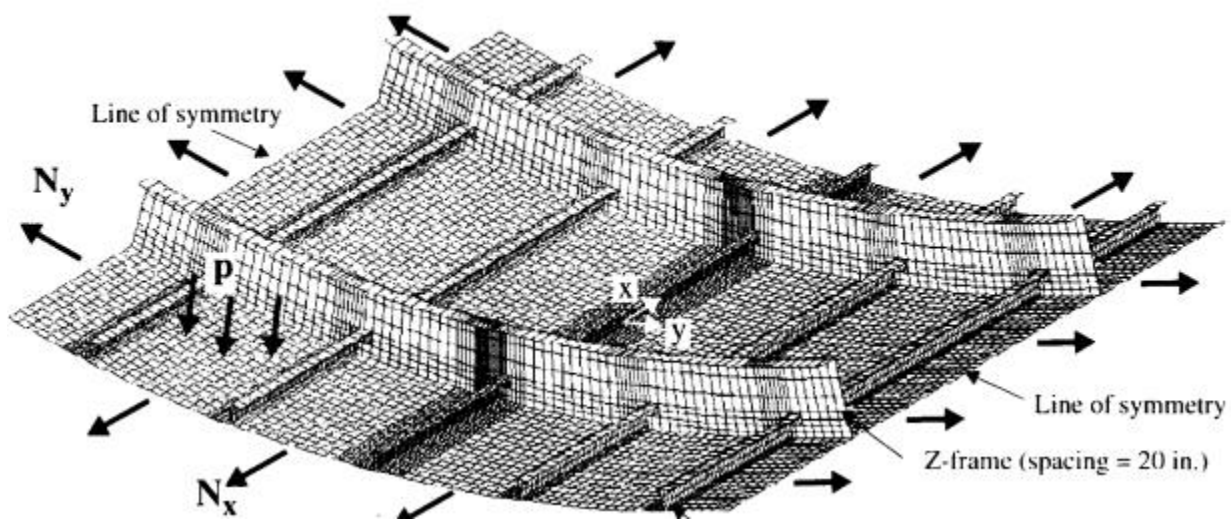


Figure 4 STAGS model of skin-stringer specimen from NASA study [5].

The results for the defect specimens placed in between the skin and stringer interface showed that when the compressive loads are applied to it the stress intensity factors near the crack

tip increases and leads to buckling of the skin. It is also seen that the crack tip in the specimen and the strength and stiffness of the material influences the failure load of the skin stringer specimen, respectively.

2.2 FEM Modeling of Skin-Stringer Structures

An analysis by Ronald et al [3,22] was performed to study the damage initiation using stress analysis and the disbonding/delamination propagation using methods of fracture mechanics. FEM models were created for pristine and defect specimens with the loads and boundary conditions to simulate the 3-point bending tests and tensile tests (Figure 5). A refined mesh configuration was used near the skin-stringer interface to monitor the crack propagation. The region near the refined mesh where the adhesive layer of the specimen is present was modeled with four elements and the skin-stringer was modeled with one element per ply in the thickness direction (Figure 6). The defect specimen was modeled with an initial damage in bonding region to predict the onset propagation of the crack during the simulation and the virtual crack closure technique (VCCT) was used to calculate the strain energy release rate when the crack starts to propagate through the specimen during the test. From (VCCT) virtual crack closure technique we obtain the strain energy release rate, and the fracture toughness of the specimen is also determined which helps to understand the delamination/disbonding [29].

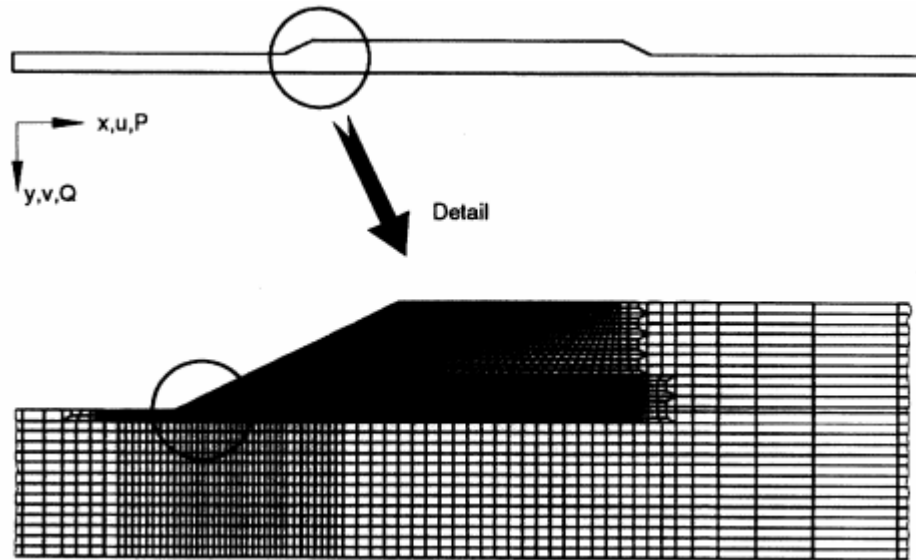


Figure 5 FEM modeling of skin-stringer specimen [3].

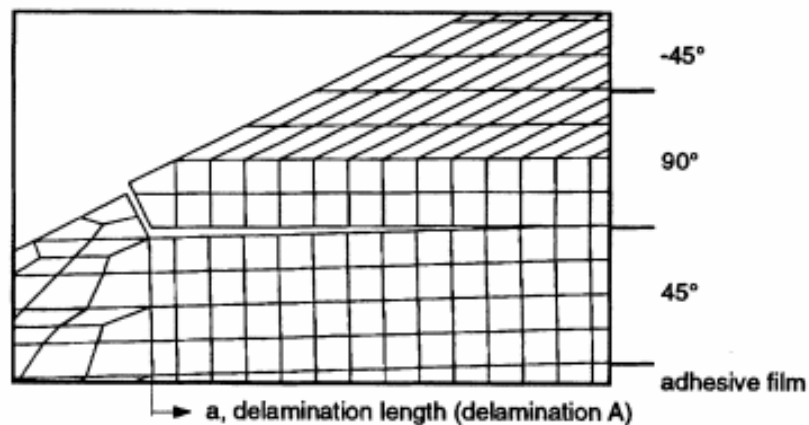


Figure 6 Initial crack modeled in the defect specimen [3].

The displacement of the skin-stringer specimen in the three-point bending test was investigated and compared with the experimental results. A geometrically non-linear analysis was performed in the finite element analysis because of the complexity. The load-displacement curves were compared for both the analytical and experimental methods (Figure 7), and it was observed that there was a 10% difference between both the above mentioned methods. The initial crack

appeared to be dependent of the stress distribution in the bonding area between the skin and stringer. Using the method of fracture mechanics and the virtual crack closure technique (VCCT), Mode I and Mode II strain energy release rate was computed and proved that the initial crack present in the defect sample grows in an unstable manner between the adhesive film and the top skin. The strain energy release rate determined using the VCCT was higher during the debonding of skin and stringer than the energy released at the stage of crack initiation. Comparison between the computational and experimental data had proved that all the samples which were tested and simulated had non-linearities in the skin/stringer panels above the ultimate debond load of the sample when the specimens was tested in 3-point bending and tensile tests.

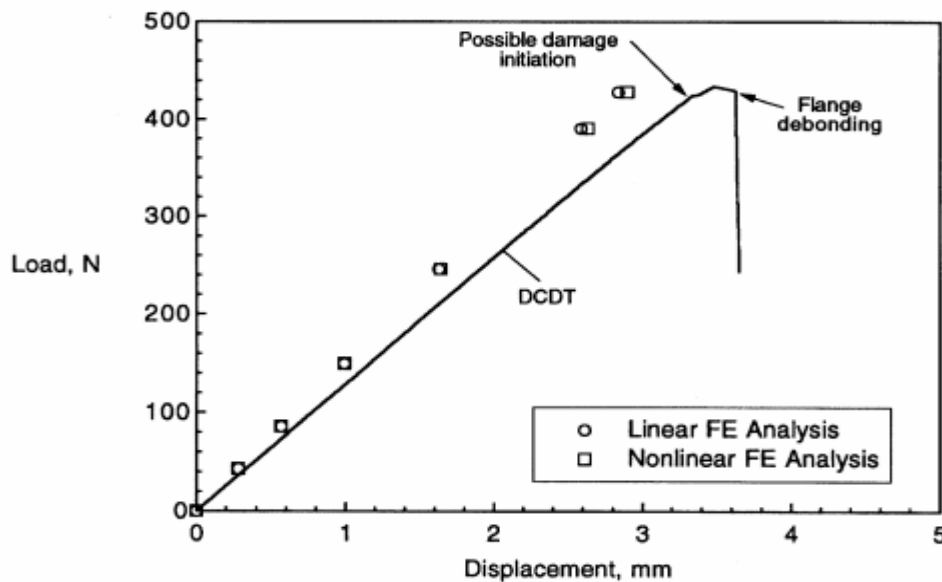


Figure 7 Load-Displacement plot for linear and Non-linear analysis [3].

2.3 Effect of Adhesive Layer in Bonded Joints

There are many advantages of using an adhesive film rather than conventional methods such as mechanical fastening, welding, and bolting. For example, in the case of mechanical fastening it is seen that the stress concentration around the bolts increase, and initiates crack which

is avoided using adhesive joints. From the study of Kinloch et al. [7] the joint durability of the specimen was examined using linear-elastic fracture mechanics. The fracture behavior is being investigated over high displacement rates during the experiment. The adhesive layer used between the skin-stringer specimen was a hot-curing rubber toughened epoxy adhesive. Before bonding the specimens, the adhesive layer was cleaned using acetone and then cured for bonding. To prepare the defect sample a thin layer of silicon substance was applied on the adhesive layer to form an initial crack. The adhesive was cured at 130C and cooled at room temperature. Sample were tested in Mode I loading in two different environment such as dry with 55% of humidity and wet (immersed in water).

It was observed three different crack propagation behaviors were present and were named region I, region II, and region III. The region I crack occurred at low displacement rates and was stable till it reached fracture. The crack growth was stable throughout the adhesive layer. For region III, the crack growth was at high velocity and failure was cohesive in the adhesive layer and region II was the transition of the crack propagation from region I to region III. Results show that testing in dry condition with 55% humidity the crack growth rate was not dependent with the fracture energy but in wet condition they were constant which indicated that the adhesive joints have better efficiency in humidity conditions than immersed in water.

Another research of J.A.B.P. Neto et al. [8] carried out experiments with ductile and brittle adhesives to predict the failure loads using several analytical and numerical methods. The study using brittle adhesive (AV138) and ductile adhesive (Silkforce 7888) were tested experimentally and compared with the numerical results (Figure 8 & 9). The numerical model of the specimen is built using FEM and the finer mesh is generated near the interface of the skin and stringer because

the smaller region is said to experience major peel and high shear peak stresses. The purpose to use small size mesh is to monitor the displacement and stress variations.

Experimental results show that using a brittle adhesive in the bonding process has a cohesive failure in the adhesive and then progresses to the interlaminar failure of the specimen. It is also seen that the maximum peak load for the sample is very low and the adhesive ability to withstand the load is very poor. The ductile adhesive is proved to reach the full shear strength capacity during the experiment and fails at a higher maximum load when compared with the brittle adhesive. The failure load for the specimen using a ductile adhesive depends on the strength of the adhesive and the length of the skin-stringer overlap so when the overlap/bonded length increases the failure load increases and the failure load of the brittle adhesive solely depends on the strength of the composite.

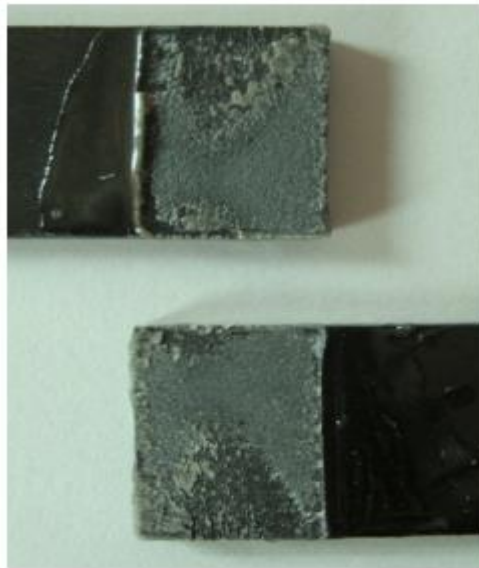


Figure 8 Adhesive AV138 specimen [8].

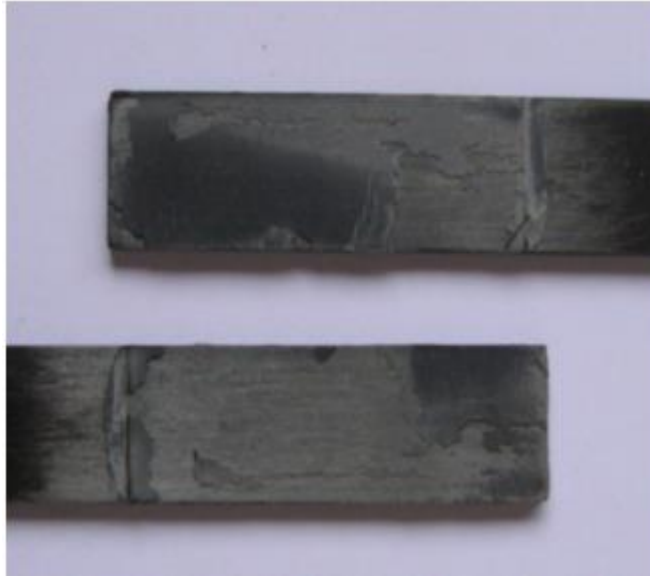


Figure 9 Adhesive silkforce 7888 specimen [8].

The load-displacement plots show the difference in the strength of the brittle and ductile adhesives and the failure loads of the specimen, respectively (Figure 10). The squares black in color denote the Sikaforce7888 adhesive and the black dots denote the LAV138 adhesive. The L_o in the figure 10 denotes the length of the bonded region in the plate. The difference in linear curve shows the efficiency of skin-stringer specimen using two different adhesives.

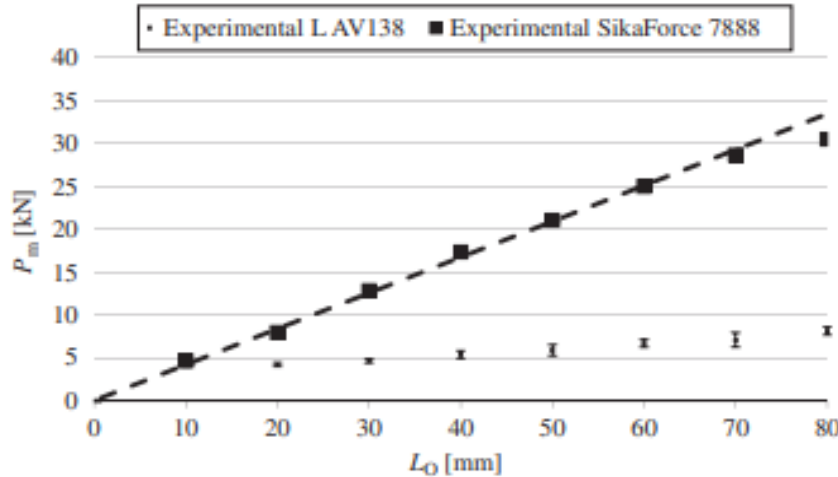


Figure 10 Load-Displacement plot for brittle and ductile adhesives [8].

2.4 Effect of Tufting on Skin/Stringer Panels

The frequent failure in the skin-stringer specimen is seen to be the disbonding/delamination which needs to be repaired for high strength and stiffness. If not repaired, the delamination leads to the separation of the stringer from the skin. A solution to reduce the crack propagation is to reinforce between the layers of the specimen layup. To prevent the delamination between skin and stringer and to avoid the crack propagation between the interface, different reinforcement methods are used such as tufting, selective stitching, Z-pinning. It was observed from various studies that the specimens reinforced with tufting exhibit high strength and stiffness than the specimens tested with the adhesive layer in the interface of Skin-stringer[26].

A research by James et al. [9] shows that the stitching has improved the in-plane properties of the composite structures but the tensile and compressive moduli will reduce due to the disturbed fiber network in the panel. The stitching of the specimen at the damaged area of the specimen will provide more resistance for crack initiation and propagation [10]. It is also recommended to repair the critical area to avoid the knockdown in the young's moduli of the specimen. Tufting is a process

where a single needle inserts a thread into reinforcement without tension (Figure 11). This method has been successful in resisting the crack initiation and propagation[9].

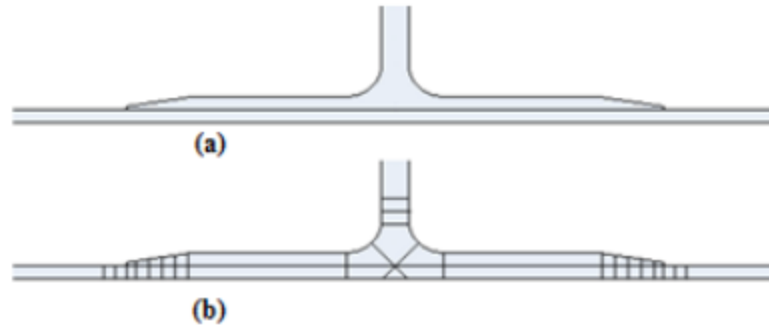


Figure 11 a) Un-tufted specimen and b) tufted reinforcement in the specimen [10].

Researchers at the National Composite Center used a Kuka robot (Figure 12) to perform the tufting reinforcement on the specimens. They used a foam covered with a low temperature vacuum bagging film below the specimen to help the needle of the robot to penetrate and to retain the tufting in the specimen.



Figure 12 Kuka robot performing the tufting reinforcement [9].

The four point bending test was performed for testing the Skin-Stringer specimens. The goal of the study was to determine the first load drop of the specimen. Untufted specimen show a low peak load before the crack propagation (Figure 13) but the tufted skin and stringer are seen to increase the stiffness of the joint and resistance to crack initiation which clearly indicates the improved damage tolerance and higher loads required [10] to initiate the crack. Inserting tufts into the specimen prevented the delamination of the skin and stringer and the increase in the peak load was 16% higher than the untufted specimen.

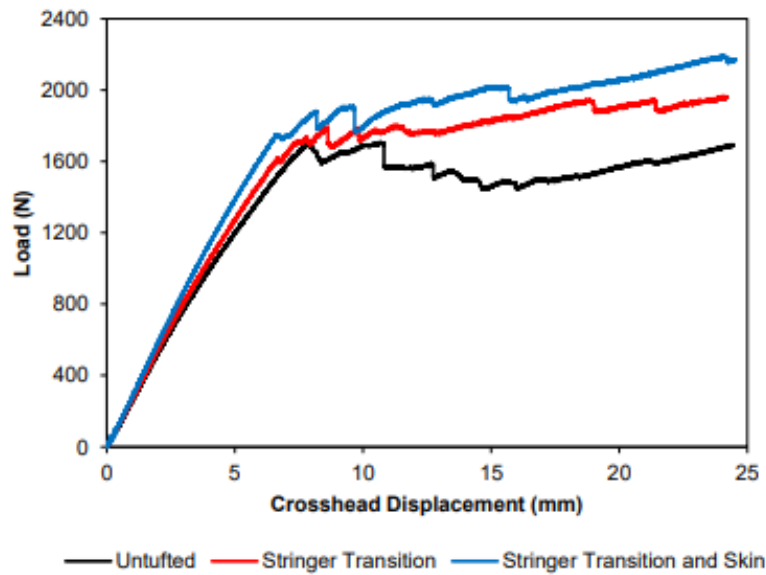


Figure 13 Load-Displacement curve of skin-stringer specimen [9].

2.4.1 Effect of Z-pining Method on Skin/Stringer Panels

The compression strength of the skin-stringer specimen made from Uni-directional carbon-fiber are lower than the tensile strength. The Z-pinning method was developed for the reinforcement of prepreg laminates. Stitching or tufting has a better efficiency for dry fabrics and Z-pinning is used in the prepregs of the material. Z-pins are made from carbon fiber and epoxy matrix which are inserted in the specimen layup and then cured in a autoclave or heat press. A study conducted by T. Kevin et al. [11] investigated the strength of the lamina with the use of Z-pins. The layup of the specimen had 24 -ply combination for both the skin and stringer and the Z-pins with diameter of 0.28mm was inserted and cured. Results show Z-pins when inserted into the prepreg of the specimen disrupted the fibers and causes reduction in the compressive strength. When the diameter of the Z-pins are large the disruption is high and reduces the strength so the study suggested that the increase in the pin density had a increase in strength and high failure loads of the specimen.

NASA research by Zhang et al. [12] developed a skin/flange specimen to investigate the effect of the Z-pin on crack propagation. The Skin and Stringer were made from carbon-fiber resin prepregs and the pins were manufactured from epoxy composites (Figure 14). Pins were inserted into the specimen in a specific grid configuration (Figure 15) in a oven which was preheated to 60 degree celcius to avoid friction while insertion of the rods.

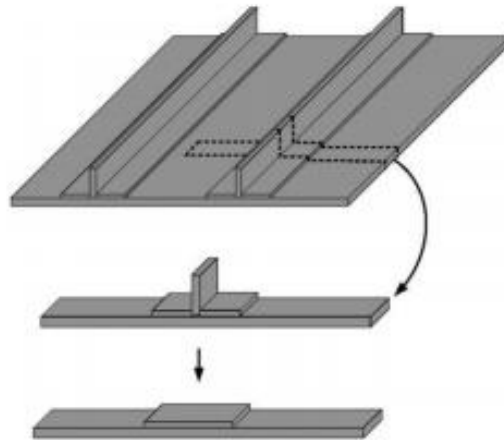


Figure 14 Simplification of skin-stringer specimen [12].

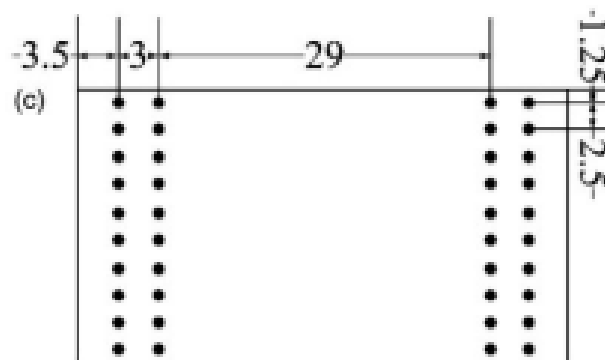


Figure 15 Grid configuration of Z-pins [12].

The results of the experiment prove that crack initiation load of the specimen is higher than the pristine sample without the reinforcement and indicates the reduction in elastic stiffness of the specimen (Figure 16). Due to reduction in the elasticity of the Skin-stringer specimen the disbonding/delamination the strength of the specimen to restrict the crack is increased upto 54.6% when compared with the pristine sample without reinforcement. The peak load for the tufted specimen was 16% but the Z-pins exhibit a high failure load or load to initiate crack which is 38% efficient that the reinforcement by tufting.

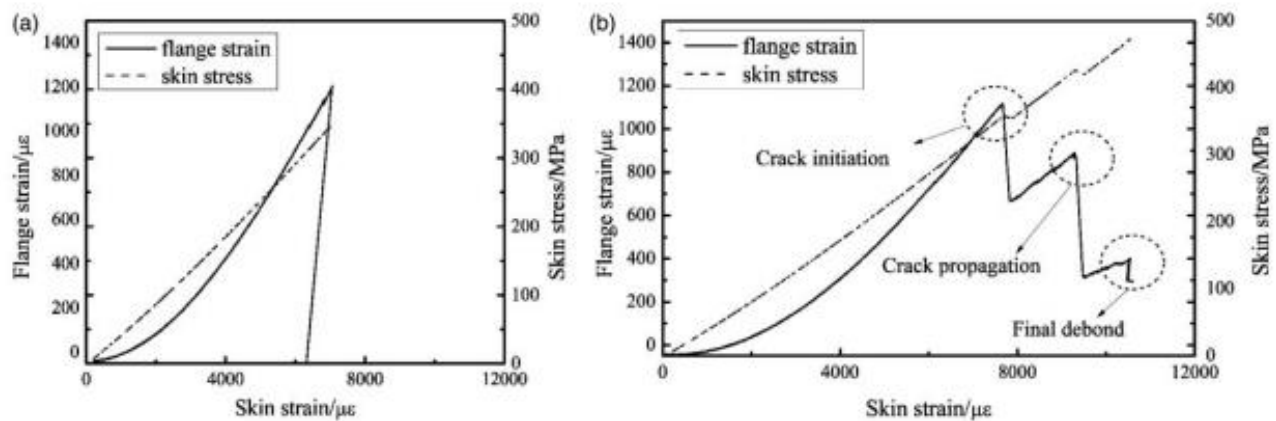


Figure 16 Stress-Strain curves for a) pristine sample and b) Z-pins inserted samples [12].

2.4.2 Effect of Welding on Bonded Plates

Welding techniques to join composite structures as a reinforcement methods was considered [13,27]. The methods to join composite parts in aerospace industries are divided into various catagories. The heat generation mechanism at the skin-stringer interface was analyzed to determine the suitable method for reinforcing the composites. A study by Dube et al. [14,28] proved that the resistance welding was efficient to join aerospace structures because of its weld quality and strength and the ease to use the technique. When the welding is performed at the

interface the material starts to soften due to the high temperature around the weld and then after the weld is completed the material is left to cool down. For the experimental part two materials such as carbon-fiber and glass fibers were used. The results of the load-displacement plot show that the carbon-fiber specimen has higher strength than the glass-fiber specimen. The carbon-fiber specimen shows a linear response until its failure loads and fractures. The glass-fiber specimen exhibited a elastic linear curve followed by a non-linear response till failure load.

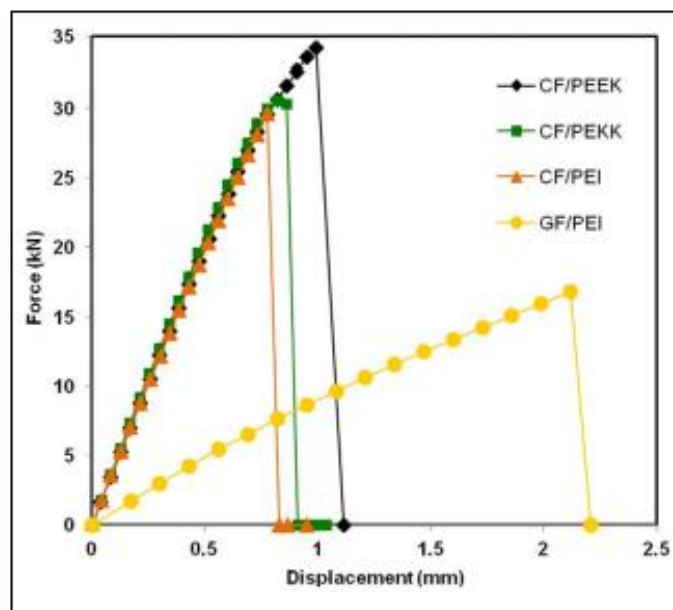


Figure 17 Load-Displacement plot for resistance welding specimens [14].

2.5 Effect Of Through Thickness Reinforcement in Laminated Composite Structures

The method of Through Thickness Reinforcement (TTR) is different from the Z-pinning and Tufting techniques. The Z-pinning is a process where the rods are driven into the specimen layup and when the rods are placed into the prepreg the fiber orientation is disturbed and the alignment of the z-pinning is difficult to control. Also, the Z-pinning reinforcement provides around 35% increase in compressive strength and the TTR in cured composite provides a

advantage to reinforce the weak area or the area of concern which will debond by drilling the holes and inserting rods of smaller diameter into it. Study by Kravchenko et al. [2] proved that the insertion of Through thickness reinforcement (TTR) on post-cured Skin-Stringer specimens improves the strength without the fiber damage. To investigate the strength of the specimen pristine and defect samples were fabricated. To understand the effect of Through Thickness Reinforcement (TTR) one defect sample had TTR placed in the undamaged zone and another sample had TTR in the start of the delamination zone (Figure 18)

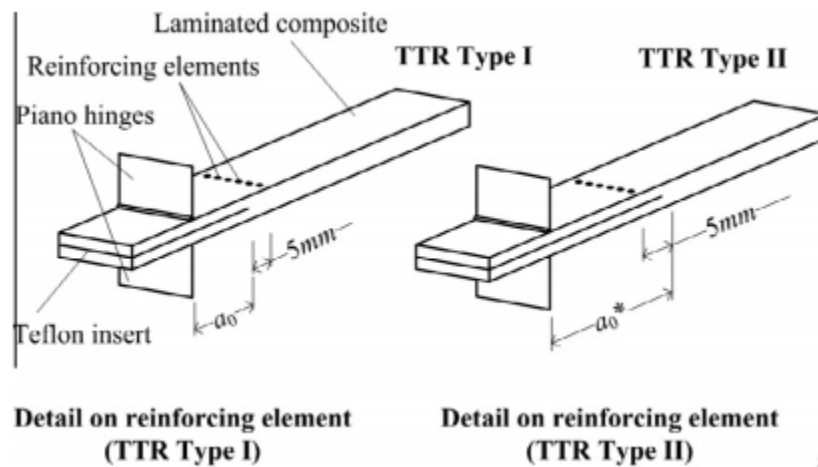


Figure 18 Defect specimens with TTR [2]

The type I TTR configuration with pin inserted in the undamaged zone is seen to be higher than the Z-pin specimens. There was a first load drop because of the crack initiation and then the failure load was obtained. From the results of the TTR specimen Type II, the pins were placed in the delamination zone, the crack propagation was prevented and had increased strength and stiffness. The strength of the Type II specimen was observed to be twice as the pristine sample and no delamination growth was observed until the fracture load was reached. So comparing with Z-

pins methodology it was seen that damage behavior of the specimen changed with respect to the position of the TTR pins inserted in the specimens.

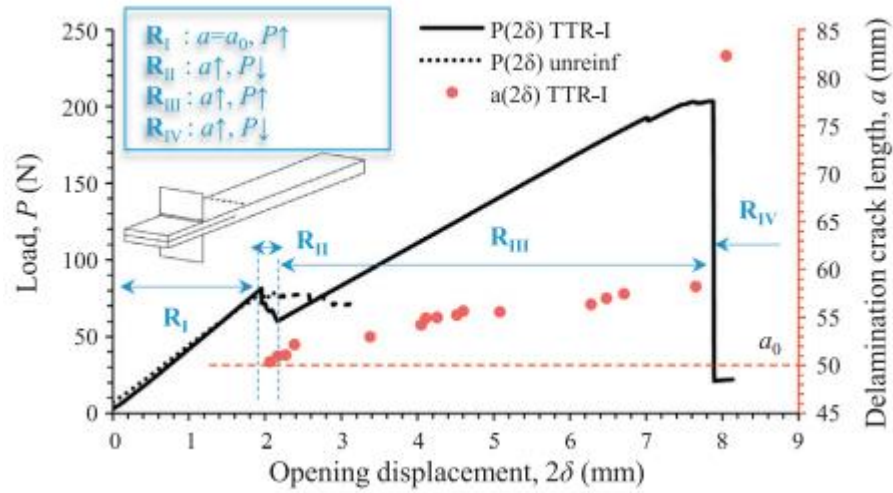


Figure 19 Specimen with TTR positioned in the undamaged area [2].

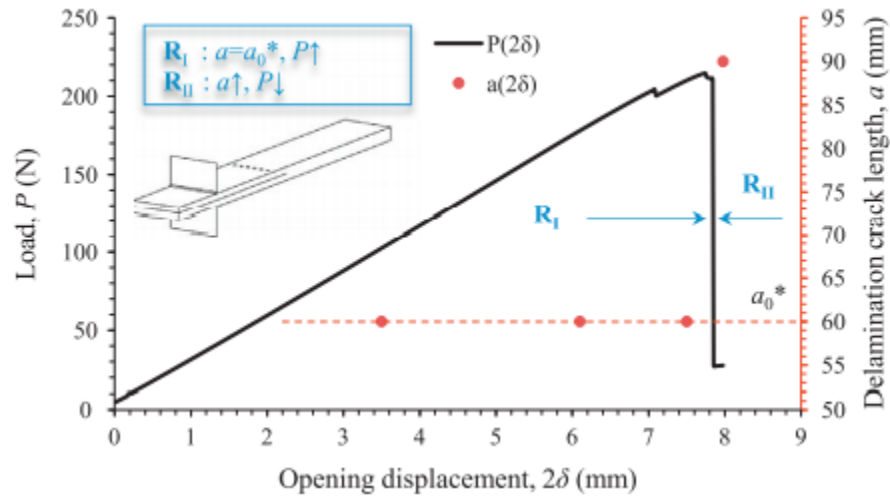


Figure 20 Specimen with TTR positioned in delamination area [2].

Another study by Kravchenko et al. on the effect of aspect ratio on the strength of Skin-Stringer specimens was investigated [15]. The aspect ratio is defined as the ratio of length to diameter of the rods inserted for reinforcement. It was seen there are two ways to improve the aspect ratio 1) By increasing the laminate thickness and 2) decrease the size of the rods. From the results of the experiments it was proved that increase in aspect ratio, increases the strength of the material and arrests the delamination in the interface of the Skin-Stringer specimen.

For lower aspect ratio rods the fracture load was higher than the load of a pristine sample, so the delamination resistance depends on the aspect ratio of the rods used in TTR. Increasing the aspect ratio increases the strength of the specimen and the fracture resistance.

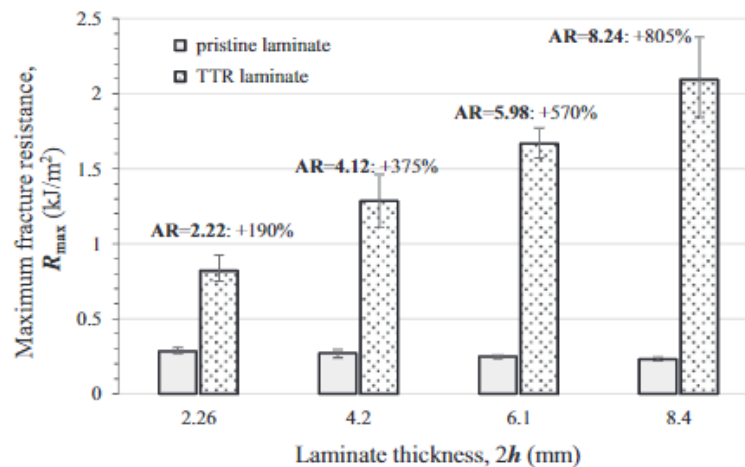


Figure 21 Aspect ratio of rods used for TTR in specimens [15].

CHAPTER 3

METHODOLOGY

This research is focused on improving the stiffness and the strength of the Skin-Stringer specimen made from carbon fiber. The through thickness reinforcement is used to improve the efficiency of the composite. The holes are drilled in the post-cured Skin-Stringer specimen and then rods are inserted in the thickness direction. The other important goal of this study is to investigate the efficiency of TTR by using two different spacings of the through thickness reinforcement (TTR) installed in the specimen. For the experimental part samples are fabricated in two types using carbon fiber prepreg. The two types are 1) Pristine and 2) defect sample. The Skin-Stringer specimens have different layup configurations, and they are cured separately using a heat press. After curing them an adhesive layer is used between the Skin-Stringer to complete the bonding. The Pristine specimen is fabricated without any defect and the defect sample is fabricated by inserting a Teflon defect under the adhesive layer and the specimen is bonded. The Teflon insert placed under the adhesive serves as an initial crack in the specimen. The experimental tests are carried out using Three-Point bending and Tensile test. Load -Displacement plots of the pristine and defect samples are observed [30](Figure 22).



Figure 22 Tensile and Flexural tests setup for skin-stringer specimen.

Digital Image Correlation (DIC) is a method used to track the surface changes of the specimen during the flexural and tensile tests. The Digital Image Correlation (DIC) is used during the testing of the Skin-Stringer specimens to understand the measurement of strain at the point of crack initiation and crack propagation until fracture of the sample.

Ultrasonic scanning equipment provided by omni scan are used to investigate the Skin-Stringer specimen after experiments. This Non-Destructive testing method (NDT) is performed by scanning the samples with a sensor which emits signals back and forth through the sample with a help of a medium such as water or gel. This Non-Destructive Testing method (NDT) is used to determine the location and the size of the defects in the specimens.

3.1 Fabrication of Skin-Stringer Specimen

The use of composites in aerospace sectors are increasing because of its compatibility and material properties. The carbon fiber provides several advantages such as light weight due to high strength and stiffness, fatigue resistance and corrosion resistance, capability to fabricate large shapes in less time. In this study the unidirectional carbon fiber prepreg fabric made by fiberglass (Figure 23) is used to fabricate the specimens. The specimens are prepared by the hand layup process and then cured in the heat press.

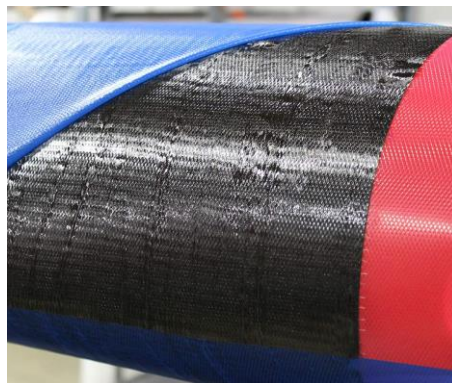


Figure 23 Unidirectional carbon fiber prepreg fabric.

The stacking sequence of the skin and stringer were different. The skin laminate had a configuration of $[0_2/90_2/0_2/90_2]_s$. The unidirectional prepreg fabric was cut in 10" x 10" dimensions for each ply and a total of 16 plies in the above-mentioned layup orientation was fabricated. The stringer panel was fabricated using the unidirectional carbon fiber prepreg with a following layup $[0/90/0/90]_s$. Each ply of the stringer specimen was cut into 10" x 2.75" and a total of 8 piles were laid up to fabricate the stringer specimen. The layup process was carried out in a plate where a release film was first placed on it and then each ply was laid up on the release film. After laying each ply the roller was used on the surface to remove the trapped air bubbles [16, 19] from the ply. Vacuum bagging for both the skin and stringer was done separately and cured. While performing the vacuum bagging for the Stringer specimen a few extra layers of breather film was added on top to provide uniform pressure on the top surface as the dimensions were smaller compared to the skin specimen.



Figure 24 Vacuum bagging of the skin-stringer laminate

3.2 Curing Process of the Prepreg Fabric

Composites are generally cured by autoclaving but in this study a different method called the Thermal Press Curing (TPC) is suggested [17]. The thermal press curing (TPC) is a process where the prepreg layup is placed between two pre-heated plates at constant temperature and pressure for a particular duration. The “caul plate” a plate placed on top of the vacuum bagging plate was used to provide uniform pressure over the surface of the specimen. The curing cycle for the Skin and stringer was similar.



Figure 25 Wabash Heat Press

The Wabash heat press with 75 metric ton capacity was used for curing the skin/stringer laminate (Figure 25). The curing process consisted of two stages: 1) the first stage of the curing process was set to 80 C at 15 psi for 120 minutes. 2) the second stage was set to 129C at 80 psi for 150 minutes. Once the curing of both the skin and stringer is completed, the edges of the surface were cut with water jet so that the bonding of the skin and stringer is performed evenly throughout the interface.



Figure 26 Skin laminate after curing.



Figure 27 Stringer laminate

3.3 Bonding Process of Skin-Stringer Panels

After the post curing of the Skin and Stringer separately (Figure 26 & 27) the bonding of the specimen is carried out. To bond them the surfaces of the skin and stringer are rubbed with sandpaper gently and then cleaned with acetone. The bonding of the specimens is performed with the help of Locitite 9696 Aero, an epoxy adhesive film which is placed in the interface of the skin and stringer. For obtaining the pristine samples only the adhesive layer was inserted in between the skin and stringer. To fabricate defect samples an initial Teflon inert of the dimensions 0.25” inches were placed under the epoxy adhesive film to provide an initial crack in the specimen. The curing cycle for the bonding is performed in heat press at two stages: 1) First stage is set to 80C at 0 psi for 90 minutes, 2) Second stage is set to 129C at 0 psi for 240 minutes. After post curing the samples were cut using water jet provided by Protomax (Figure 28) from the plate (Figure 29) to obtain the skin-stringer specimen.



Figure 28 Protomax Waterjet

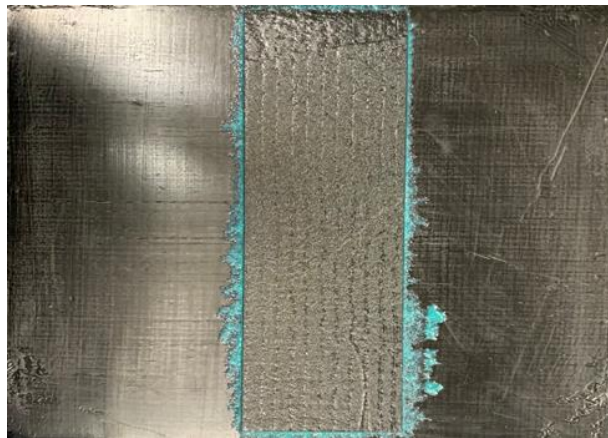


Figure 29 Completely cured skin-stringer plate

3.4 Installation of Through Thickness Reinforcement (TTR)

To Install the Through Thickness Reinforcement (TTR) in both pristine and defect samples a specific configuration of drilling using a Dremel equipment was performed on the samples. The configuration was chosen to avoid the crack propagation during the three-point bending and tensile

tests. To avoid the growth of initial defect in the defect samples the TTR was inserted very near to the edge of the skin and stringer specimen.

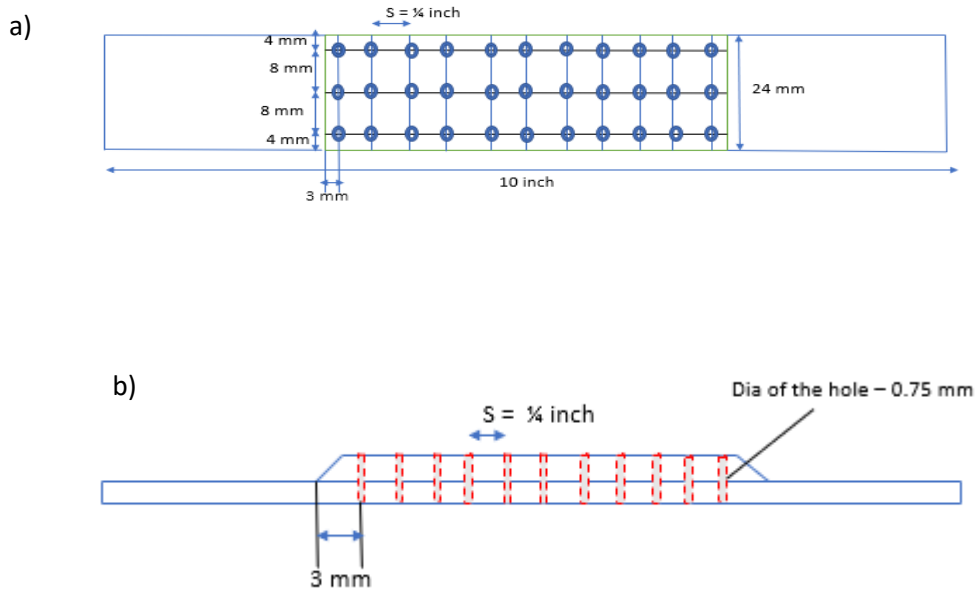


Figure 30 a) Top view and b) Side view of the TTR configuration with $\frac{1}{4}$ inch spacing, c) dremel equipment, and d) sawyer robot drilling machine.

The first row of the TTR starts at 3mm from the edge of the skin-stringer to the center of the hole to avoid the crack propagation as in Figure 30(a). The dimensions of the TTR are measured from center to center of each hole that is being drilled in the sample. The through thickness reinforcement (TTR) is performed for two different spacing (S) mentioned in the Figure 30 (a & b) along the length direction: 1) $\frac{1}{2}$ inch and 2) $\frac{1}{4}$ inch and the diameter of the drilled hole in the sample is 0.75 mm.

The drilling was carried out using the Dremel equipment with electroplated diamond drill bits. After completion, the carbon rods were inserted in the specimen for increasing the strength and stiffness [2]. The round pultruded carbon rods used for TTR was manufactured by Rock West

composites with a diameter of 0.019 inches. To insert and bond the TTR into the specimen an epoxy resin and hardener was used.

The drilling of the holes was also carried out with the help of sawyer robot from rethink robotics [18] (Figure 30(d)). The drilling operation was performed by specifying the grid configuration and the speed of the drill into the system which eases the complexity and increases the accuracy in drilling each hole in the exact position. The drilling with the Dremel equipment was a bit complex because the schematics was done on the sample by hand and then the holes were drilled.



Fig 30. (c) Dremel drilling equipment



(d) Robotic drilling equipment [18]

The Epoxy resin used for bonding the carbon rods are INF-114 and INF-211. The epoxy resin and hardener were mixed in a ratio of 3:1 (Epoxy Resin: Hardener) and the rods were dipped into the mixture and inserted into the holes.

Once the rods are inserted into the holes a little amount of resin is poured into the holes to make the bonding of the rods intact within the sample. A Teflon tape was used on the back surface of the Skin to avoid the resin flow out of the sample. Thus, this made sure that the resin stayed inside each hole and the carbon rods were cured to finish the Through Thickness Reinforcement process (TTR)[19].



Figure 31 Epoxy Resin and Hardener.



Figure 32 TTR installed skin-stringer sample

The samples are cured in the room temperature for more than 8 hours after the through thickness reinforcement (TTR) is installed. Once the curing is completed the extra portion of the rods pointing outwards the sample are cut and filed to obtain an even finish on the skin surface. The uneven surface may cause stress concentrations and affect the experimental results, so the surface is filed after the TTR installation.

3.5 Fabrication of Skin-Stringer Specimens for Tensile Test

For the tensile test unlike three-point bending the specimens need to have grips at both the ends to avoid slipping during the experiment. The grips used to attach at the ends are made from fiber glass. The required amount of grip is cut with the help of water jet and then it is cleaned with acetone. To bond the grips tightly, the ends of the sample and the grips are being rubbed with sandpaper. An epoxy glue is used to bond the grips to the sample, it is important to evenly spread the glue so that the grips are bonded in line with the sample. After the epoxy is applied, clippers are used on both the ends of the specimen and left to cure in room temperature for 10 hours (Figure 33). Once the bonding is completed the specimens are mounted to the MTS machine for testing.



Figure 33 Tabs bonding to the skin-stringer specimen.

3.6 Ultrasonic Scanning using Omniscan

The Ultrasonic scanning is a Non-Destructive Testing technique which is used in evaluation of cracks in airplanes after certain life cycles. The test is performed mostly in aviation sectors to determine the damage in parts of aircrafts. The Omniscan Ultrasonic scanner device is used in this study to investigate the crack/delamination in the interface of the skin-stringer specimen after the three-point bending and tensile tests.

The Ultrasonic scanner is calibrated to determine the location and size of the crack in the specimen.

The following steps are being followed to get the desired output:

Step 1: The Omniscan power is switched on and the software MX4.4 version is selected to obtain the working interface which shows a split screen of A-Scan, C-Scan and S-Scan (Figure 34)

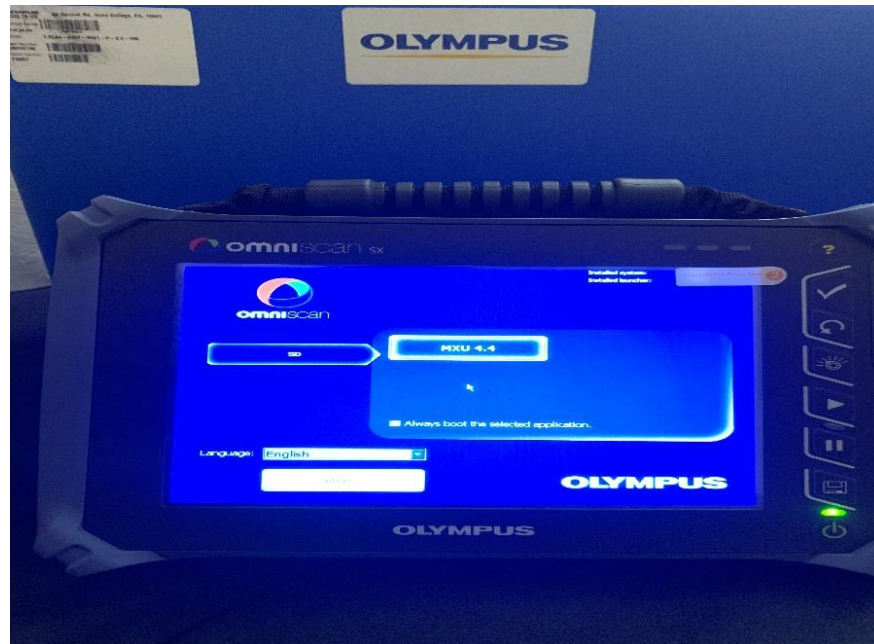


Figure 34 Interface of the Omniscan.

Step 2: Select the file option towards the left and click wizard option, this option opens the setup panel which is used to specify the settings for the Skin-Stringer specimens and has sub options such as Part & Weld, setup, and calibration under it.

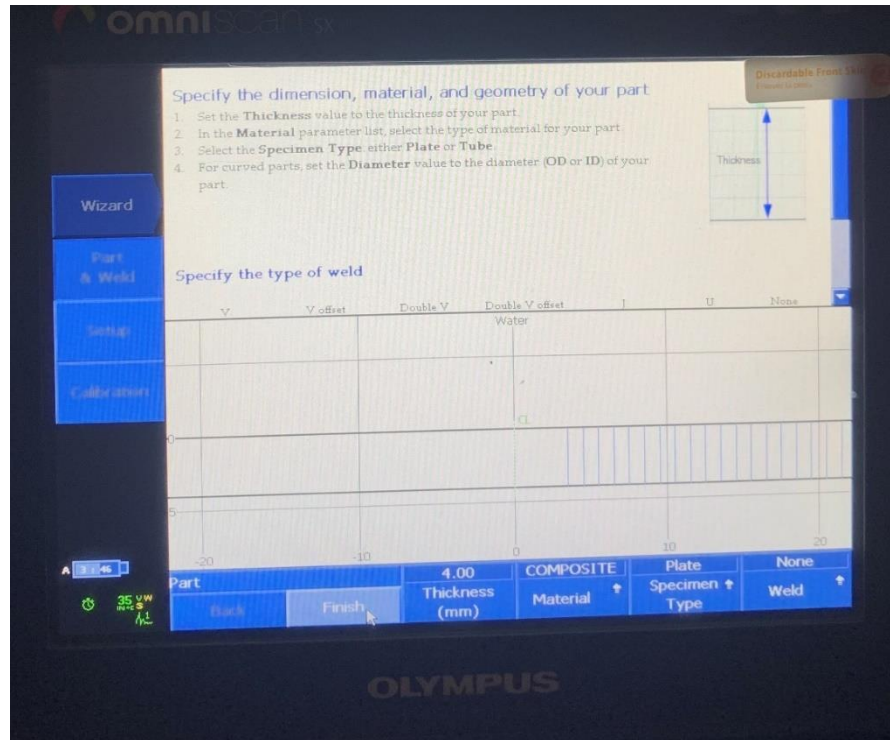


Figure 35 Part & Weld screen of Omniscan.

Step 3: Once the set-up screen is opened the dropdown menu on the left will have four options such as Part & Weld, Setup and Calibration.

Step 4: The Specimens are scanned using the probe which emits signals through the sample and collects the data of the defects present in them. The probe is connected to the Omniscan in the port located on top right corner.

Step 5: Select the Part & Weld option and click start at the bottom. In this step the thickness of the specimen, the material and the specimen type should be entered in the respective field and click finish (Figure 35). An extra 0.5 mm is specified above the original thickness so that the ultrasonic scanner detects the back wall of the sample.

Step 6: After the Part & Weld, select the setup option. In this option the probe type is automatically recognized by the Omniscan and then wedge type is selected as water (Figure 36)

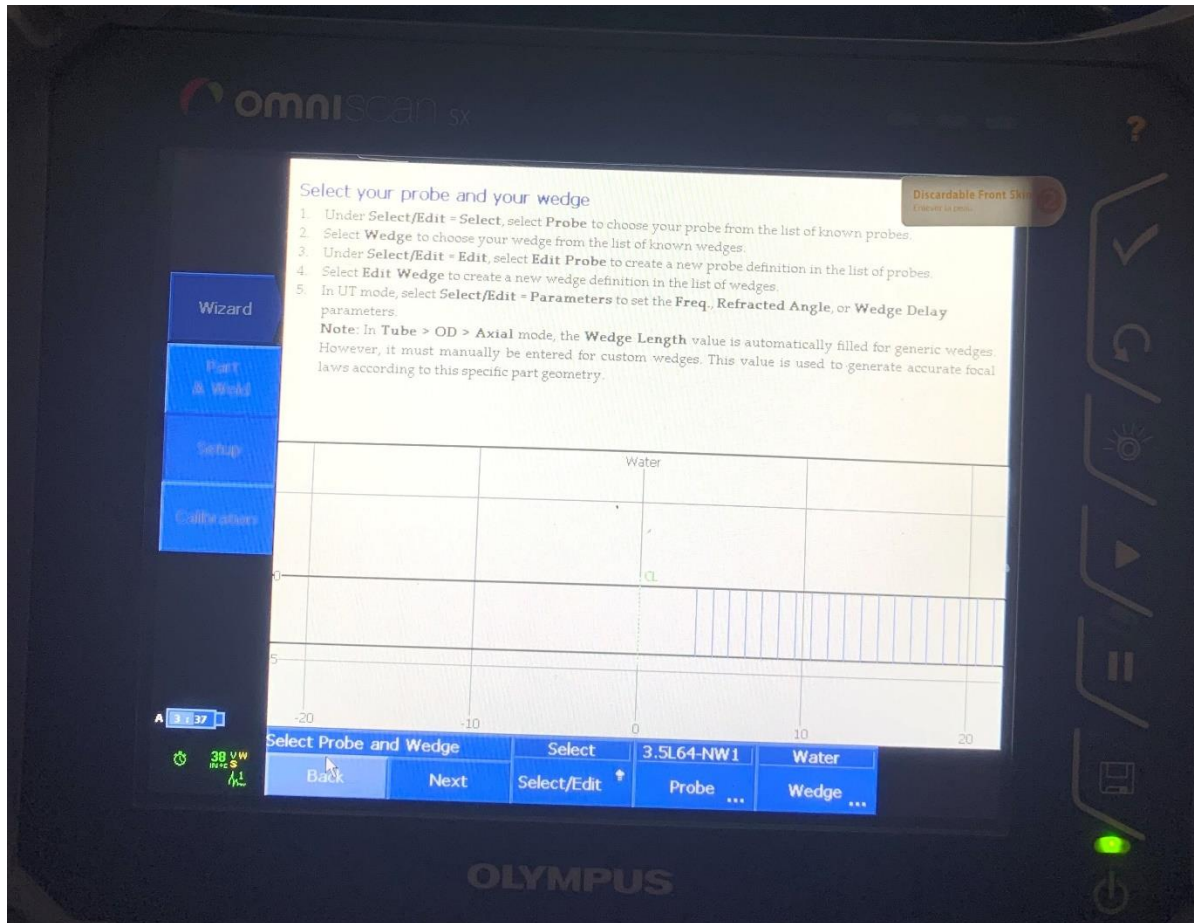


Figure 36 Setup screen of the Omniscan Sx.

Then click next to verify the number of elements the probe uses to scan the specimen (which should be specified as 64) and click the generate button to complete the set up (Figure 37).

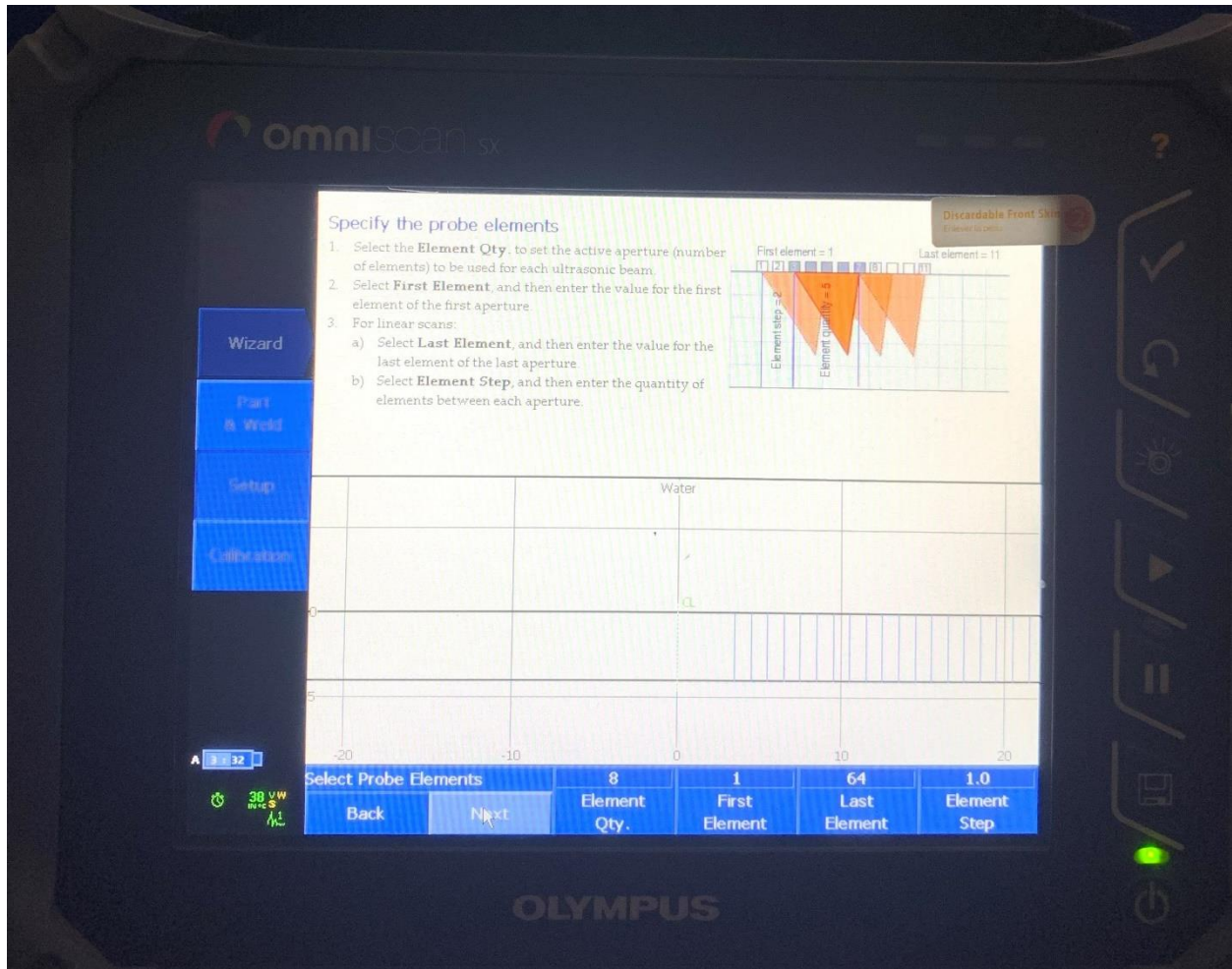
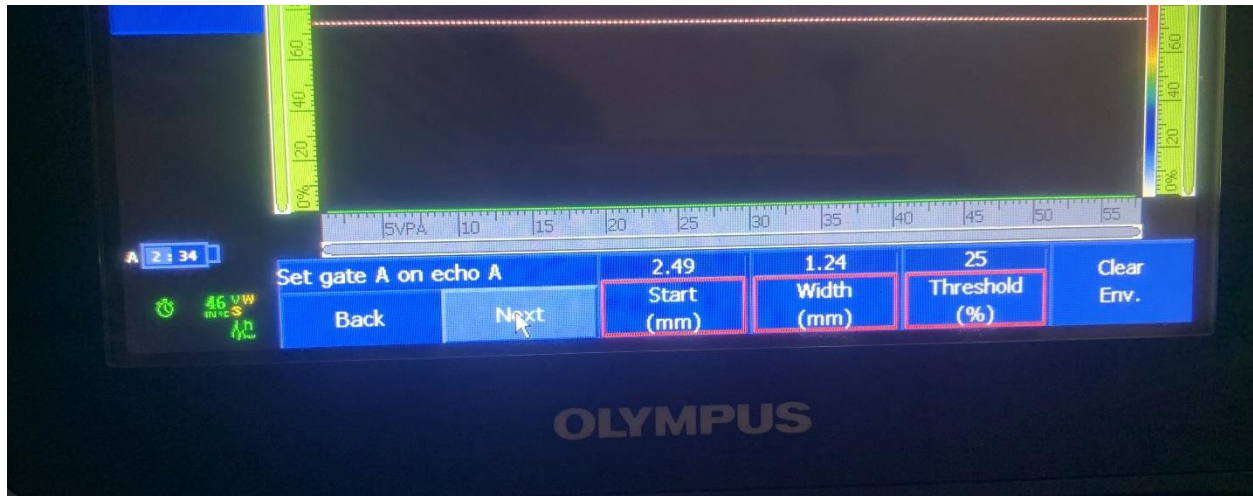


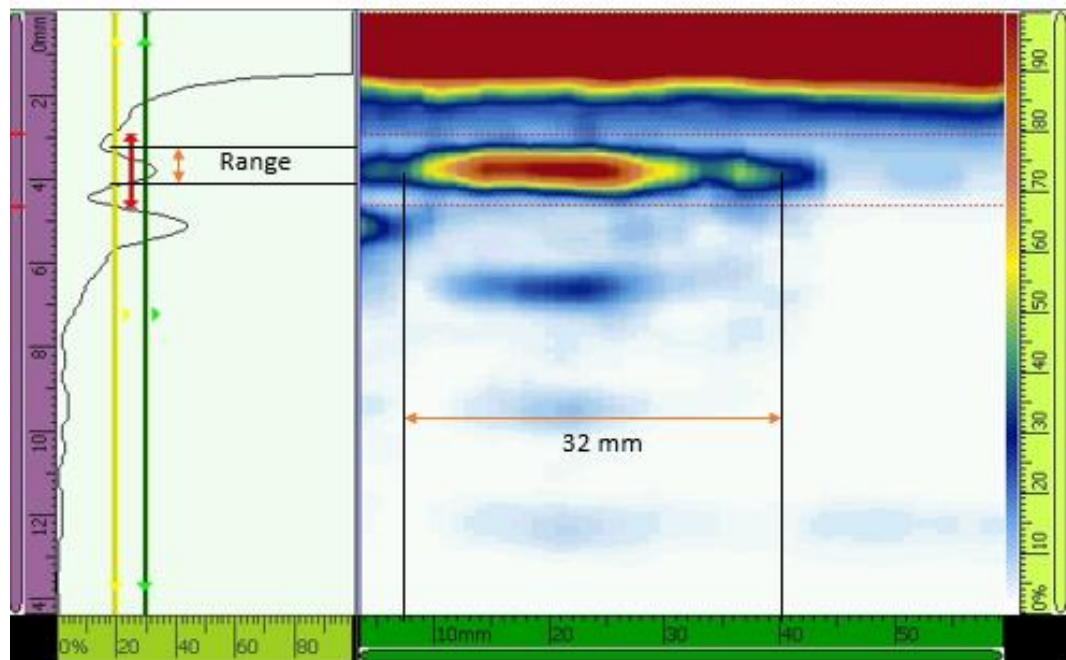
Figure 37 Confirmation screen for checking the probe elements.

Step 7: Now the calibration option is selected (Figure 38(a)). The medium used for scanning the sample is water, so a small amount of water is poured on the sample and the probe is moved through the sample. The reference amplitude for scanning should be specified at around 80%. After that click next twice, the set gate A option appears on the screen. In this option the probe is kept at the top of the stringer and the signal is received by the system. Once the signal is received, the start point (the red line) value and the width values of the signal detected by the probe are specified. For example, in the figure 38 (b) below: a pristine sample without TTR is shown for better understanding.

a)



b)



To understand the setting of Gate A sample figure 38(b) is presented. The left side is the A-scan where the signals are seen while scanning the sample. To set the Gate A, the probe is moved through the sample and a signal is received. The red line on the screen should be adjusted in such a way that it should start from the start point of the signal and end with respect to the end point of the signal. In the above the image the red line starts at 2.5mm and ends at 4.3 mm which covers

the total range of the signal received. The important role of setting the Gate A is to predict the position of the defects present when the sample is scanned. The total thickness of the pristine sample is around 3.9 mm and the Gate A is set on 2.5 mm to 4.3 mm which means that the crack in the sample is present in between the specified thickness range. The red color on the top of the screen represents the top surface of the sample that is scanned and the pattern that appears in between the two red lines is the size and length of the defect present in the sample. In Figure 38(c) the transducer is placed on the edge of the pristine skin/stringer to capture the delamination.



Figure 38 a) Calibration for scanning the specimens b) Example of setting Gate A thickness of pristine sample c) Image of the transducer scanning the sample with water as scanning gel.

3.9 Simulation of Skin/Stringer Sample Using Finite Element Analysis

The Skin/Stringer sample are modeled using the ABAQUS software. The modeling is done using same properties of the sample that were tested in three-point bending. The Skin was modeled with the configuration of [0/0/90/90/0/0/90/90]s. A total of 16 plies have been modelled with the

above configuration shown in figure 39 and figure 40. The thickness of the skin is 2.44mm. The mechanical properties used for the skin/stringer part is $E_1 = 143000 \text{ Mpa}$, $E_2 = E_3 = 8000 \text{ Mpa}$, $G_{12} = G_{13} = 3000 \text{ Mpa}$, $G_{23} = 2758 \text{ Mpa}$, $\nu_{12} = \nu_{13} = 0.32$, $\nu_{23} = 0.45$. These material properties were used for both the skin and stringer specimen. The roller used in the modelling is assigned as a rigid body and no material properties are assigned to all the three rollers.

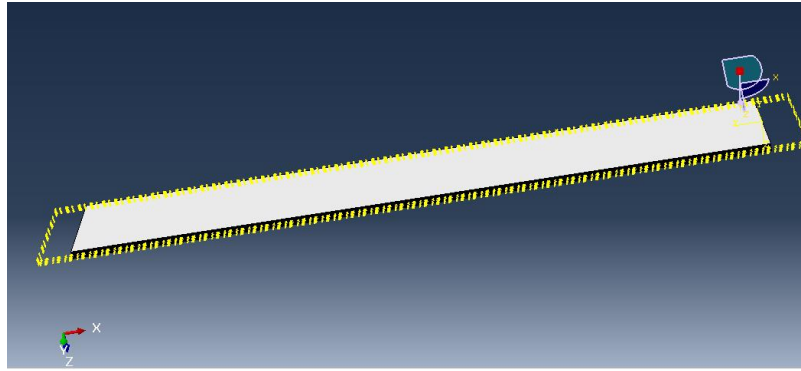


Figure 39 Modeled Skin Surface.

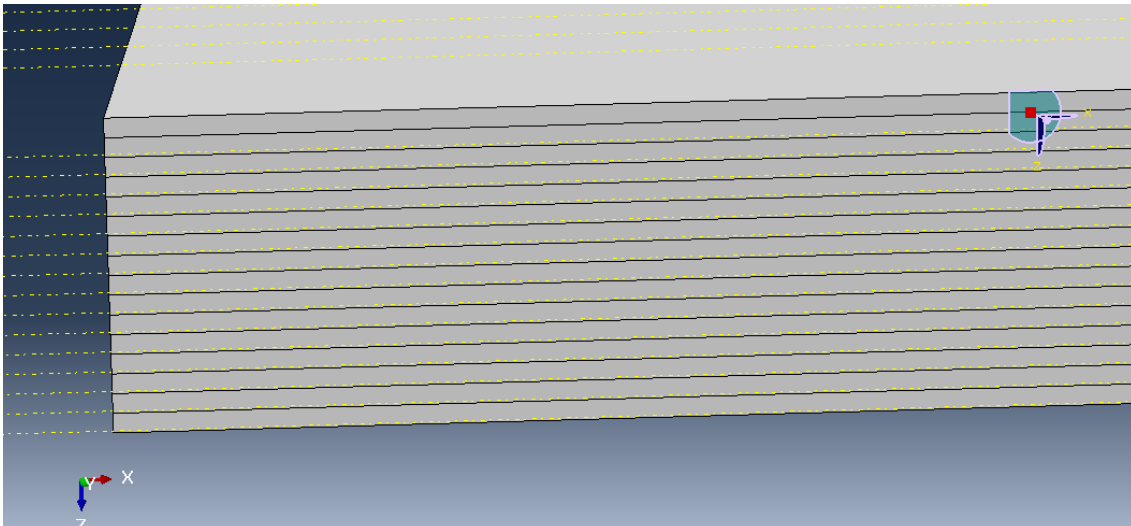


Figure 40 Partitioned Layers of Skin Specimen

The Stringer part is also modeled (Figure 41 & 42) in a similar manner of the skin with different layup configuration. The ply configuration is $[0/90/0/90]_s$. The dimension of the sample is 2.75-inch x 1 inch, thickness of the stringer is 1.22 mm. The sample is partitioned by 8 plies.

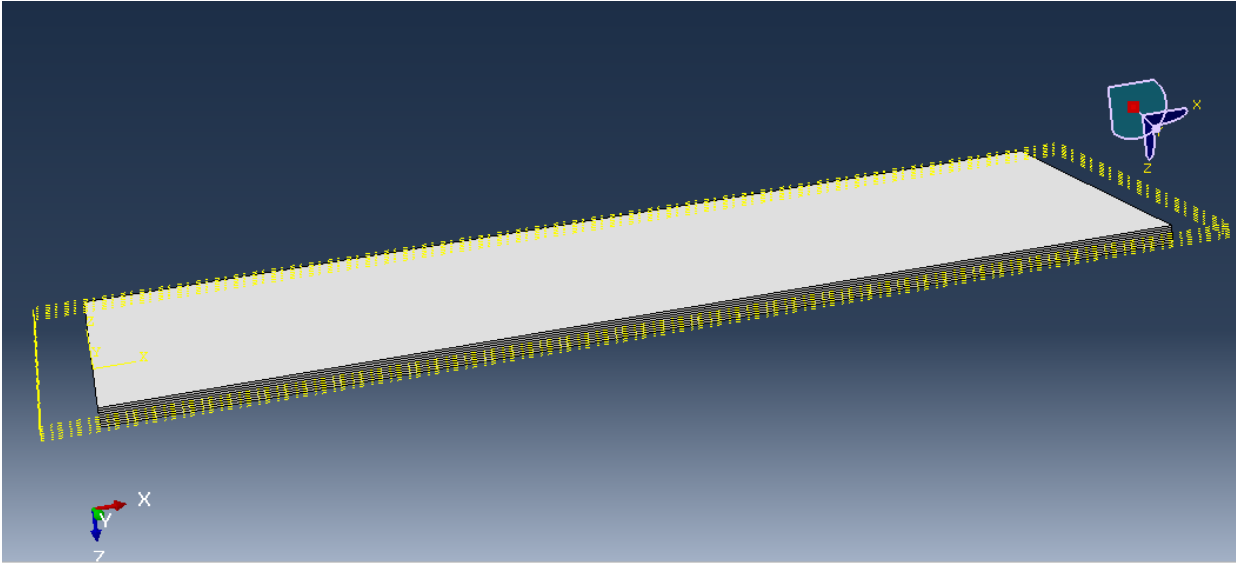


Figure 41 Modeled Stringer Specimen.

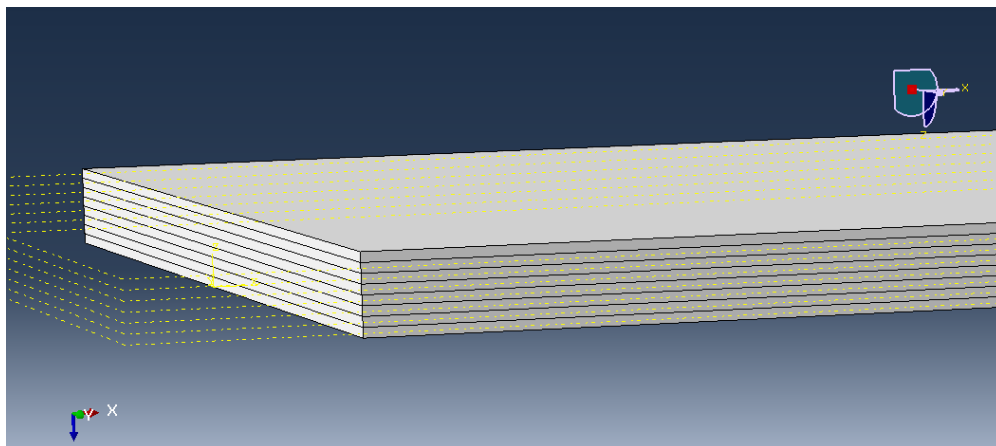


Figure 42 Partitioned Layers of Stringer Specimen

The adhesive layer in the skin-stringer specimen used in the interface for the bonding purpose is also modelled with help of cohesive elements. The cohesive elements in ABAQUS acts as a layer of adhesive between the skin/stringer. The dimension of the element is 2.75 in x 1 inch and the thickness is 0.001mm. The properties and the model of the cohesive elements are shown in Figure 43 and Figure 44.

Damage Evolution

Type: Energy

Softening: Linear

Degradation: Maximum

Mixed mode behavior: BK

Mode mix ratio: Energy

☒ Power 2.1

☐ Use temperature-dependent data

Number of field variables: 0

Data

	Normal Mode Fracture Energy	Shear Mode Fracture Energy First Direction	Shear Mode Fracture Energy Second Direction
1	0.24	0.74	0.74

OK Cancel

Figure 43 Properties of the Cohesive Elements

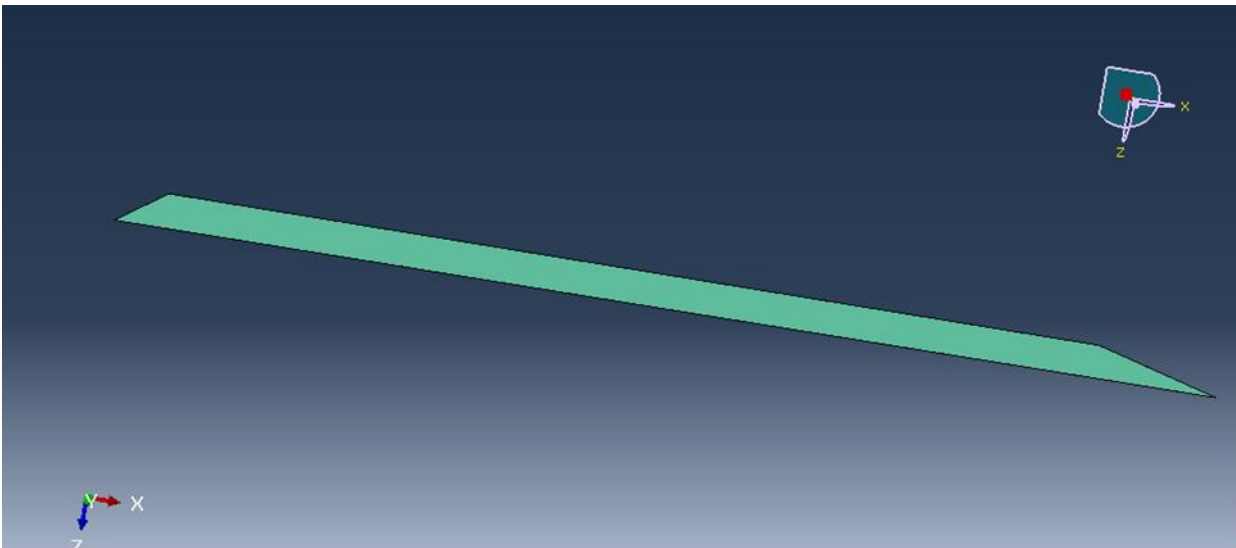


Figure 44 ABAQUS modelling of cohesive element.

The layup of the plies for both the skin and stringer was done by hand and the stacking sequence was followed. For modelling them in Abaqus the material orientation option was used. In the material orientation option, the orientation of each ply in the skin/stringer part was specified. The

datum axis was also created, and the angle of each ply was mentioned in the software. The orientation of the plies is shown in the figure below.

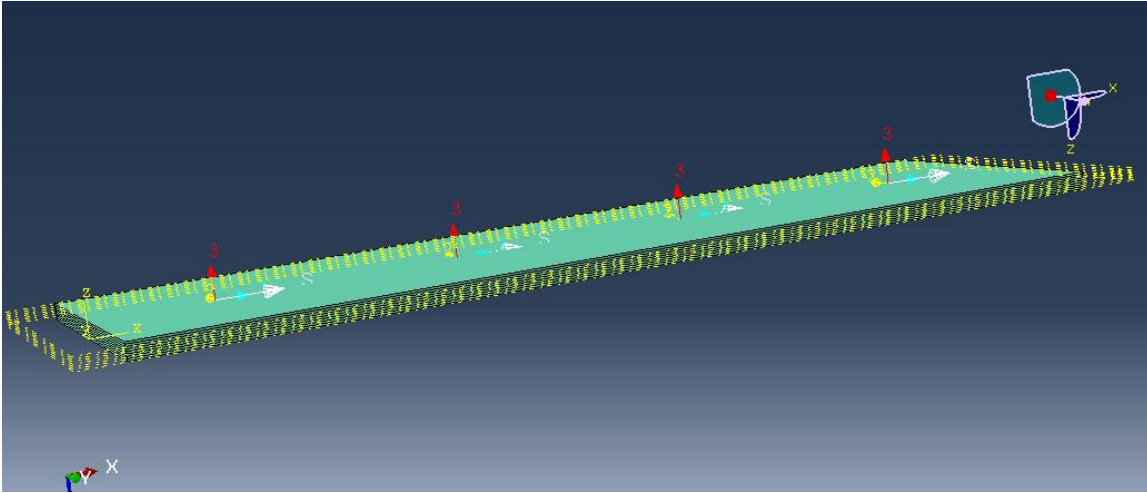




Figure 45 Orientation of the plies in Skin/Stringer Specimen.




Certain constraints and boundary condition were also specified to the model. The boundary condition was specified to restrict motion at the edge of the specimen in all directions. The purpose of the constraints is to restrict the slipping or movement of parts when the simulation is carried out. The boundary condition Encastre is used at the edges of the sample to restrict the rotational motion during the simulation. For example, a tie constraint has been assigned between the upper part of the cohesive layer and the lower part of the skin so that when the bending takes place the cohesive layer between the skin and stringer does not move and acts as an adhesive layer. The same constraint is specified for the rollers so that it does not penetrate the sample. An interaction known as surface-to-surface contact was used to the top roller which also avoids the penetration into the specimen. The interaction condition and boundary condition are shown in the figure below.

Name: Int-1


Type: Surface-to-surface contact (Standard)

Step: Step-1 (Static, General)

 Master surface: (Picked) 

 Slave surface: (Picked)  

Sliding formulation: ☒ Finite sliding ☐ Small sliding

Discretization method: Surface to surface 

☐ Exclude shell/membrane element thickness

Degree of smoothing for master surface: 0.2

Use supplementary contact points: ☒ Selectively ☐ Never ☐ Always

Contact tracking: ☒ Two configurations (path) ☐ Single configuration (state)

Slave Adjustment Surface Smoothing Clearance Bonding

☒ No adjustment

☐ Adjust only to remove overclosure

☐ Specify tolerance for adjustment zone: 0


☐ Adjust slave nodes in set: 

Figure 46 Interactions Settings Used for Skin/Stringer Sample.

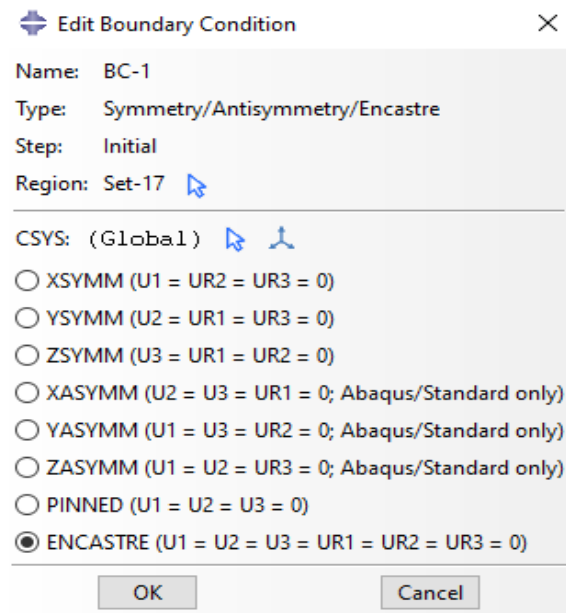


Figure 47 Boundary conditions of the Skin/Stringer Sample

After the conditions are specified the meshing of the assembly is carried out and then the job is submitted for the simulation. The results of the simulation are plotted as Load vs Displacement and compared with the experimental results.

CHAPTER 4

EXPERIMENTAL RESULTS

The main aim of the study is to investigate the effect of the Through Thickness Reinforcement (TTR) on the strength and stiffness of the pristine and defect sample. The key role of this research is also to determine the effect of the TTR spacing on the strength and stiffness, and the ability of the reinforcement to suppress the crack propagation. The results are presented accordingly for the following groups:

- 1) Pristine Specimen
- 2) Defect Specimen
- 3) Pristine Specimen with TTR
- 4) Defect Specimen with TTR
- 5) Failed Skin-Stringer Specimen repaired with TTR.

Each of the group have been tested with few samples and the Load-Displacement plots are compared with other respective specimens to determine the crack initiation (first load drop) and the fracture point. The DIC is used to understand the strain concentration on the surface of the specimens.

4.1 Comparison of Pristine Skin-Stringer Sample and Sample with Initial Disbond

The Pristine specimens are fabricated by using an adhesive layer between skin and stringer without any defect whereas the defect specimens had a Teflon initial disbond of 0.25” inches from

the edge of the skin-stringer interface on both the sides of the sample. After curing, the specimens are cut from the plate using the waterjet machine. The dimension of each pristine specimen is 0.85” x 10” (inches). Once the specimens are cut from the plate they are cleaned with acetone and painted with black paint. In addition to the black layer, white paint is speckled over the specimen to obtain a good surface pattern while using DIC.

The Skin-Stringer Specimen is placed in the Tinius Olsen testing machine and the three-point bending test is performed. The data collection was set at 0.5mm/min at the rate of 1Hz and the same setting was used for the Digital Image Correlation (DIC).

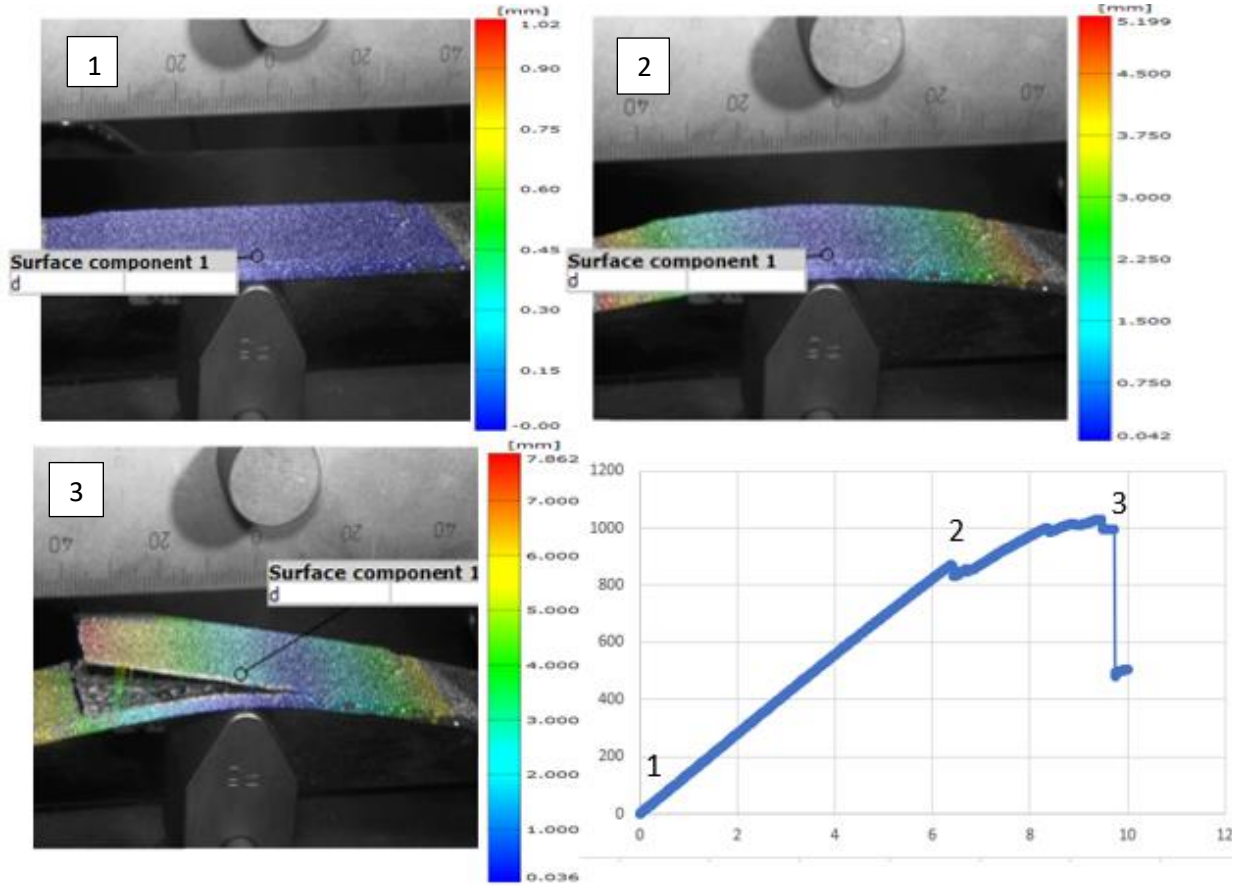


Figure 48 DIC images of displacement for the pristine skin/stringer sample.

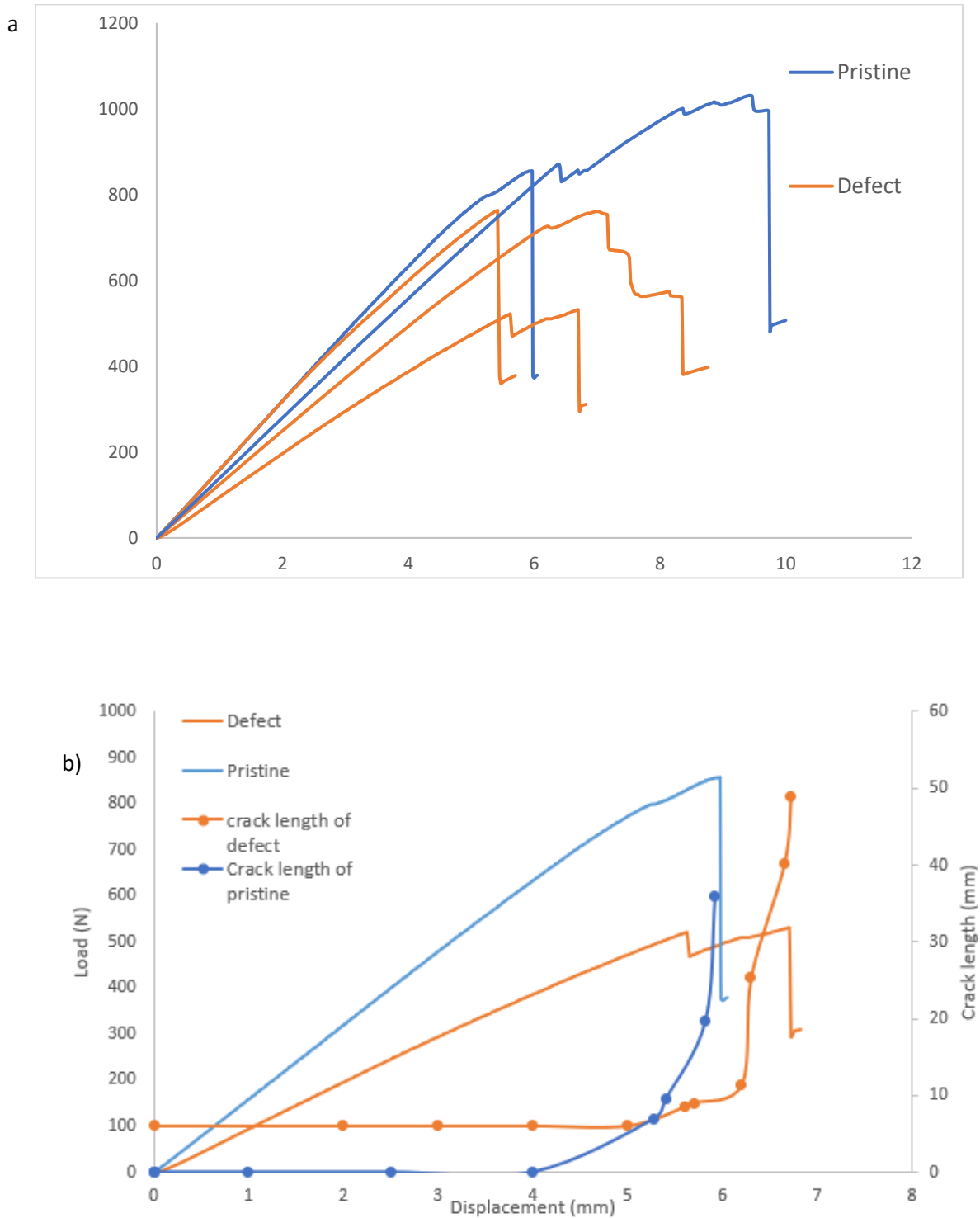


Figure 49 a) Load vs Displacement plot for pristine vs defect skin-stringer samples b) Crack propagation behavior of pristine and defect samples.

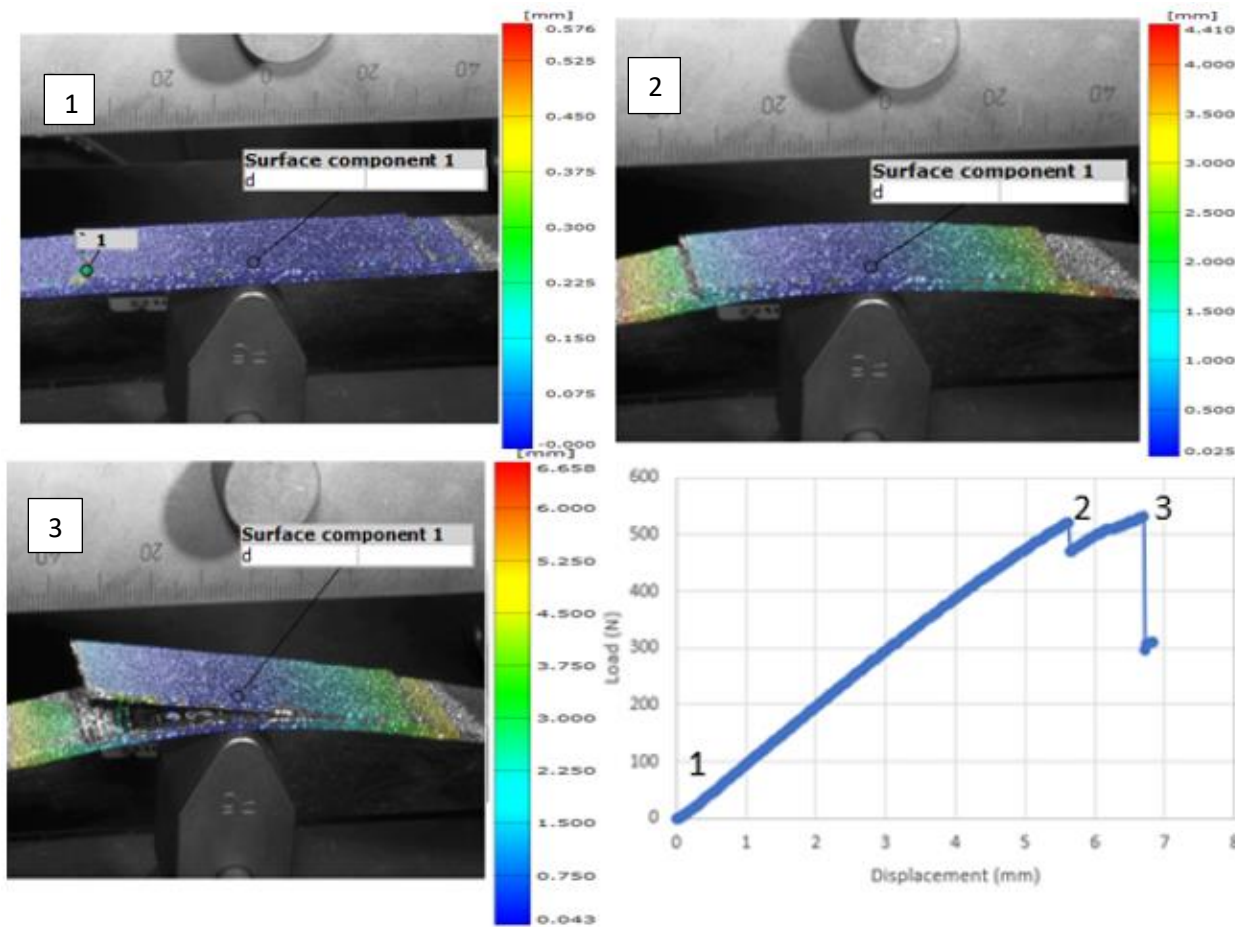


Figure 50 DIC images of displacement for initial debonded skin/stringer samples.

Using the results of the pristine and defect specimens a significant difference in the strength and stiffness is investigated. The crack initiation point (First Load drop) for the pristine samples is higher than the defect samples as seen in the above Figure 49. Even after the crack initiation point of the pristine sample, the failure/fracture occurs at higher load which shows the higher stiffness and strength in the pristine sample delays the crack propagation (Figure 49(b)). Comparing the pristine with the defect specimens the initial defect in the sample starts to propagate at lower loads and failure is observed. Since there is a pre-crack present in the specimen lower loads are sufficient to propagate the crack and develop failure. The failure load of the pristine

sample is 853 N and the failure load for the defect sample is 547. This shows that the strength and stiffness of the pristine samples are 36% higher than the defect samples.

The DIC images of the pristine skin/stringer and the defect skin/stringer at the start of the testing and after delamination are showed in figure 48 and figure 50. The crack initiation in the pristine sample (figure 48) where the strain concentration in the DIC image changes at the edge of the skin and stringer interface are seen as the color changes from blue to green where the blue color denotes small displacement and green shows increase displacement. The crack initiation for the pristine sample near the edge of the skin/stringer interface had a displacement buildup around 5.5 mm and the corresponding load drop was around 800 N. The load started to increase after the first load drop and the crack growth was stable until failure which was measured at a displacement of 7 -7.5 mm. The crack propagation for the defect specimen in figure 50 starts at a lower load, of 520N, compared to the pristine because of the pre-crack present in the sample and reaches failure at 546 N. The crack initiation starts around a displacement of the 4.5 – 5 mm. The crack growth after the first load drop is seen to be developing under minor loads but the crack propagation is stable due to the increase in load seen in Figure 50. The failure of the initial debond sample is observed around 6.5 mm which is comparatively less than the pristine sample.

4.2 Effect of 1/2" TTR Spacing on Skin-Stringer Debonding Behavior

The TTR repair was installed in the samples with a distance of 1/2 inch in between each row. The sample after curing was tested using similar settings to that of the pristine sample. The configuration of the TTR mentioned in the section 3.4 was followed and a total of 5 rows of TTR was installed. The initial disbond in the sample is created by placing a teflon film under the adhesive layer which is of the length 6 mm from the edge. The TTR is placed at 3 mm from the edge to avoid the crack propagation at the earlier stage of the experiment. The TTR in the disbond sample is placed in the center of the defect so that the disbond region has an increase in strength.

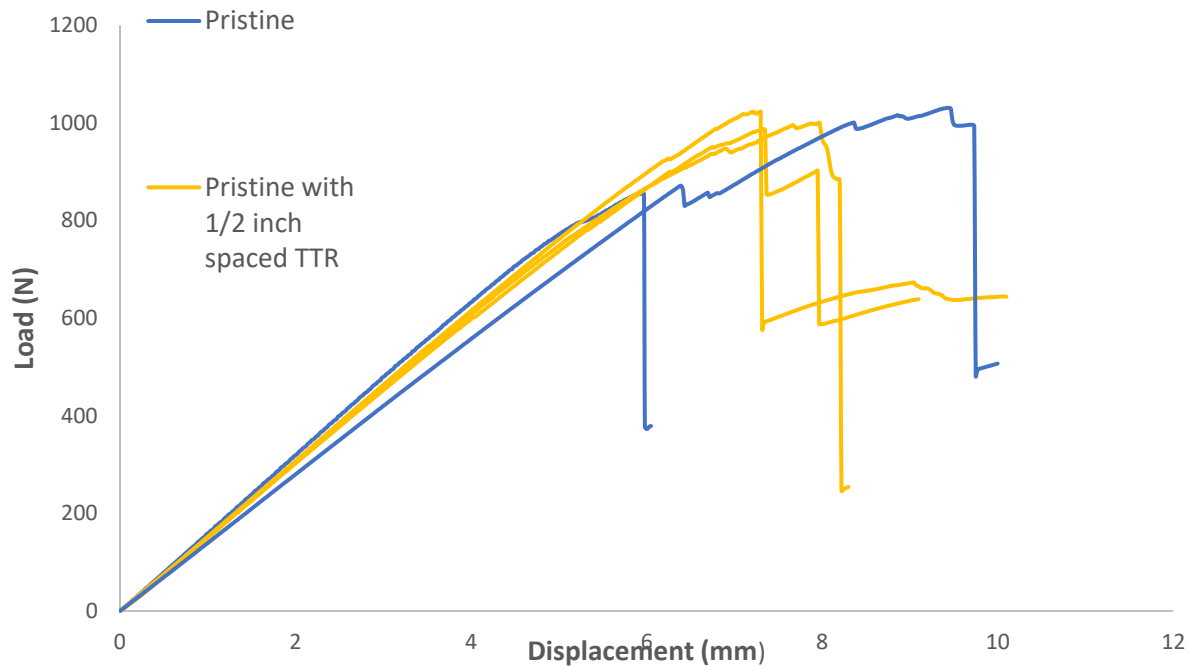


Figure 51 Load vs Displacement plot for pristine vs pristine repaired TTR.

The figure 52 is the initial skin/stringer specimen mounted for the three-point bending test. The load at which the specimen fails is 975 N and the displacement of the specimen is shown using

DIC in figure 52 where the crack propagates extensively from the edge of the interface into the sample which creates the delamination between the skin and stringer.

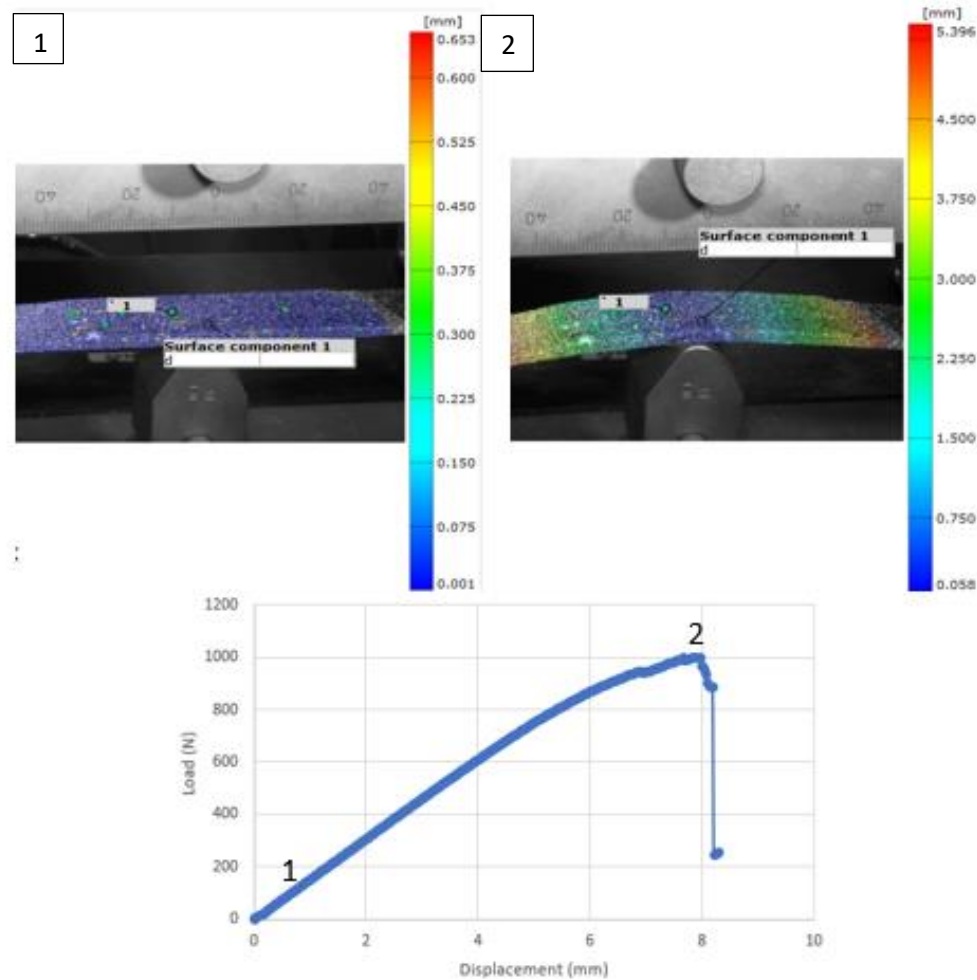


Figure 52 DIC images of displacement for 1/2 inch spaced TTR in pristine skin/stringer sample.

The aim to determine the effectiveness of improving strength in 1/2 inch spaced TTR on pristine sample is discussed, the pristine with no TTR is included in figure 51. The load drop for the pristine

was observed at 841 N and the TTR pristine sample had a load drop at 975 N. The failure load of both the samples does not differ drastically when compared but the difference is observed when the load required for pristine with TTR to propagate the crack is little higher than the pristine without TTR. From the DIC images the displacement of the specimen is monitored, and the failure of the specimen is due to extensive crack propagation in the interface of the skin/stringer. The reinforcement with $\frac{1}{2}$ inch spacing in the samples was not effective in arresting the crack and the crack propagated till the center of the interface. It is seen that this TTR configuration did not have a greater efficiency and did not improve the strength and stiffness of the specimen.

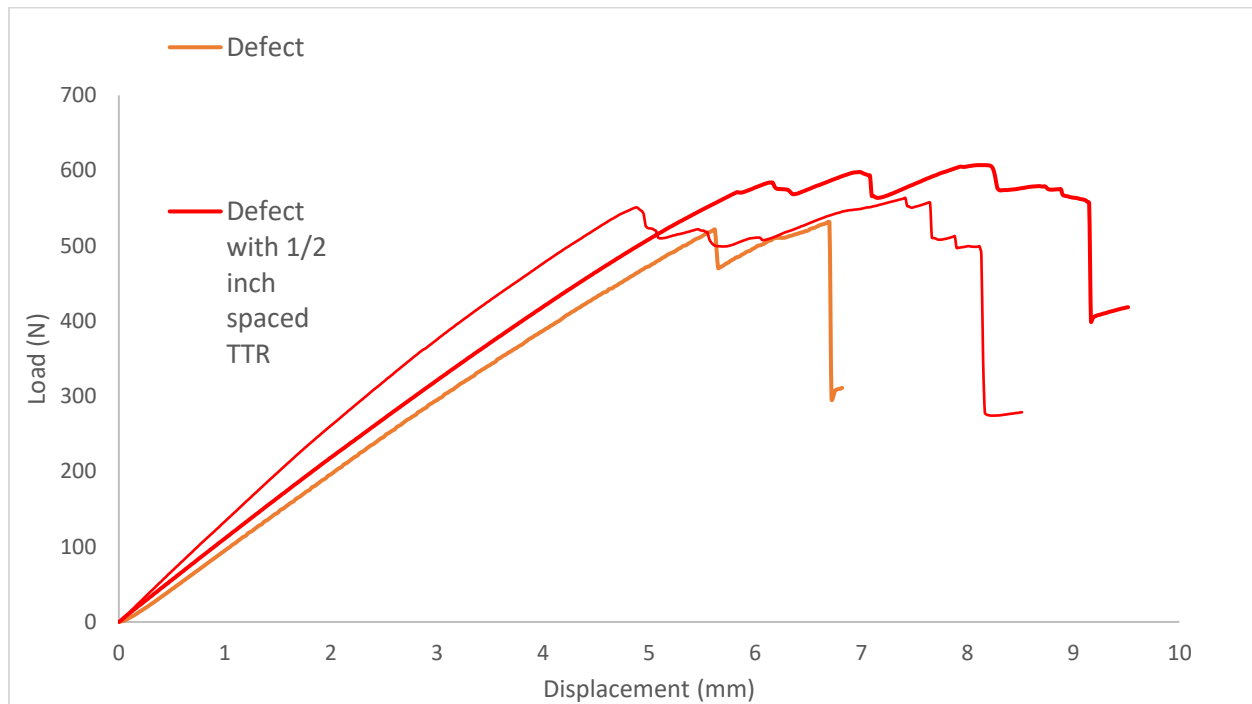


Figure 53 Load vs Displacement for defect vs TTR repaired defect.

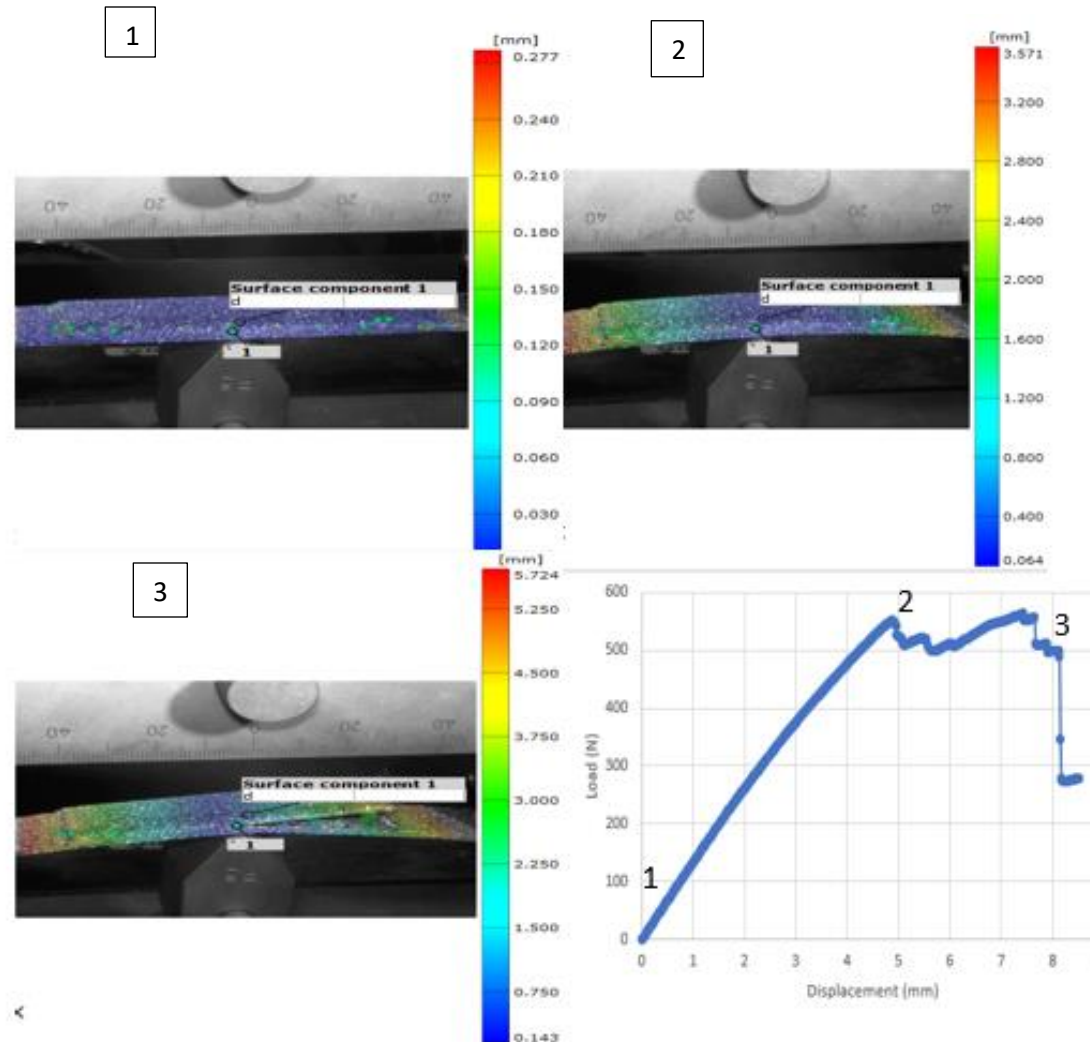


Figure 54 DIC image of displacement for 1/2 inch spaced TTR in initial disbond sample.

The defect sample with 1/2 inch spaced TTR is investigated to understand the effectiveness of TTR on defect skin/stringer samples. The point where the load drop/ crack propagation starts is same as the defect without TTR. Using figure 53 the first load drop was observed at 517 N for the defect sample and 545 N for the TTR repaired defect sample with 1/2 inch spacing. The failure load for the defect specimens is 545 N and failure point for the TTR repaired specimen is 558 N. These

results show that the TTR configuration has not improved the efficiency and strength of the samples.

From the DIC Images in Figure 54, the displacement of the defect skin/stringer samples with ½ inch spaced TTR are shown and disbonding of the specimens is observed at the failure load of 558 N. The change in concentration on the top surface and interface shows the start of crack propagation after the pre-crack. The disbond region is initially 6mm length and the TTR are installed at 3mm which makes the disbond region strong and higher loads are achieved for the propagation of a crack. The rate of crack propagation after the first load drop at 545 N was high, so the defect skin/stringer starts to disbond quickly but the installed TTR in the initial disbond sample stables the crack growth and fails at a higher load when compared to the sample without TTR. The sample with TTR installed fails at a larger displacement which is due to the increase in strength achieved by TTR and marginal increase in failure load of the range 580 -600 N is observed.

Using the DIC images the displacement (Figure 52) at which the pristine with 1/2” spaced TTR develops crack propagation is around 7 mm where the load drop occurs, then with the influence of TTR the crack growth was steady while considering the load-displacement curve and it was observed the sample failed under the roller at a load of 975 N with a displacement around 8 mm. The pristine with 1/2” spaced TTR failed at a displacement around 8 mm higher than the pristine without TTR.

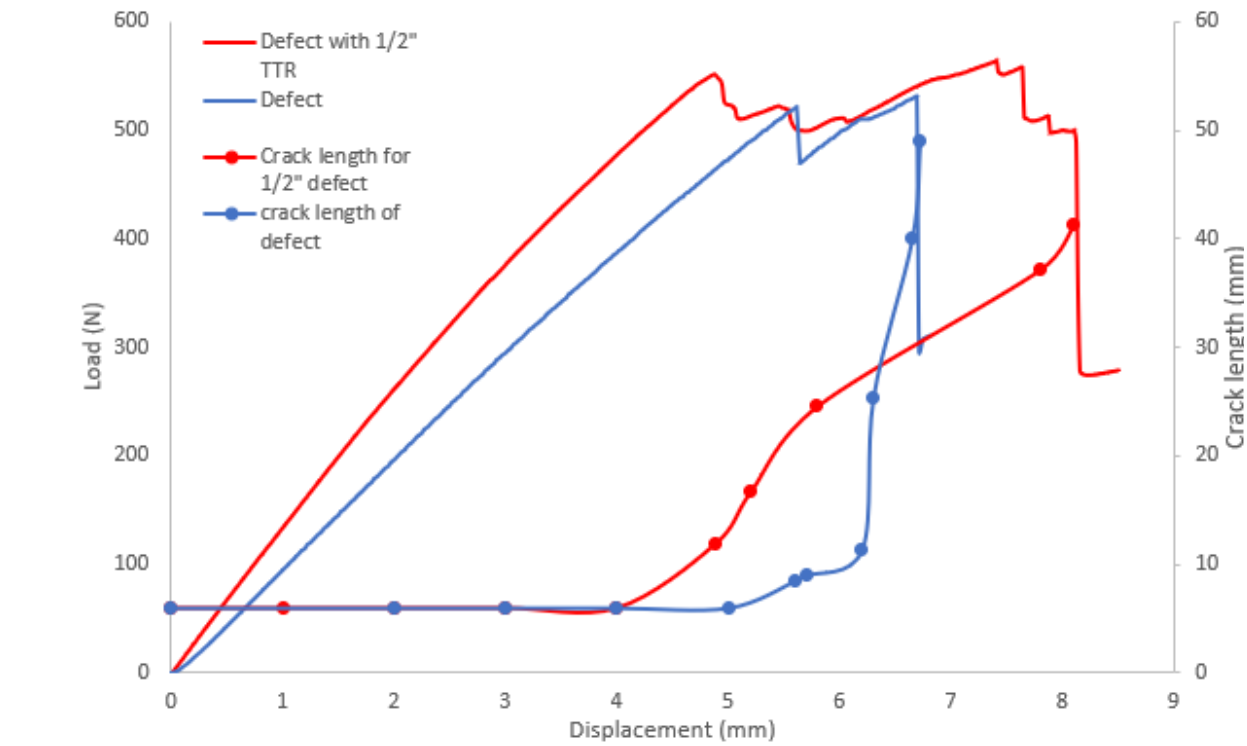


Figure 55 Behavior of crack propagation for defect vs defect with 1/2\" TTR samples.

The crack propagation of the defect sample is measured using the DIC images in Figure 54, the initial crack in the defect sample without TTR initiates the crack propagation at the range of 520 N when the sample is displaced at 5.6 mm and the corresponding crack length is 8.5 mm. The crack behavior is steady and without TTR it grows rapidly until failure when the sample is displaced at 6.7 mm. For the defect with 1/2\" spaced TTR , the TTR is installed in the initial disbond region to improve the strength and the load required for the crack to propagate is at 540 N. After that the crack growth is steady with increase in load because of the TTR and the displacement at which the sample fails is higher at 8 mm. From this it is observed that TTR influences the ability to suppress the propagation of cracks in minor loads.

The ½ inch spacing TTR was seen to be not effective in the pristine skin/stringer specimen but the defect specimen with the same configuration had a considerable effect because of the TTR for which the load was lesser than the pristine specimen.

4.3 Effect of 1/4” TTR Spacing on Skin-Stringer Debonding Behavior

For fabrication of the pristine specimen with ¼ inch TTR the distance between the rows is reduced from ½ inch to ¼ inch. The holes are drilled in the sample using the configuration specified in section 3.4. The curing process followed is similar to the ½ inch spacing specimens.

The DIC images for the pristine with ¼ inch spaced TTR specimen are given in figure 57 in which the displacement of the sample during the crack propagation stage and at the failure point is observed. After capturing the experiment using the DIC, the GOM correlate software is used to analyze the strain concentrations and displacement of the skin/stringer sample. The distance of the crack is measured to understand the effect of TTR on the pristine skin/stringer samples by applying the “Two-point distance technique” given by the GOM correlate software. This technique gives the distance of the delaminated region at failure.

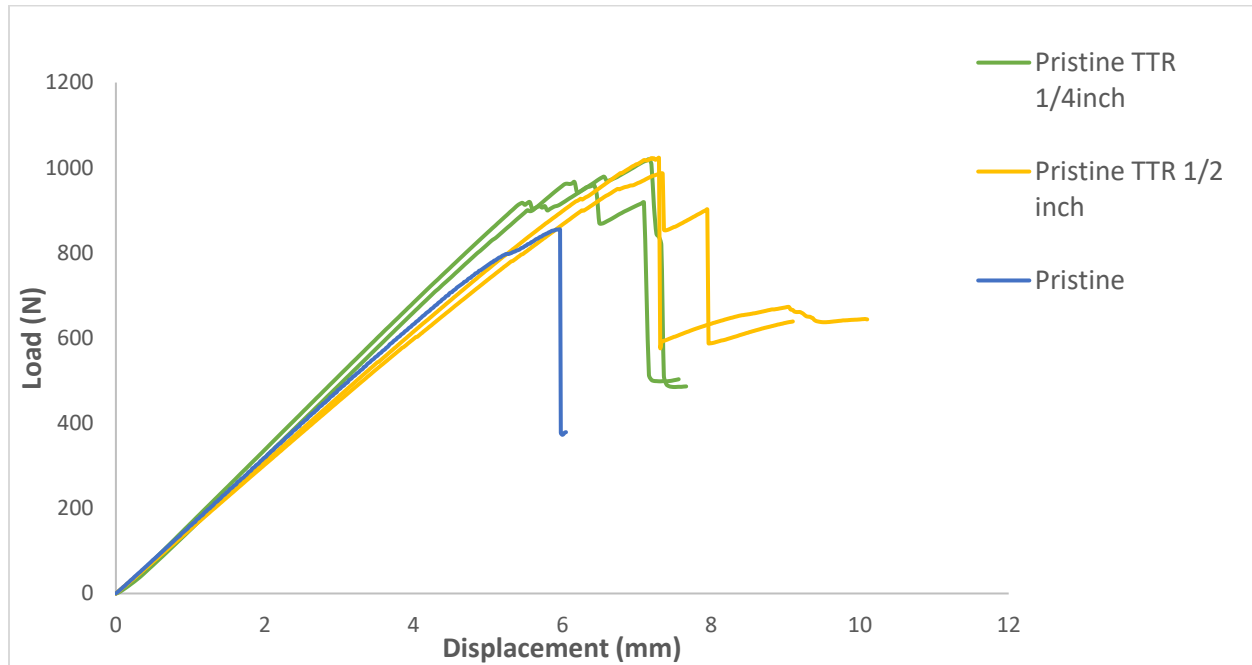


Figure 56 Load vs Displacement curves for $\frac{1}{2}$ inch spaced TTR vs $\frac{1}{4}$ inch spaced TTR.

Addition of pristine samples without TTR are also added to the figure 56 to better understand the effect of the TTR in pristine specimens. The behavior of the $\frac{1}{2}$ inch TTR spaced and the pristine without any TTR had large delamination lengths at the interface. The Skin-Stringer specimens with $\frac{1}{4}$ inch spaced TTR was tested using three-point bending was observed to have a high stiffness and strength as the crack propagation point where the first load drop occurs at 918 N which is higher than the pristine without TTR and $\frac{1}{2}$ inch spaced TTR specimens. There is a small deviation after the linear response of the curve which increases to a higher load and the crack propagation takes place. The load drop for the $\frac{1}{2}$ inch spaced TTR was around 800 N and the $\frac{1}{4}$ inch spaced TTR specimens developed the first load drop at 875 N. The failure of the $\frac{1}{4}$ inch spaced TTR specimens is observed a load of 910 N. From the results it is understood that the $\frac{1}{4}$ inch spacing of TTR has increased the strength of the specimen has resulted to suppress the crack propagation

in the specimen. The efficiency of the $\frac{1}{4}$ inch spacing is higher when compared to the $\frac{1}{2}$ inch spacing of TTR.

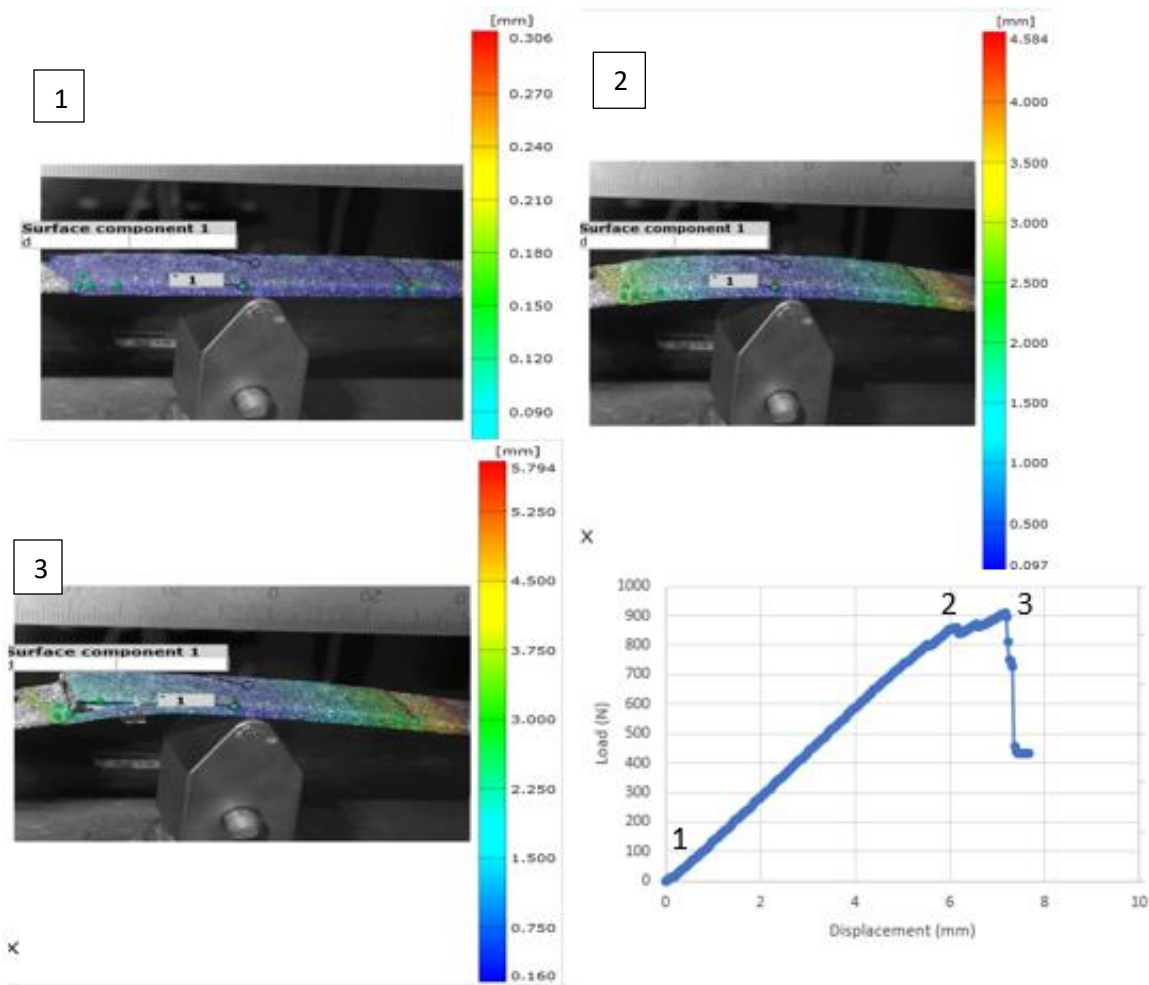


Figure 57 DIC image of displacement for $\frac{1}{4}$ inch spaced TTR in pristine skin/stringer sample.

Using the two-point rule in GOM correlate software the crack propagation in the samples is measured using DIC images (Figure 57 & 58) and the disbonding behavior of the sample is understood. The slope of the pristine sample without TTR changes after the initial curve because

of the crack initiation and growth present in the sample. After the crack initiation the load increases until failure at load of 854 N.

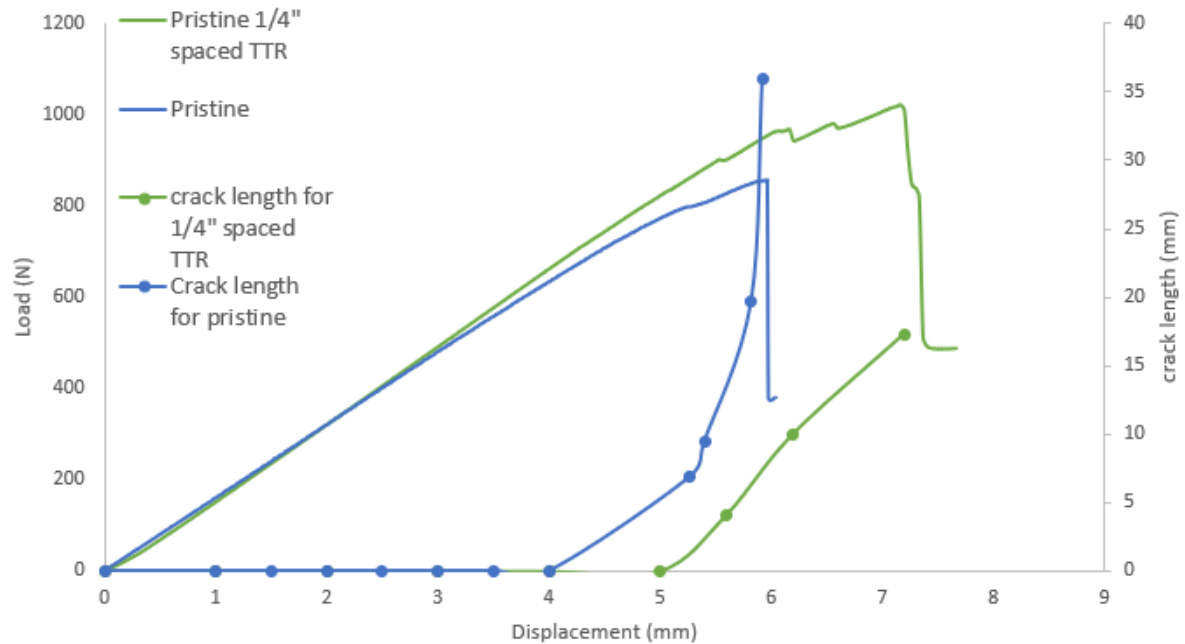


Figure 58 Behavior of crack propagation for pristine vs pristine with 1/4" spaced TTR.

The pristine with 1/4" spaced TTR has a better improvement in slope than the pristine sample and the crack propagation in the sample is steady even at higher loads. The difference between the specimens is that the displacement at which the failure occurs is higher at 7.5 mm than the pristine without TTR which fails at a displacement of 6 mm. The crack length at failure is less for the reinforced pristine sample which proves the effect of TTR in suppressing the crack.

The effect on the spacing for the defect skin/stringer samples are observed in a similar fashion of the pristine specimen. The fabrication is done by inserting the TTR with 1/4 inch spacing

across the length direction. The Load-Displacement plots for all the defect skin/stringer samples are given. The DIC images for the specimen are evaluated for the overall crack length at failure to understand the efficiency in $\frac{1}{4}$ inch spacing.

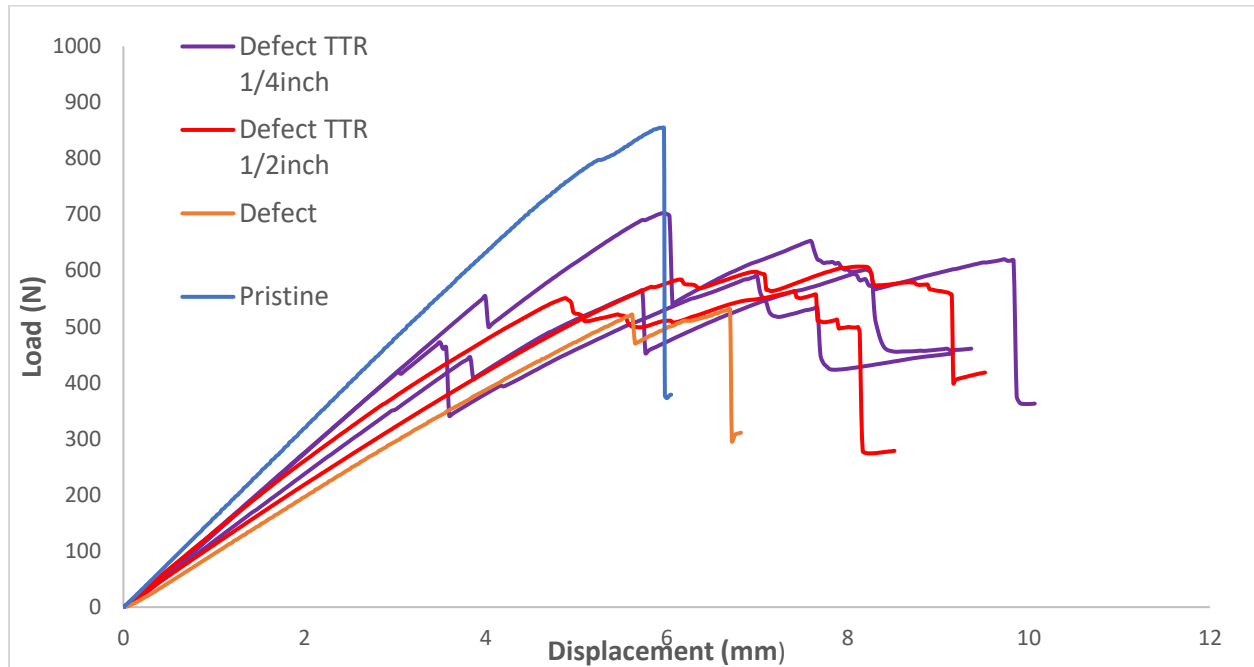
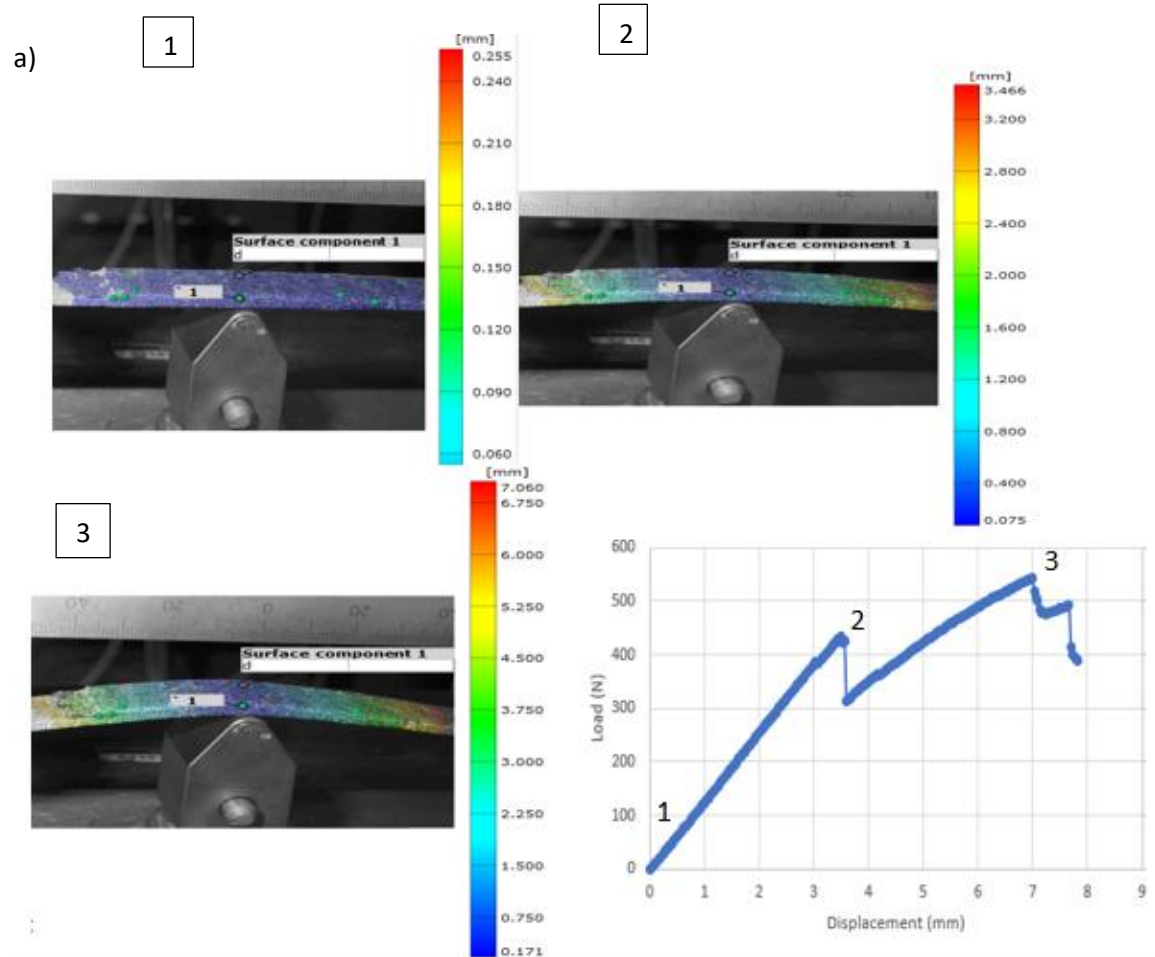


Figure 59 Load vs Displacement plots for $\frac{1}{2}$ inch and $\frac{1}{4}$ inch spaced TTR defect skin/stringer.

The defect samples with $\frac{1}{4}$ inch spacing were observed to develop the crack propagation at higher loads unlike the defect without TTR and $\frac{1}{2}$ inch spaced TTR defect samples. The ability of the skin-stringer specimen to resist the crack growth has increased and resulted in the crack propagation at higher loads shown in Figure 59. The samples with $\frac{1}{4}$ inch spaced TTR which were tested exhibited a crack propagation at higher loads even with the presence of the pre-crack in the defect specimens. The average of the samples of $\frac{1}{4}$ inch spaced was higher than the average of the other two groups which shows the effectiveness of the TTR spacing. The difference in linear behavior of the load-displacement plot is observed and the load drop is found at 500 N. The failure load of the $\frac{1}{4}$ inch spaced TTR specimen is at 630 N and the failure of $\frac{1}{2}$ inch spaced TTR defect

specimen is found at 530 N. From this it is concluded that there is 16% increase in failure loads for the $\frac{1}{4}$ inch spaced TTR specimen when compared to $\frac{1}{2}$ inch spaced TTR defect specimen.



(a). DIC images of displacement for $\frac{1}{4}$ inch spaced TTR in defect skin/stringer sample

From the DIC images and the GOM correlate software (Figure 60) the length of the crack at failure for the defect skin/stringer sample with $\frac{1}{4}$ inch spaced TTR is 26 mm and the crack length for $\frac{1}{2}$ inch spaced TTR is 41 mm. The crack for the defect sample without TTR is 49 mm is measured to compare with the omniscan ultrasonic scanning results. The DIC images are used to

track the crack propagation in the sample and the behavior of the crack propagation is plotted in Figure 61. From Figure 60, the crack propagation after the first load drop in the TTR installed specimen is seen when the load increases for both the 1/2" spaced initial disbond samples and 1/4" spaced samples. The defect sample without TTR has the crack growth with minor loads until failure occurs. For all the three groups the crack growth is steady but the ability to suppress the

b) crack is influenced by the presence of TTR in the initial disbond samples.

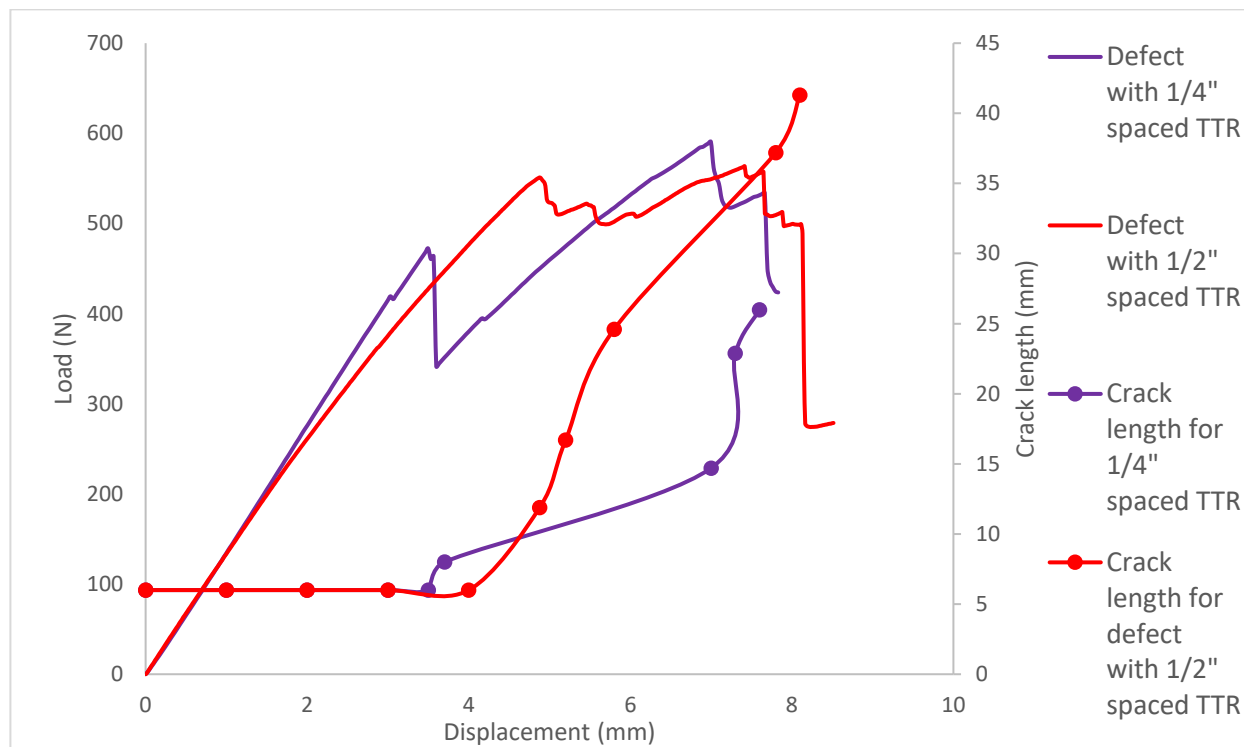


Figure 60 a) DIC images of displacement for ¼ inch spaced TTR in defect skin/stringer sample
b) Behavior of crack propagation in defect with 1/2" vs defect with 1/4" spaced TTR samples.

The behavior of the crack propagation for the defect with 1/4" is seen when there is increase in load, the disbond propagation is initiated at the load of 480 N and the growth of the disbond is seen to increase with the increase in load (figure 60(b)). The first load drop occurs at a displacement of 4mm and the sample failure occurs at a higher displacement of 8 mm which is

higher than both the groups. The failure of the 1/4" spaced TTR sample is seen at higher load of 590 N and the crack propagated through the sample during failure is less than the defect with 1/2" TTR and 1/4" TTR proving the effectiveness of 1/4" spacing is higher in improving the strength and stiffness than the 1/2" inch spacing.

The bar chart given below in Figure 61 with all the tested samples makes us to understand the effectiveness of the TTR spacing on pristine and defect skin/stringer specimens. The average of all the samples manufactured and tested are used in the bar chart.

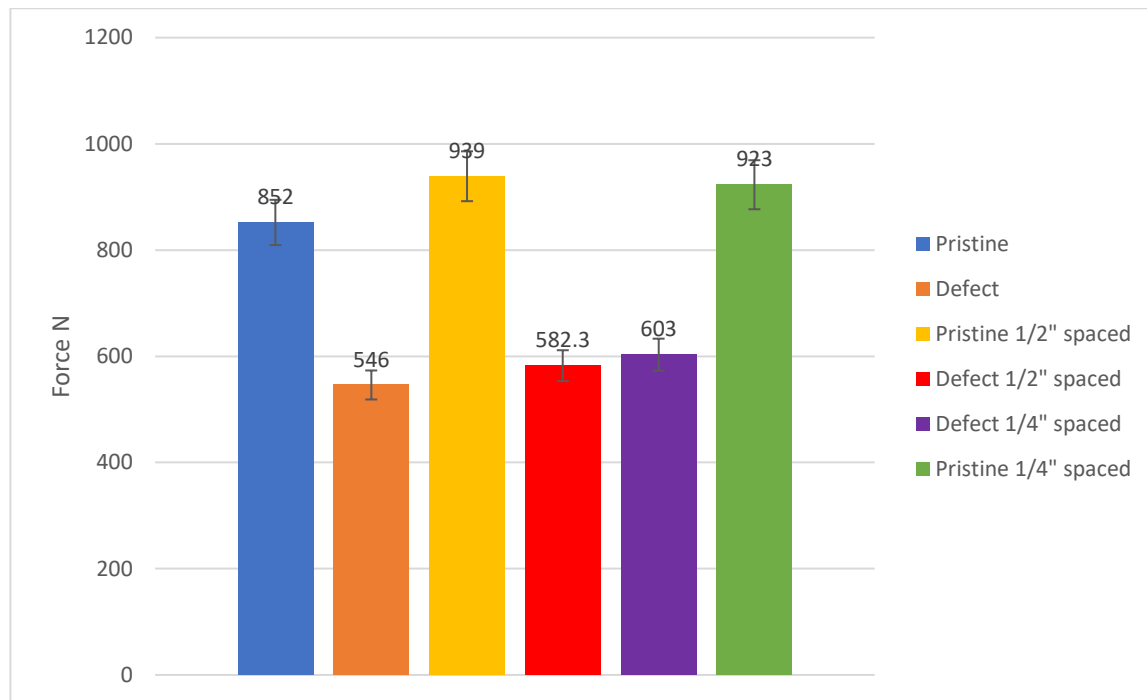


Figure 61 Effectiveness of TTR spacing on pristine and initially disbonded skin/stringer samples.

Using the group of samples specified above the effect of TTR for both the spacings fail at a higher load than the other sample groups. The 1/2 inch and 1/4 inch spaced TTR pristine skin/stringer samples fail at 939 N and 922 N but the when the load-displacement curve of the samples are compared the linear behavior of the curve for the 1/4 inch spaced pristine specimens

are higher than the $\frac{1}{2}$ inch spaced specimens. So, from the plots it is seen that the strength and stiffness of the sample are higher for the $\frac{1}{4}$ inch spaced specimens and increase the effect of suppressing the propagation of the crack.

The pristine sample without TTR has the second highest load of 852 N but lesser than the TTR spaced specimens. The defect sample without TTR experienced the failure at lower load of 546.5 N which is the least among the other groups.

The efficiency of TTR on defect skin/stringer samples was also seen to be similar to pristine samples where the average failure load for the $\frac{1}{4}$ inch spaced was at 603 N and $\frac{1}{2}$ inch spaced TTR sample had a failure load of 582 N. Both the specimens did not have a large difference but the linear response of the $\frac{1}{4}$ inch spaced TTR specimen proved that there is an increase in the stiffness of the specimen.

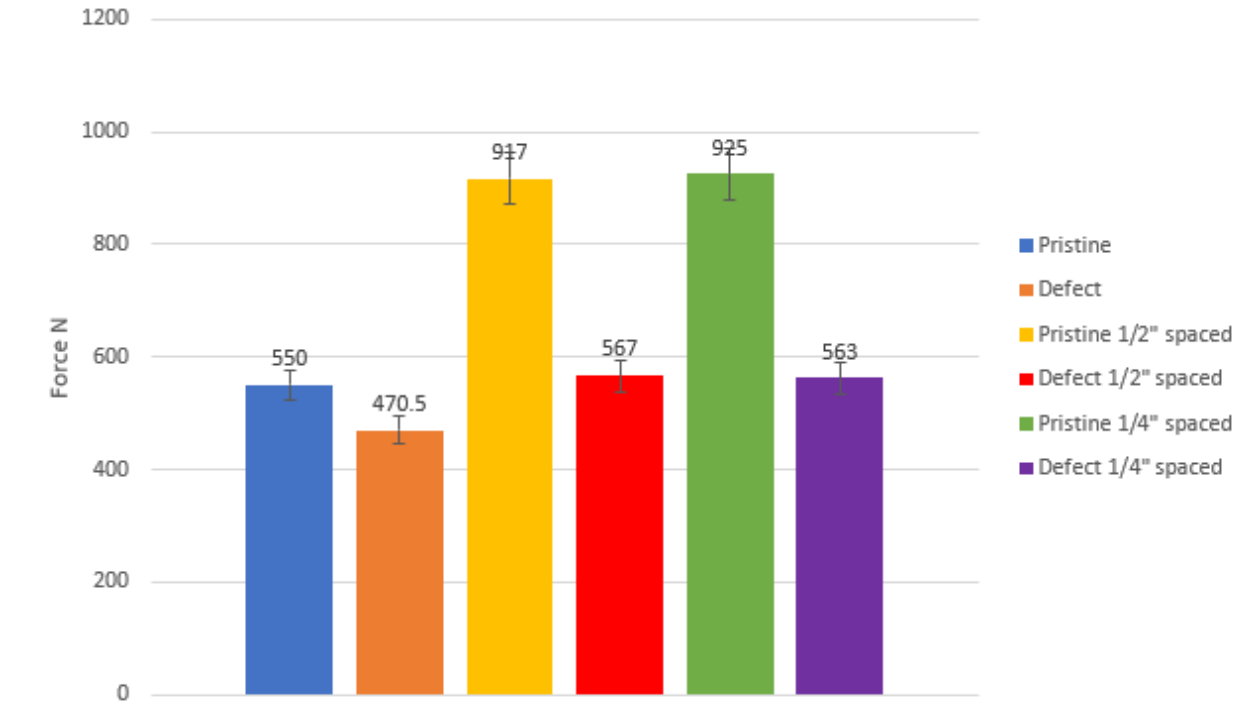


Figure 62 Comparison of crack initiation load in all sample groups.

From Fig 62 the crack initiation in the pristine sample with 1/4" spacing is seen to be higher because of the spacing of TTR. The crack propagation resistance is higher when the TTR spacing is reduced, thus having a slow and stable growth after each row of TTR fails. The crack initiation of the 1/4" spaced TTR pristine sample is observed at a load of 925 N. The crack initiation in other samples is comparatively less and due to the difference in spacing of TTR.

Similarly for the 1/4" spaced defect skin/stringer the crack initiation load is seen to have a minor difference but the crack propagation in the sample is suppressed when the rows of the TTR are increased. The initial disbond present in the sample creates the crack initiation at a minor load when compared to the pristine but while tracking the crack growth in Figure 62 the resistance for the 1/4" samples is higher and has a promising efficiency in suppressing the crack.

4.4 Effect of 1/2" and 1/4" TTR Spacing on Failed Skin-Stringer Panels

The Skin-Stringer specimens used in this section were completely disbonded with the skin surface. After failure, the specimens were repaired using both the 1/2 inch TTR spacing and 1/4 inch TTR spacing. Using the experimental results shown in Figure 63 the failure load of 1/2 inch spaced TTR is around 750 N and the failure load of the 1/4 inch spaced TTR specimens is at 822 N. The failed samples when repaired with the 1/4 inch spacing of TTR has the tendency to restore its strength and stiffness close to the strength of the pristine sample. The linear curve of the load-displacement plot has a similar behavior to that of the pristine sample but after the initial curve a deviation is observed in the plot of both the 1/2" and 1/4" spaced failed samples. The deviation in the load-displacement plot is observed due to the pull out of the first row of TTR in the sample. After the pull out of first TTR row the disbond grows with increase in load but the damage of individual rods are also seen which weakens the sample and leads to failure less than failure load of pristine. So, from these results when the 1/4 inch TTR is installed in the failed specimen it restores 80% of the strength and stiffness and 69% when repaired with 1/2 inch spacing. The efficiency of the 1/4 inch spaced TTR is higher than the 1/2 inch spaced TTR.

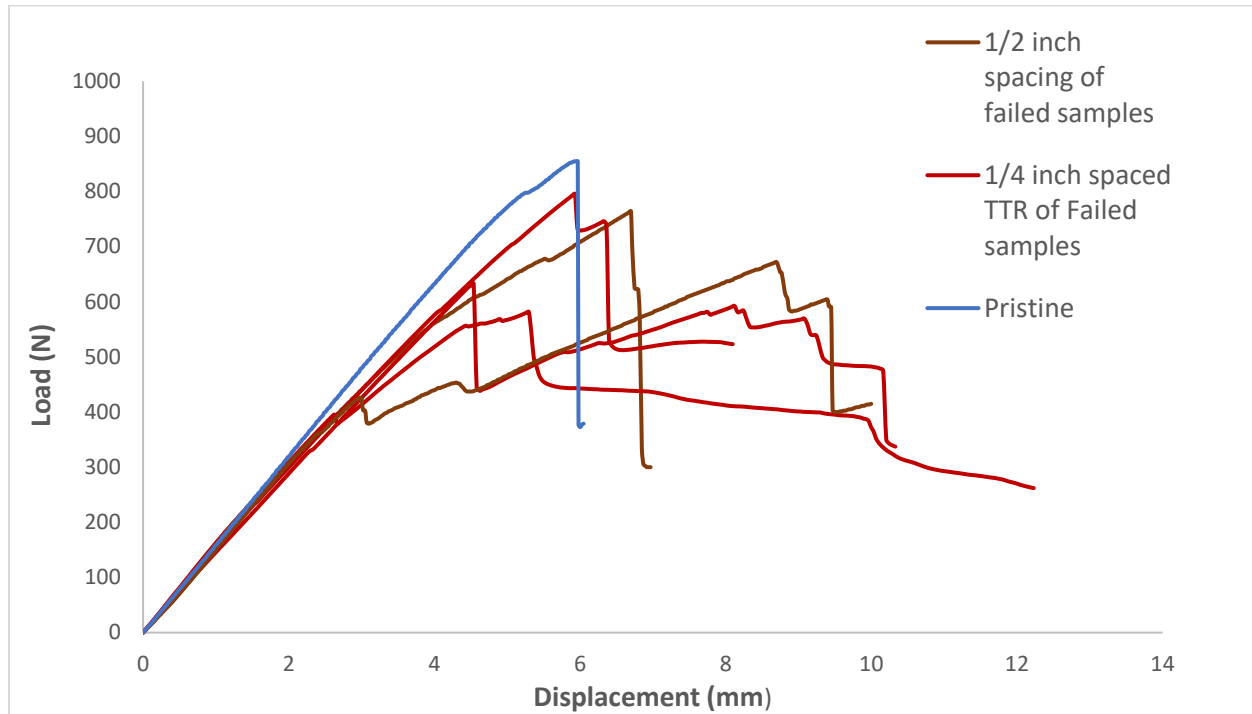


Figure 63 Load vs Displacement for completely failed and repaired specimens.

The repaired and tested specimens were compared to the pristine and defect skin/stringer samples with TTR to investigate the efficiency of TTR which is given in the image given below. Using the Figure 64, it is understood that the repaired specimens with $\frac{1}{2}$ inch and $\frac{1}{4}$ inch spaced TTR have a similar trend in the failure load but the load at which the first load drop or the crack propagation occurs is higher at a load of 682 N in the $\frac{1}{4}$ inch spaced skin/stringer sample than the $\frac{1}{2}$ inch spaced TTR samples where the failure occurs at 672 N. This difference in the load at which the crack propagation begins is observed in the load-displacement plots and proves that the efficiency of $\frac{1}{4}$ inch spaced TTR specimens is better than the specimens repaired with $\frac{1}{2}$ inch spaced TTR.

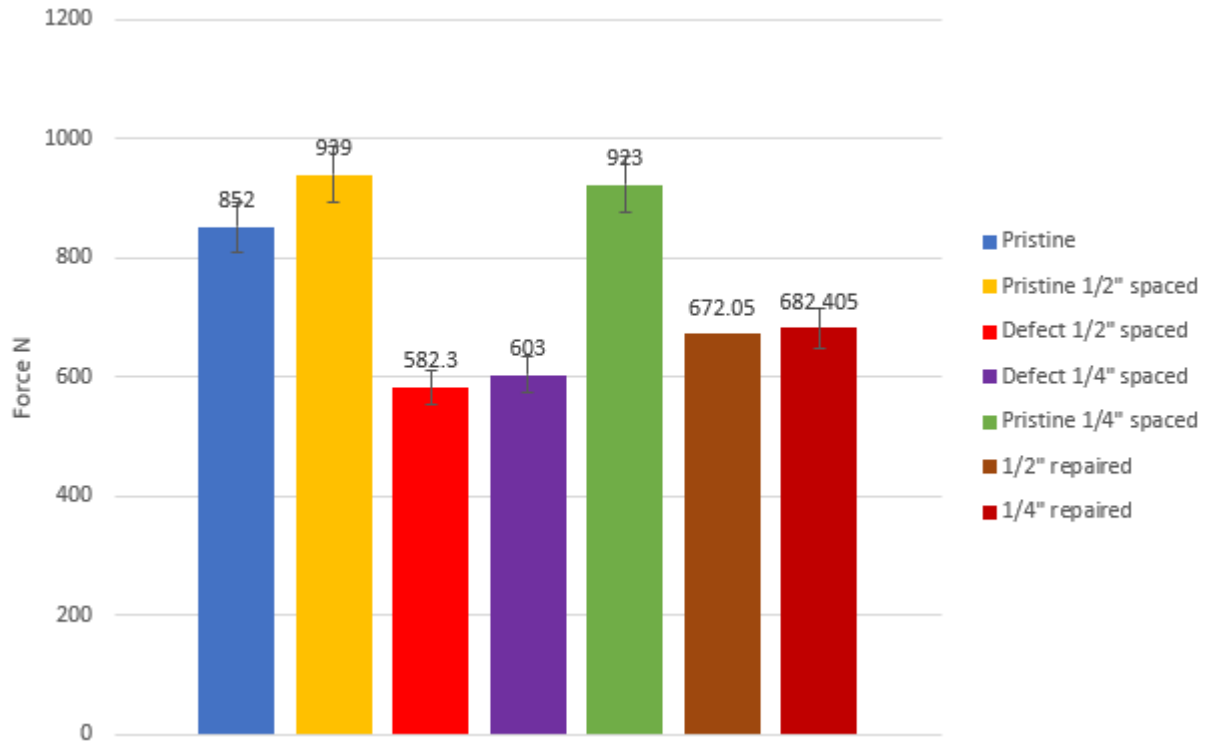


Figure 64 Effectiveness of TTR on repaired skin/stringer specimens.

4.5 Effect of TTR in Tensile test

The tensile tests were carried out for Skin-stringer defect specimens and ¼ inch spaced TTR specimens for both pristine and defect samples. To perform the tensile testing the specimens were bonded to grips at both the ends and cured for 10 hours. After the grips are left to dry in room temperature the specimens were clamped to the tensile tool. Unlike the three-point bending test the specimens exhibited high strength and stiffness during the tensile test. The linear curve of the defect sample without any TTR has a major difference when compared to the ¼ inch spaced TTR samples. The pristine specimen with ¼ inch spaced TTR has a higher strength and fails at 38.6

KN. The TTR efficiency has proved to be effective in increasing the strength of the specimens when tested in tensile direction.



Figure 65 Failed Pristine with TTR Skin/Stringer.

The pristine skin/stringer sample with $\frac{1}{4}$ inch spaced TTR was seen to have high strength and stiffness which exhibited failure at the load of 38.6 KN and the defect skin/stringer specimen had a first load drop which may have been caused due to the inserted pre-crack and then failed after reaching 21.4 KN shown in Figure 66. The pristine skin/stringer sample was removed from the MTS machine and the delamination was observed (Figure 65). The specimen was completely damaged and the damage in the TTR is seen which led to the disbonding of the specimen. In Figure 67 the crack in the defect sample without any TTR is observed.

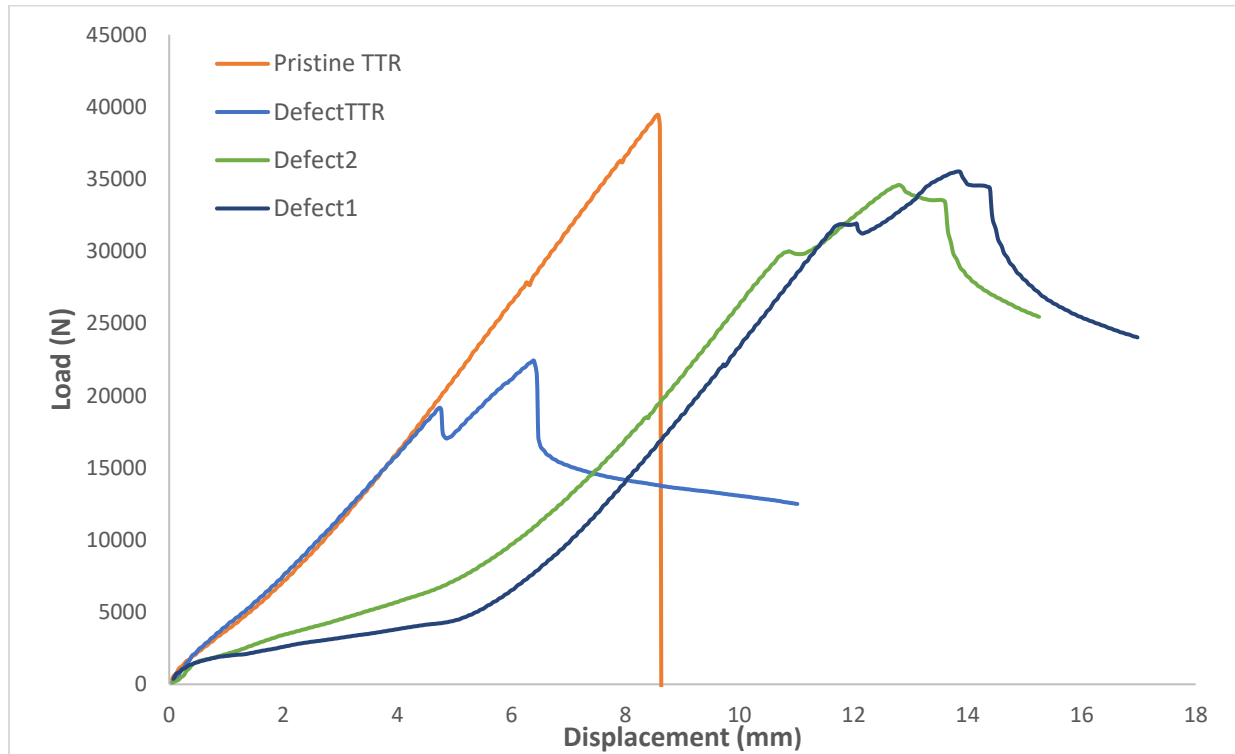


Figure 66 Tensile test results of skin-stringer specimens.



Figure 67 Crack in the defect skin/stringer sample.

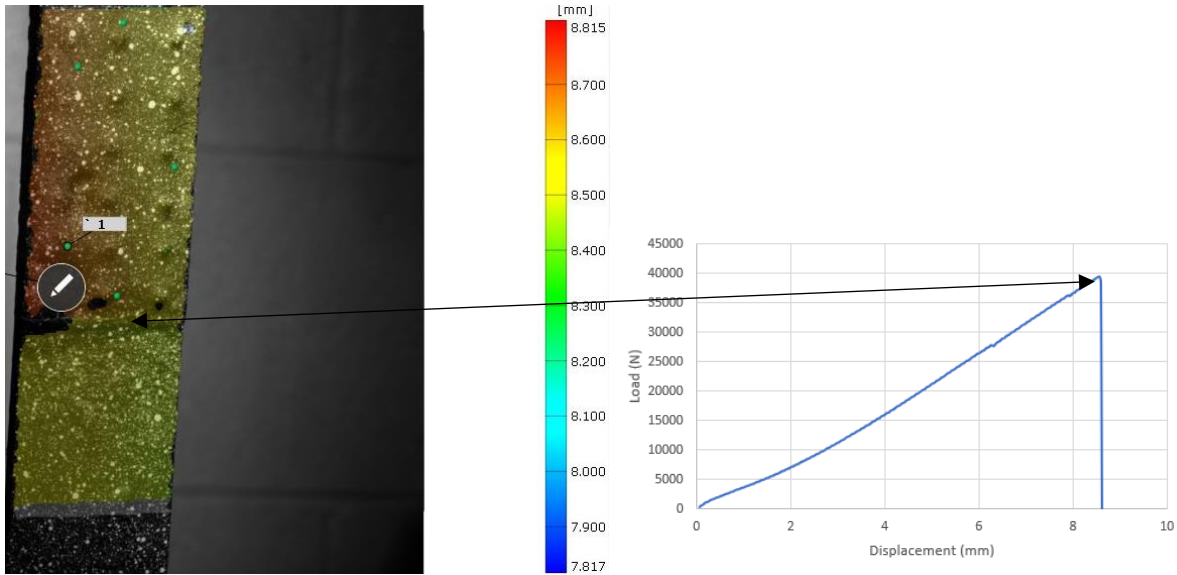


Figure 68 DIC image of displacement of pristine skin/stringer with ¼ inch spaced TTR.

In the above Figure 68 the DIC image and the displacement concentration from the GOM correlate is seen at the edge of the interface indicating the disbonding region of the skin/stringer. The crack propagation cannot be seen on this surface, but it is seen in the corresponding load-displacement plot there is an increase in the load to reach failure. For the defect specimen with TTR, there was a load drop observed which is shown in Figure 69 and then a load increase was seen to reach failure. The bottom left corner on the specimen has a change in displacement concentration when the crack starts to propagate and the delamination in the interface begins.

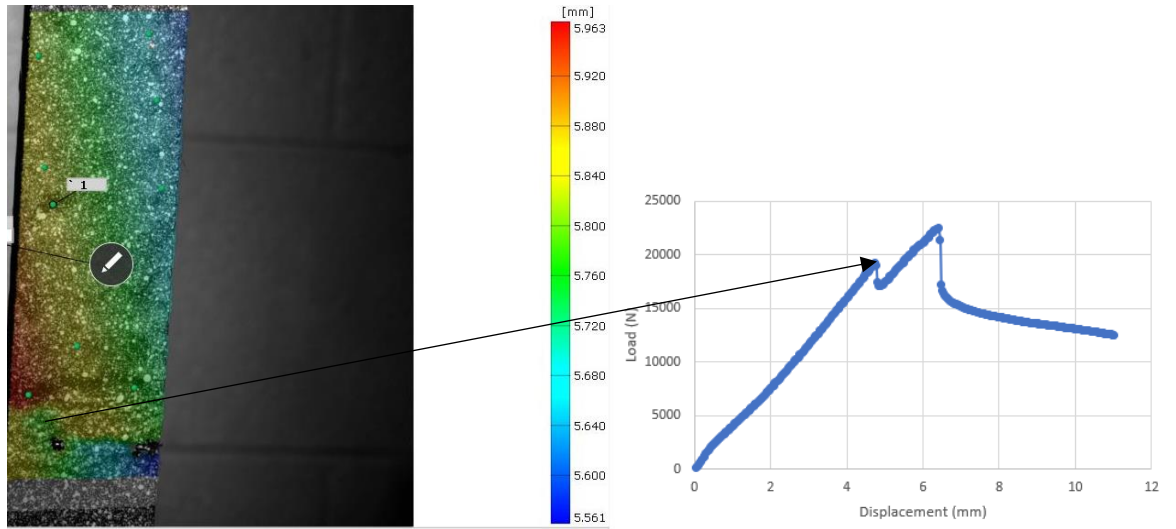


Figure 69 DIC image of displacement of the defect skin/stringer sample with 1/4 inch spaced TTR.

4.6 Ultrasonic Scanning of Skin-Stringer Specimens

The ultrasonic scanning is performed on the skin/stringer samples to determine the location of the defect and the size of the crack is determined. The setup of the Omniscan ultrasonic scanner is explained in section 3.6. The scanning of the samples is carried out with a presence of water medium or gel. A small amount of water is poured on the sample and the probe is moved through the sample front and back to find the defect in the sample. In this section the pristine and defect specimens with and without TTR are scanned and compared with crack lengths measured using the DIC images and GOM correlate software.

The length of the probe used for measuring the sample is 66 mm and the width of the probe is 10 mm. The length of the crack at failure is compared to the DIC images with help of GOM correlate. The A-scan and the S-scan images of the pristine, defect, pristine with TTR and defect

with TTR are shown below. The Gate-A setting is important in determining the range in the specimen in which the crack will appear.

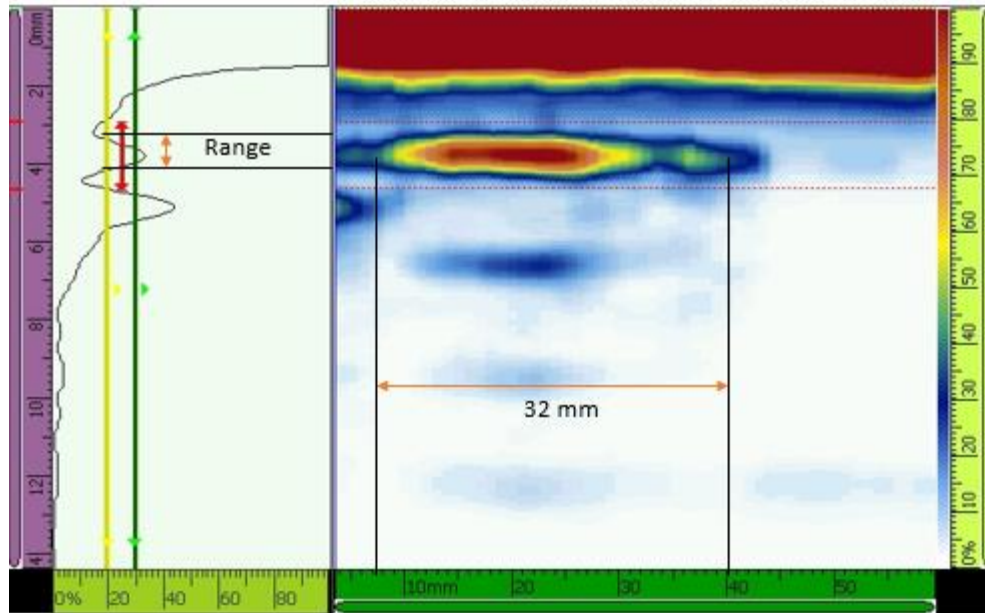


Figure 70 Ultrasonic scanning image of pristine skin/stringer sample.

The pristine sample without TTR is scanned after removing from the test setup. The omniscan scanner is calibrated by specifying the specimen thickness and setting the Gate A to predict the range in which the crack is bound to occur. While scanning the pristine sample the signal of the crack is seen in the Figure 70 and then the second signal is detected which denotes the back wall of the specimen. The left side of the image where the signals received are seen is the A-scan and the right side of the image where the crack is shown is the S-scan. The length of the crack in the S-scan is predicted to be around 20 mm in the interface of the skin/stringer. The range of the thickness at which the crack appears in the sample is in between 3mm to 4.2 mm.

The defect skin/stringer is also scanned to estimate the range of the crack and the length of the crack. Once the testing is completed the specimen is demounted and used for scanning. In defect sample there is an initial crack present which helps the crack to propagate at lower loads and is expected to have crack length higher than the pristine sample. The image of the A-scan and the S-scan are studied to determine the crack length present in the specimen.

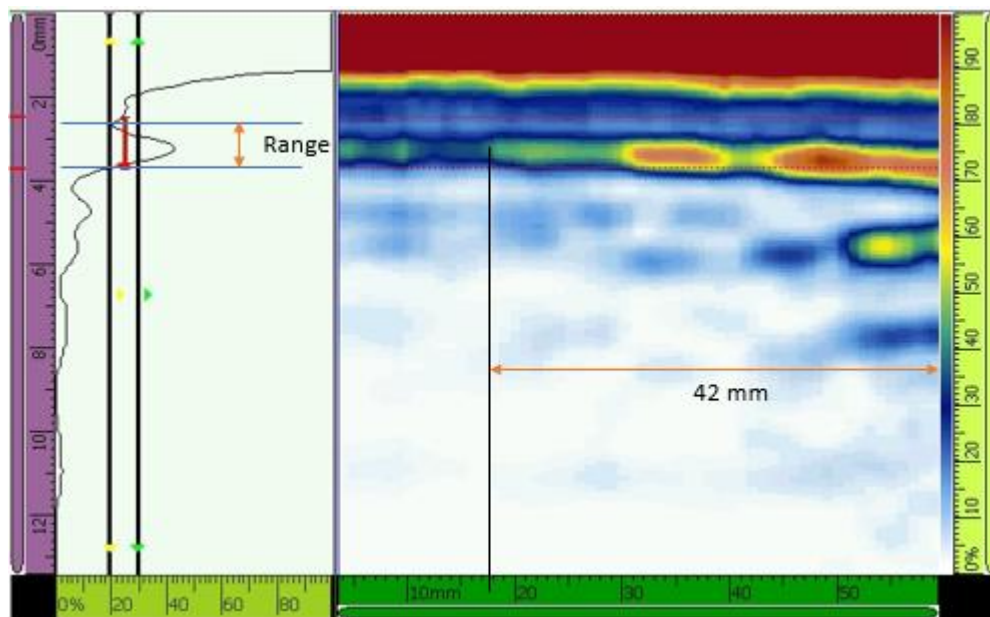


Figure 71 Ultrasonic scanning image of defect skin/stringer samples.

The A-scan of the defect sample shows the signal of the defect sample and also the range on where the crack is in the specimen. The start and end of the Gate A is the predicted range of the position of crack. The range is in between 2.6 mm to 3.6 mm (Figure 71). The S-scan on the right side is used to measure the crack length. It is given as 42 mm. The concentration of the crack in the specimen is higher as the probe is scanned through the sample. At the start of the crack the concentration is seen low which might be due to the water used for scanning. Sometimes while

scanning in some portions of the sample the water might be less on surface and you can observe the mild coloring of the crack. The crack length predicted by scanning is around 42 mm. The crack in the pristine skin/stringer is much lesser than the defect samples.

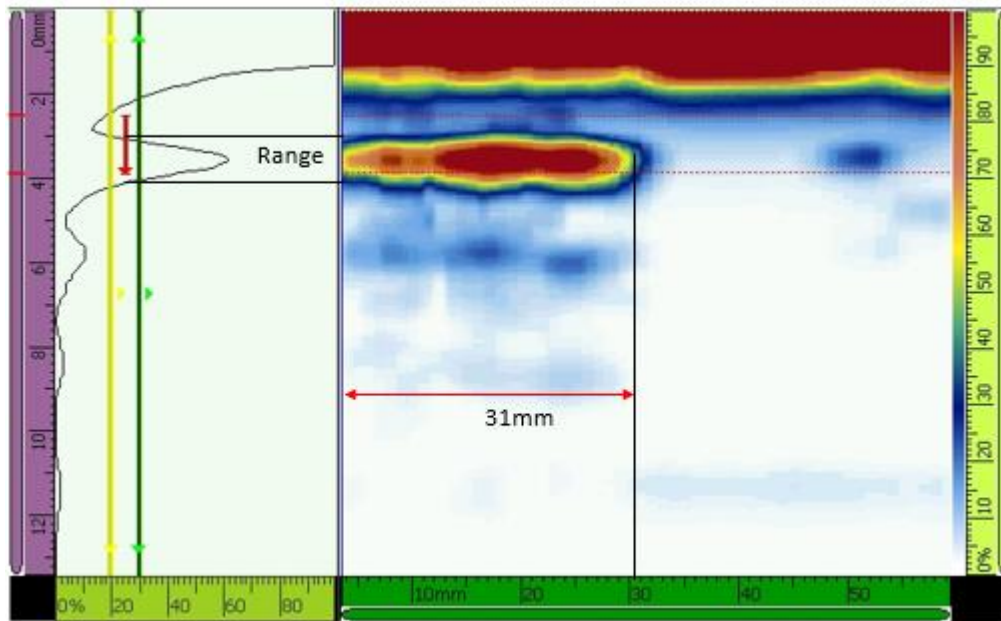


Figure 72 Ultrasonic scanning image of defect sample with $\frac{1}{2}$ inch spaced TTR.

The crack length of the defect skin/stringer without the TTR was 42 mm. After the installation of TTR in the specimen the crack propagation was reduced and the length of the crack at failure was seen to be 31 mm. The range at which the crack is predicted is around the thickness of 3mm to 4.2mm in the defect skin/stringer specimen (Figure 72). The defect with $\frac{1}{2}$ inch spacing TTR when inspected under ultrasonic scanning is seen to have higher impact in stiffness when compared with the defect without TTR.

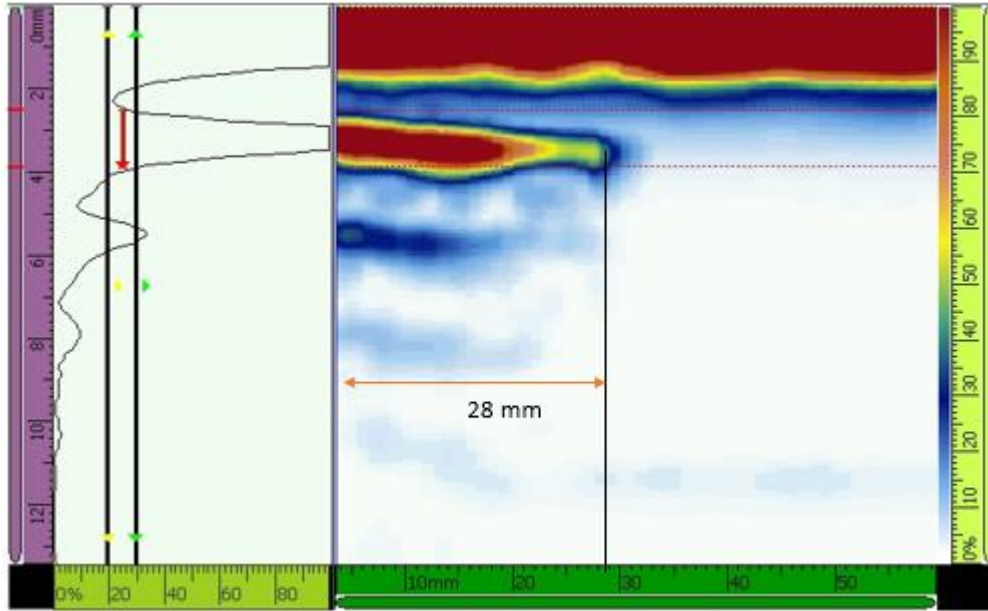


Figure 73 Ultrasonic scanning image of pristine with 1/2 inch spaced TTR.

Using the above Figure 73, the ultrasonic inspection performed on the pristine skin/stringer specimen, the length of the crack seen in the interface of the specimen is 28 mm. The range at which the delamination is observed is in between 2.4 mm to 4.2 mm given by the A-scan. The S-scan of the pristine sample with 1/2 inch TTR is not very effective in arresting the crack as the difference between the pristine without TTR and with TTR is around 3 mm. The scanning of both the samples has similar delamination length and does not suppress the crack like the defect specimens which had a difference of 10 mm.

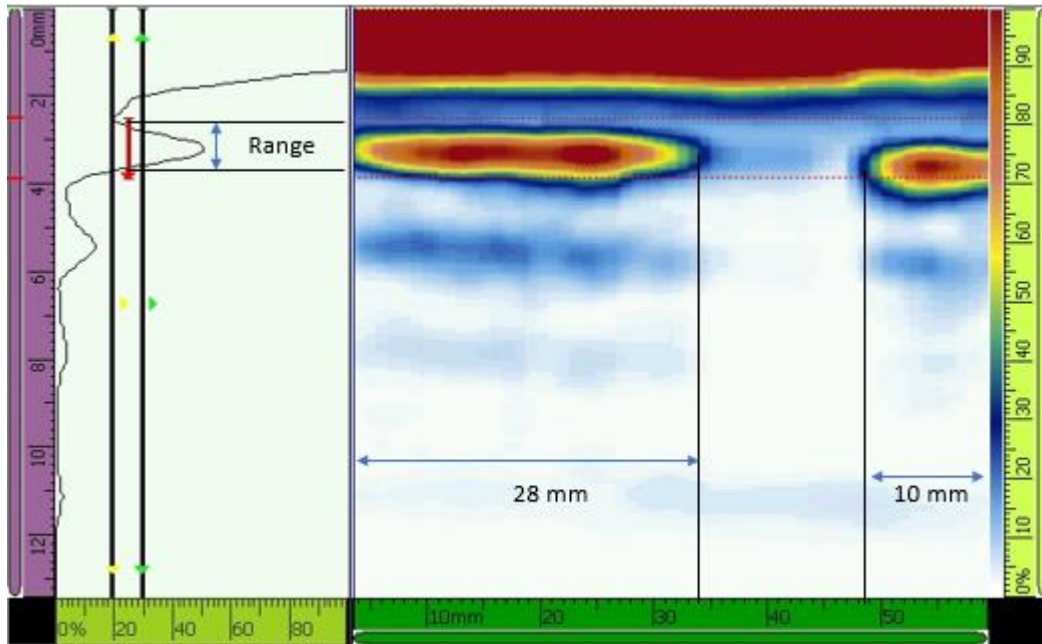


Figure 74 Ultrasonic scanning of defect skin/stringer sample with $\frac{1}{4}$ inch TTR.

After scanning the defect specimen with $\frac{1}{4}$ inch spaced TTR, the Figure 74 has cracks/defects present at both the ends of the skin/stringer sample. The delamination of the interface is seen at both ends from the right and left. The crack at the left of the sample is 28 mm and the crack at the right is around 10 mm. The range at which the crack appears is between 2.2 mm and 4 mm. In the other groups the delamination was observed at one side and the crack propagated more into the sample around an average of 40 mm. But in the defect sample with $\frac{1}{4}$ inch spaced TTR the crack propagation was not deep as the other groups with the help of reinforcement so the stiffness and strength of the defect skin/stringer with $\frac{1}{4}$ inch TTR was highly effective.

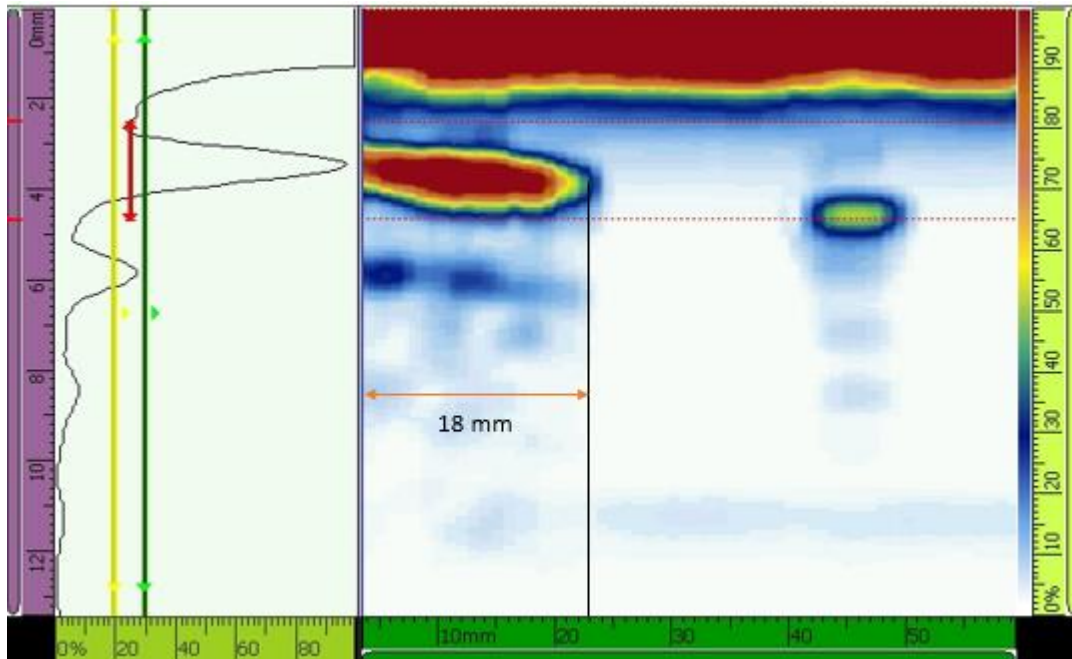


Figure 75 Ultrasonic scanning for pristine samples with $\frac{1}{4}$ inch spaced TTR.

Investigating the ultrasonic scanning images of the all the groups of specimens with and without TTR, the pristine sample with the $\frac{1}{4}$ inch spaced TTR has the least length of delamination of the interface. The S-scan on the right from Figure 75 shows the least crack length of 18 mm in the pristine sample. The A-scan of the image gives the range about 2.2 mm to 4.2 mm. The pristine sample without TTR has 32mm and the $\frac{1}{4}$ inch spaced TTR has a crack of 18 mm which shows the effectiveness of the TTR in the samples. Another factor when compared with the defect specimens is that the initial crack is not inserted, and crack propagation does not start at lower loads. The $\frac{1}{4}$ inch TTR configuration in pristine skin/stringer samples is more effective in arresting the crack and increase the strength and stiffness among other groups of samples.

4.7 Simulation Results of Skin/Stringer Specimen

After the submission of the modelling the simulation takes place at a specified step size, and it increases with respect to step size. Once the iteration of each step is completed the results can be plotted as Load-Displacement plots. When the roller starts to contact the top layer of the skin the changes in the stress concentrations are seen at the top layer. The point where the roller makes direct contact is the region of high stress and sample starts to bend when the displacement increases. The simulation is displacement controlled and a value is specified for the top roller. The image of stress concentration is shown in figure below (Figure 76).

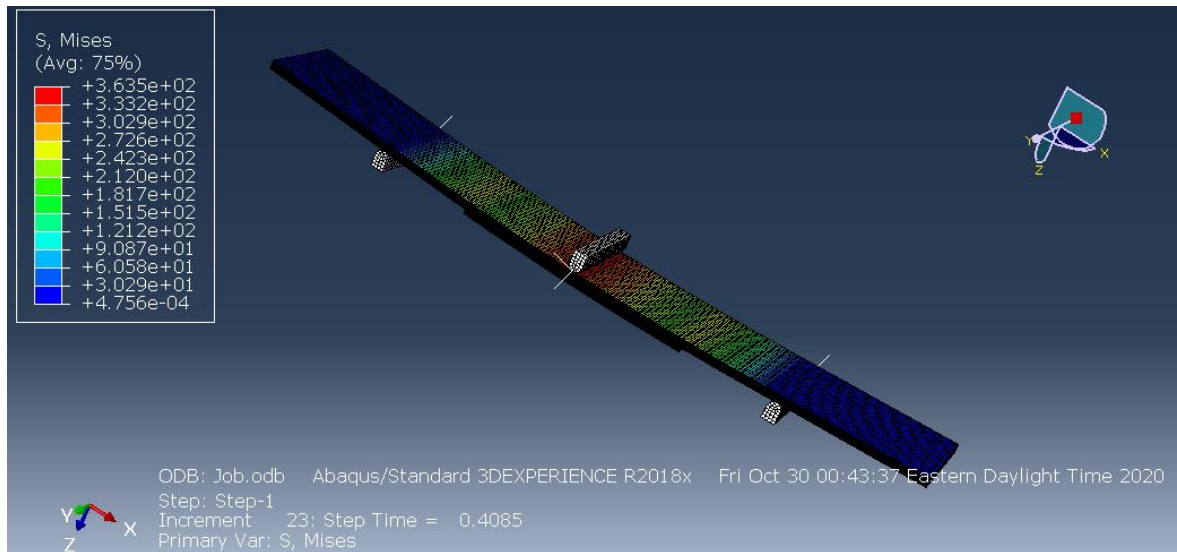


Figure 76 Stress concentration of skin/stringer specimen.

To determine the failure of the interface between the skin/stringer samples, the option that displays the failure of the interface at certain steps is selected and the images are shown in the figures below. The cohesive layer starts to fail at the edges and then starts to propagate. To view

the failure in cohesive layers the SDEG technique in Abaqus is used. The images of the SDEG are shown in the figures below (Figure 77 & 78)

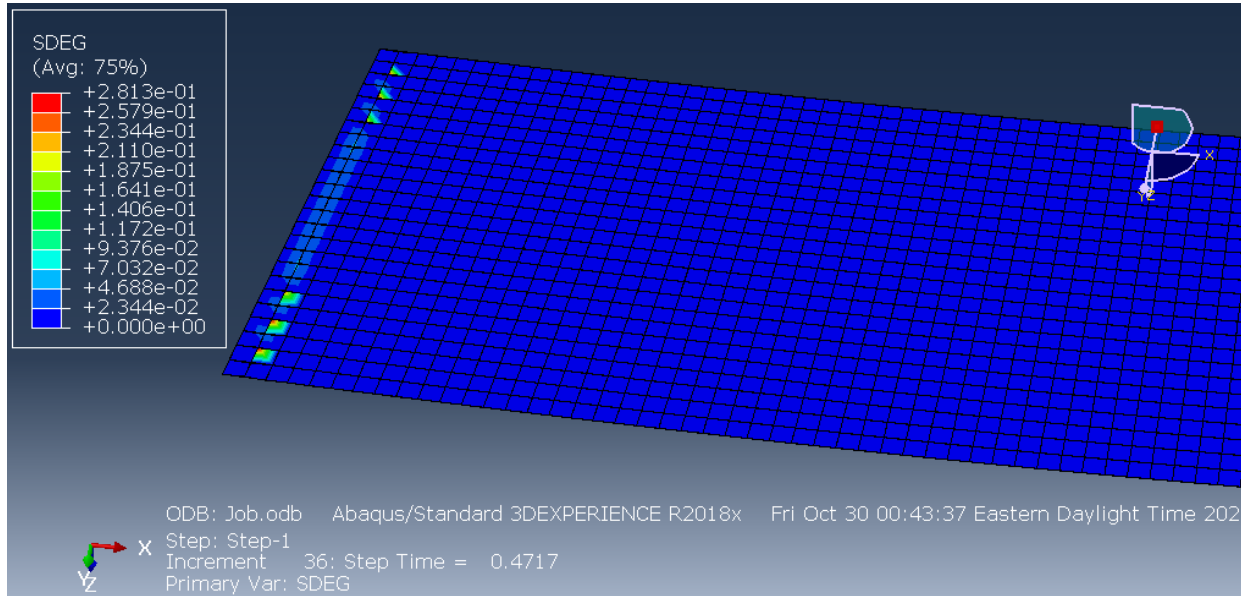


Figure 77 Failure of cohesive layer at the load of 495 N.

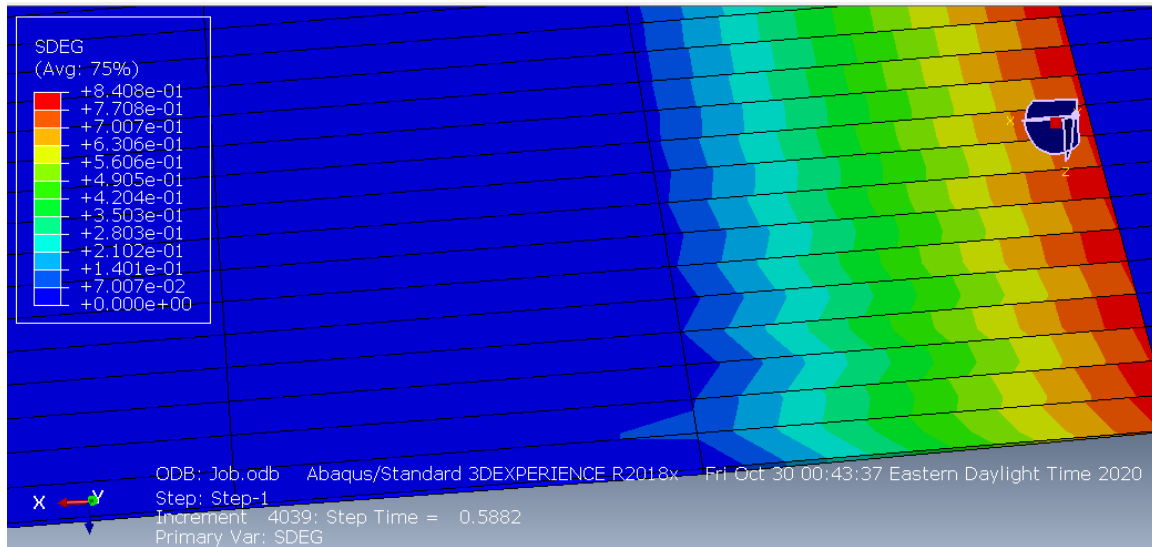


Figure 78 Failure of cohesive layer at the load of 620 N.

Load-Displacement plot of the simulation from Abaqus and the experimental results of the pristine are compared in the Figure 79. The linear curve of the simulation results is similar with the experimental results. The stiffness of the Abaqus model is higher than the pristine sample tested under the three-point bending test. In future work the modelling of the specimen can be done with the TTR installation and insertion of the defect in the interface can also be modelled and compared with their respective groups.

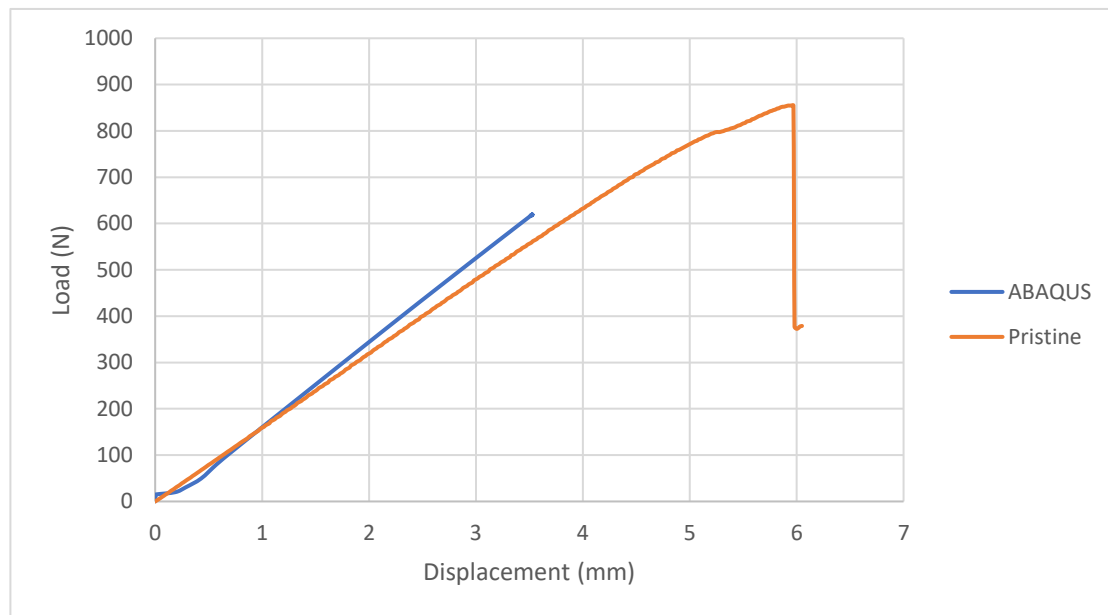


Figure 79 Load vs Displacement of ABAQUS for pristine skin/stringer sample.

The response of the Abaqus is higher than the pristine sample after following a same pattern till 300 N. From the SDEG images it is observed that the damage occurs in the interface of the skin/stringer at a load of 620 N but there is no load drop observed which indicates that the material has the ability to withstand the load and restrict the crack propagation. Due to the high strength of the material a deviation is observed which is higher than the pristine curve.

CHAPTER 5

CONCLUSION

The main aim of this study was to understand the effectiveness of TTR and the spacing of the TTR in skin/stringer samples. The samples are manufactured by laying up the prepreg and curing it using the heat press. After the curing process the skin/stringer plate is cut using the protomax waterjet. The TTR configuration mentioned in Figure 30 is installed in the sample for both the spacings. The pristine and initially debonded skin/stringer are tested in 3PB test and tensile test. A total of 5 groups pristine, defect, pristine with TTR, defect with TTR and totally failed and repaired skin/stringer samples are tested to determine the effectiveness of TTR on skin/stringer samples. For each group three samples were tested, and the crack propagation was investigated using DIC images and load-displacement plots.

Using the results shown in the previous section, the first load drop or the load at which the crack starts to propagate seen to be higher in pristine skin/stringer samples with 1/4" and 1/2" spaced TTR when compared with other groups. The failure load for 1/4" spaced TTR was around 930 N and the failure load for 1/2" spaced TTR was around 932 N. The failure load for both the samples was almost similar but studying the crack propagation in both the 1/2" and 1/4" skin/stringer samples, the TTR effect on the strength and stiffness was higher for the 1/4" spaced samples.

The pristine without the TTR had strength lower than the pristine skin/stringer with TTR which failed at a load of 852 N. The initially debonded sample with and without TTR had failure between 540 N to 610 N and the effectiveness of resisting the crack propagation in 1/4" spaced TTR in initially debonded samples was higher than the defect without TTR. The initial debond created was seen to weaken the sample and fail at lower loads but the 1/4" TTR spacing increased the strength, the first row of the TTR was 3mm away from the edge of the skin/stringer which also increased the strength in the initial debonded region. The completely failed and repaired samples had a promising improvement in restoring the samples strength and failed at 685 N. The crack propagation behavior when analyzed using the disbond growth in all the groups, the 1/4" spaced TTR pristine sample was seen to have less crack propagation and reaches failure at a higher load proving the effectiveness of the spacing of the TTR installed in the sample. The effectiveness of spacing of the TTR in increasing the strength was seen in initial disbond samples when the disbond region was installed with TTR which suppressed the crack propagation in minor loads. Thus the presence of TTR improves the strength and stiffness in all the sample groups.

Finite element analysis of the skin/stringer samples were performed to compare the computational and experimental results. The linear curve of the Abaqus model was in a similar trend with the experimental load-displacement plot of the pristine skin/stringer sample without TTR (Figure 76). In Future work the finite element analysis of the skin/stringer samples with both the spacings of TTR can be modelled to understand the efficiency of the TTR spacing.

REFERENCES

- [1] Marshall, I. H., Arnold, W. S., Wood, J., & Mousley, R. F. (1989). Observations on bolted connections in composite structures. *Composite Structures*, 13(2), 133-151.
- [2] Kravchenko, S., Kravchenko, O., Wortmann, M., Pietrek, M., Horst, P., & Pipes, R. B. (2013). Composite toughness enhancement with interlaminar reinforcement. *Composites Part A: Applied Science and Manufacturing*, 54, 98-106.
- [3] Krueger, R., Cvitkovich, M. K., O'Brien, T. K., & Minguet, P. J. (2000). Testing and analysis of composite skin/stringer debonding under multi-axial loading. *Journal of composite Materials*, 34(15), 1263-1300.
- [4] Ciminello, M., Concilio, A., Galasso, B., & Pisano, F. M. (2018). Skin–stringer debonding detection using distributed dispersion index features. *Structural Health Monitoring*, 17(5), 1245-1254.
- [5] Young, R., Rose, C., & Starnes, Jr, K. (2001, January). Skin, stringer, and fastener loads in buckled fuselage panels. In *19th AIAA Applied Aerodynamics Conference*.
- [6] P D MANGALGIRI. Composite materials for aerospace applications. *Aeronautical Development Agency*, Vimanapura PO, Bangalore 560017, India.
- [7] Kinloch, A. J., Korenberg, C. F., & Tan, K. T. (1983). Durability of Structural Adhesive Joints. *Applied Sciences Publishers*.
- [8] Neto, J. A. B. P., Campilho, R. D., & Da Silva, L. F. M. (2012). Parametric study of adhesive joints with composites. *International Journal of Adhesion and Adhesives*, 37, 96-101.

- [9] Kratz, J., Clegg, H., Dell'Anno, G., & Partridge, I. K. (2015). Improving the damage tolerance of composite joints with tufting. In *ICCM20-20th International Conference on Composite Materials, Copenhagen, Denmark*.
- [10] Harry M. Clegg, James Kratz, Ivana Partridge and Giuseppe Dell'Anno. Evaluation of the effects of tufting on performance of composite T-JOINTS.
- [11] T.Kevin O'Brien and Ronald Krueger. Influence of Compression and Shear on the Strength of Composite Laminates with Z-Pinned Reinforcement. U.S. Army Research Lab, NASA Langley Research Center, Hampton, VA 23681, USA.
- [12] Zhang, X., Van Hoa, S., Li, Y., Xiao, J., & Tan, Y. (2018). Effect of Z-pinning on fatigue crack propagation in composite skin/stiffener structures. *Journal of Composite Materials*, 52(2), 275-285.
- [13] Yousefpour, A., Hojjati, M., & Immarigeon, J. P. (2004). Fusion bonding/welding of thermoplastic composites. *Journal of Thermoplastic composite materials*, 17(4), 303-341.
- [14] Dubé, Martine, et al. "Characterization of resistance-welded thermoplastic composite double-lap joints under static and fatigue loading." *Journal of Thermoplastic Composite Materials* 28.6 (2015): 762-776.
- [15] Kravchenko, S. G., Kravchenko, O. G., Carlsson, L. A., & Pipes, R. B. (2015). Influence of through-thickness reinforcement aspect ratio on mode I delamination fracture resistance. *Composite Structures*, 125, 13-22.

- [16] Balasubramanian, K., Mohamed TH Sultan, and N. Rajeswari. "Manufacturing techniques of composites for aerospace applications." *Sustainable Composites for Aerospace Applications*. Woodhead Publishing, 2018. 55-67.
- [17] Walczyk, Daniel, and Jaron Koppers. "Thermal press curing of advanced thermoset composite laminate parts." *Composites Part A: Applied Science and Manufacturing* 43.4 (2012): 635-646.
- [18] M. Suresh, A. Sanders, P. Prajapati, K. Kaipa, O. G. Kravchenko, "Composite Sandwich Repair using Through-Thickness Reinforcement with Robotic Hand Micro-Drilling, "Master's Thesis, Department of Mechanical and Aerospace Engineering, Old Dominion University, Norfolk, VA, 2020.
- [19] Kravchenko, Oleksandr G., et al. "Conductive interlaminar interfaces for structural health monitoring in composite laminates under fatigue loading." *Materials & Design* 160 (2018): 1217-1225.
- [20] Hart-Smith. L.J. "Mechanically fastened joints for advanced composites. Phenomenological considerations and simple analyses". *Douglas Aircraft Company Paper DP6748A*, November 1978.
- [21] Cartié, Denis DR, Manos Troulis, and Ivana K. Partridge. "Delamination of Z-pinned carbon fibre reinforced laminates." *Composites science and Technology* 66.6 (2006): 855-861.
- [22] "Bulging Cracks in Pressurized Fuselages: A Numerical Study", *NLR Report NLR-MP-87058 U*, NLR National Aerospace Laboratory, The Netherlands, 1978.
- [23] A.J. "Kinloch. Adhesion and Adhesives": Science and Technology, Chapman and Hall, London, 1987.

- [24] Adams RD, Comyn J, Wake W. “Structural Adhesive Joints in Engineering”. London: Champan and Hall; 1997.
- [25] Dell'Anno, Milton Keynes. “Effect of tufting on the mechanical behavior of carbon fabric/epoxy composites”. Cranfield University, 2007.
- [26] Dransfield K, Baillie C, Mai Y-W. “Improving the delamination resistance of CFRP by stitching—a review”. *Composites Science and Technology*, 1994. 50(3):305-17.
- [27] Stavrov D and Bersee HEN. “Resistance welding of thermoplastic composites: an overview”. *Composite Applied Science Manufacturing* 2005; 36(1): 39–54.
- [28] Hou M and Friedrich K. “Resistance welding of continuous carbon fibre/polypropylene composites”. *Plast Rubb Compos Process Appl* 1992; 18(4): 205–213.
- [29] Raimondo A, & Riccio A. (2016). “Inter-laminar and intra-laminar damage evolution in composite panels with skin-stringer debonding under compression”. *Composites Part B: Engineering*, 94, 139-151.
- [30] Cvitkovich, M. K., Krueger, R., OBrien, T., & Minguet, P. J. (2004). Debonding in composite skin/stringer configurations under multi-axial loading.